Appalachian
STATE UNIVERSITY®
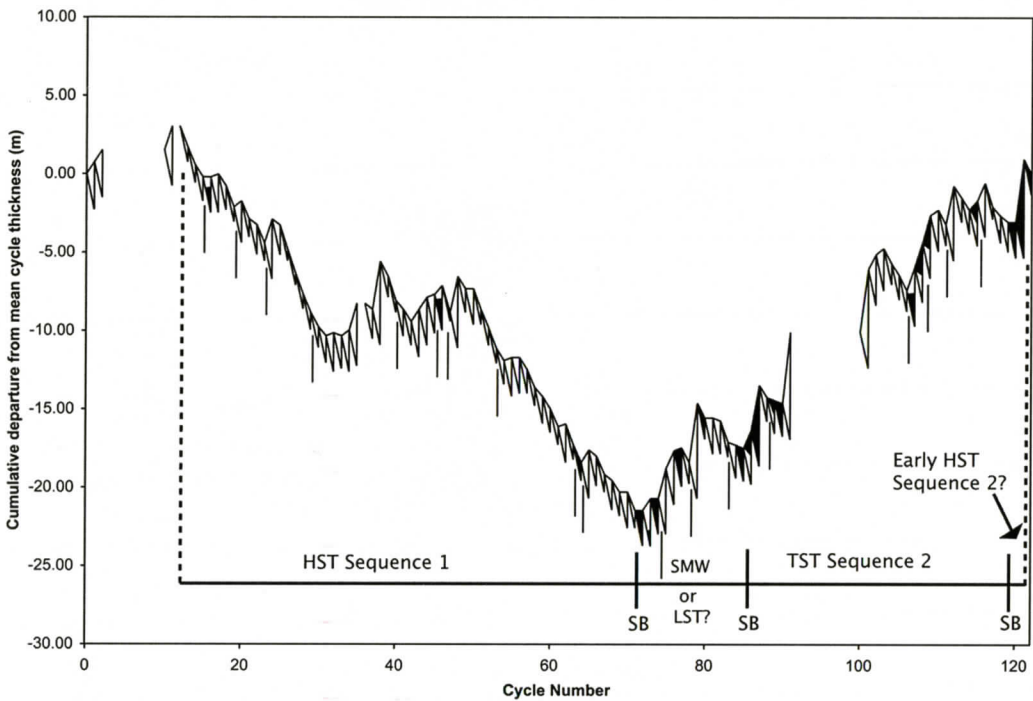BOONE, NORTH CAROLINA

Southeastern Geology: Volume 46, No. 3
July 2009

Editor in Chief: S. Duncan Heron, Jr.

Abstract

Academic journal published quarterly by the Department of Geology, Duke University.

SOUTHEASTERN GEOLOGY

Table of Contents

Volume 46, No. 3 July 2009

EVIDENCE FOR LATE EARLY CAMBRIAN GREENHOUSE CLIMATE IN PERITIDAL SHADY DOLOMITE, VIRGINIA

JASON BETZNER

4334 Sutler Hill Square
Fairfax, VA 22033

J. FRED READ

Department of Geosciences
Virginia Tech
Blacksburg, VA 24060

ABSTRACT

A relatively recently exposed road-cut section of the late Early Cambrian Shady Dolomite/Rome Formation was logged at Porters Crossroads, Virginia, to assess whether the section contained a paleoclimate record relevant to the onset of global greenhouse conditions. The cut exposes 300 meters (900 feet) of cyclic peritidal carbonate parasequences and several distinctive red-bed units that formed on the peritidal portion of a carbonate ramp with periodic siliciclastic influx. The carbonate parasequences are 0.3 to 5 m thick (1-15 feet). The major facies comprise red mudrock (terrestrial or intertidal mud-flat), red and white sandstone (intertidal sand-flat), microbially laminated dolomite (upper intertidal flat), thick-laminated dolomite (lower intertidal), fenestral pelletal packstone/mudstone (intertidal to subtidal), and burrowed dolomite/wackestone-mudstone (subtidal).

A Fischer (accommodation) plot shows that the succession preserves the late highstand (Sequence 1) of the Shady carbonate platform and the transgressive systems tract (Sequence 2) of the overlying Rome Formation. The parasequences commonly stack into groups of 4 to 6 upward-shallowing and upward-thinning cycles, which make up parasequence bundles. The roughly 5 to 1 bundling suggests precessional cycles stacked within short-term eccentricity cycles. These high frequency fourth- and fifth-order, upward-shallowing parasequences are classic greenhouse platform deposits, suggesting that the exposed Shady-Rome section formed on a relatively ice-free earth over about 2 m.y. This study extends the greenhouse climate that typifies the Middle to Late Cambrian back into the late Early Cambrian.

INTRODUCTION

This study was done to determine whether there is evidence in the Appalachian Valley and Ridge Province, southwestern Virginia, for a greenhouse global climate in the late Early Cambrian. The Shady-Rome section at Porters Crossroads (Figs. 1 and 2) was chosen because a relatively new road-cut exposed about 300 meters (900 feet) of section of peritidal facies. The Early Cambrian Shady Dolomite and overlying Rome Formation (Figs. 3 and 4) form a second order supersequence representing an overall transgression and regression of the sea (Barnaby and Read, 1990). The peritidal carbonates in the upper Shady Dolomite-Rome Formation formed on a carbonate ramp and subsequent rimmed shelf just landward of the margin.

During global greenhouse worlds, parasequences updip on aggraded ramps are dominated by 20 k.y. precessional cycles formed under meter-scale (< 10 m) sea-level fluctuations along with possible autocyclicity (Read, 1998). Cycles consist of very shallow-water facies, with regional tidal flat caps and minor disconformities (Read, 1998). Cycles are typically bundled into 100 and 400 k.y. sets, although
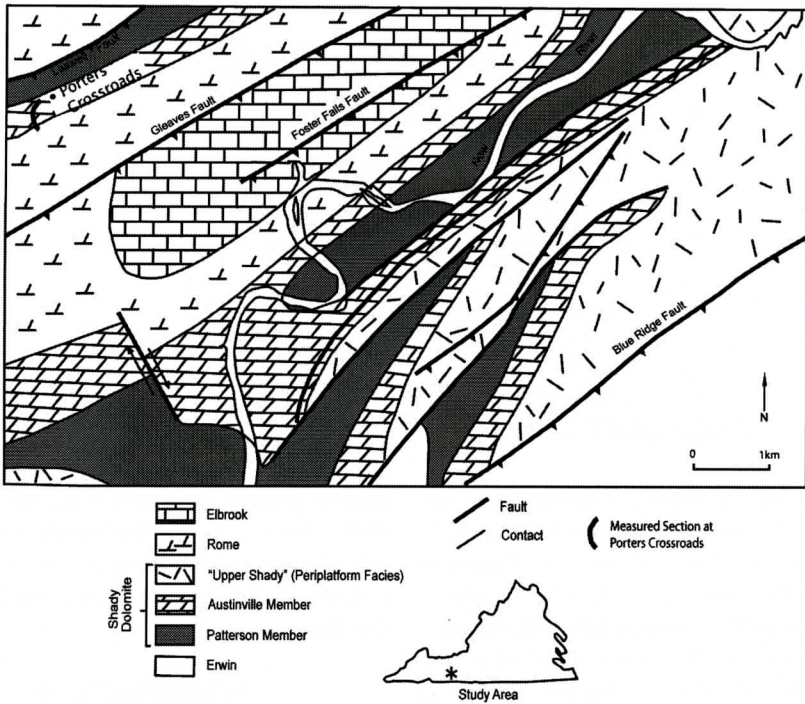
Figure 1. Locality map of study area showing location of Porters Crossroads. Modified from Barnaby and Read, 1990.

'missing beats' on the platform often make it difficult to determine simple ratios typical of Milankovitch forcing (Read 1998).
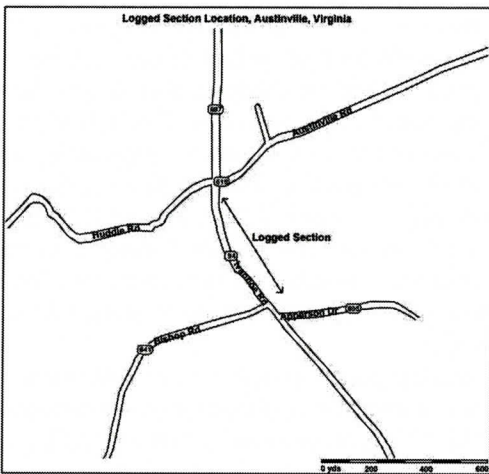
Figure 2. Locality map of Porters Crossroads section near Austinville, Virginia.

These greenhouse parasequences differ from icehouse cycles on carbonate platforms, which are dominated by 400, 100, and possibly 40 k.y. Milankovitch cycles with 50-100 m shifts in sea level (Read, 1998). Carbonate cycles during an icehouse world have regional disconformities with associated aeolianites, lack tidal-flat facies except near the shoreline, and commonly have deeper-water facies in-between shallow-water facies. There is also abundant unfilled accommodation (Read, 1998).

Greenhouse cycles also differ from transitional cycles formed during times of moderate continental ice sheets. These parasequences lack deeper-water facies, rarely have regional tidal flats, and show widespread disconformities updip (Read, 1998). They are also characterized by deep-ramp storm beds arranged in upward-coarsening units because of high-frequency eustasy (Read, 1998).

Parasequences formed during greenhouse worlds, that were relatively free of global ice, have been described along the East Coast of North America during the Middle to Late Cambrian (Read, 1998; Koerschner and Read, 1989; Demicco, 1985; Goldhammer et. al, 1990) as

110
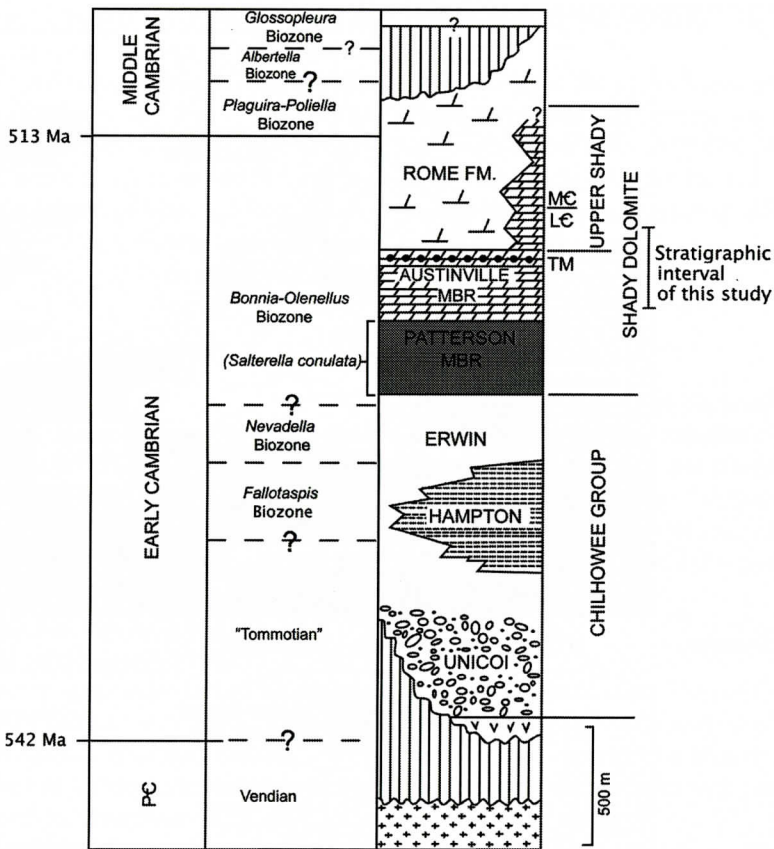
Figure 3. General stratigraphic section of Cambrian Chilhowee Group and Shady Dolomite/Rome sequence. Ivanhoe Member not shown. Modified from Barnaby and Read, 1990.

well as Late Cambrian successions in Nevada and eastern California (Montanez and Osleger, 1993).

The latest Precambrian to Middle Cambrian spans the transition from an icehouse world into a greenhouse world (Read, 1998). This study provides clues as to how early in the Cambrian, greenhouse conditions existed by examining the parasequences, stacking patterns, and sequence stratigraphy of the Shady-Rome Formation in southwestern Virginia. If the late Early Cambrian Shady Dolomite formed during a relatively ice-free greenhouse world, then parasequences and a corresponding Fischer plot should display 20 k.y. precessional cycles, minor disconformities and be bundled in 100 to 400 k.y. Milankovitch sets. Parasequences should also display shallow-water facies with tidal-flat caps.

GEOLOGIC SETTING

The section is located in the folded and thrusted Valley and Ridge Province on the Laswell Thrust Sheet, and is one of the easternmost thrust sheets in the area (Fig. 1; Barnaby and Read, 1990). It is overridden by the Blue Ridge Thrust to the southeast. The oldest unit in the area is the Early Cambrian Erwin Sandstone of the Chilhowee Group, which consists dominantly of marine quartz arenites (Barnaby and Read, 1990). It is conformably overlain by the Early Cambrian Shady Dolomite carbonate platform succession. The basal unit, the Patterson Member (300 m thick), comprises thin-bedded, nodular dolomitic lime wackestone/ mudstone deposited in a deep ramp setting. The overlying Austinville Member (300 m thick) is composed of massive upward into cyclic peloi-

111
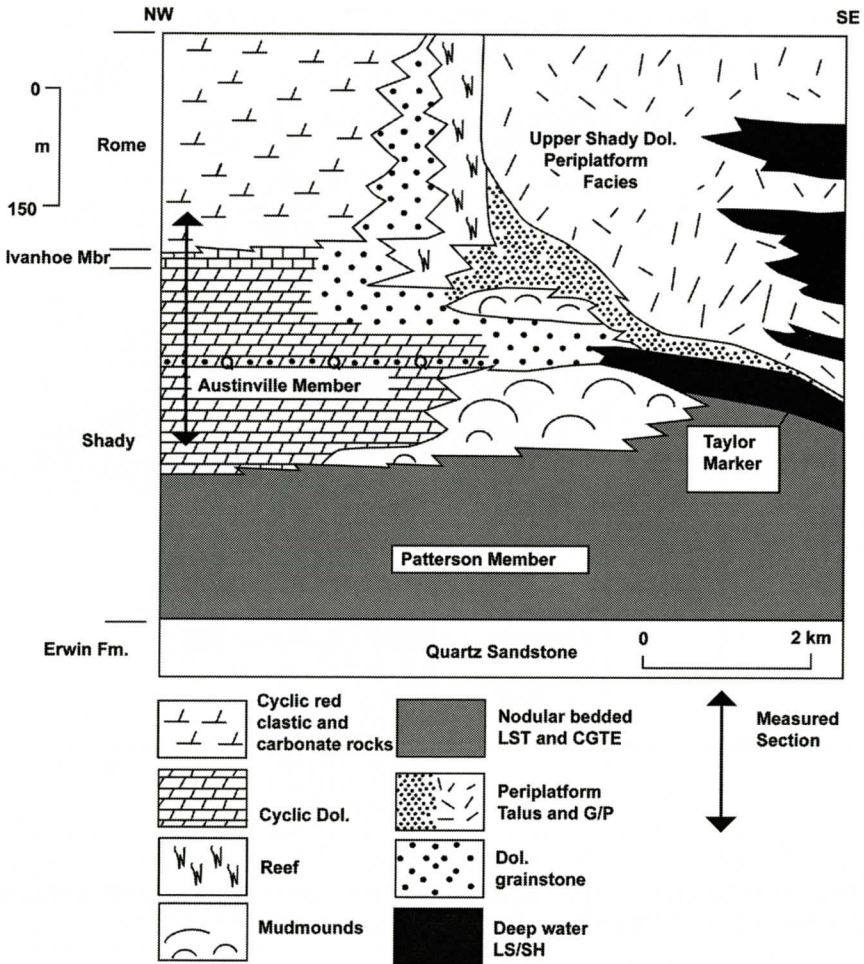
Figure 4. Generalized stratigraphic cross section of Shady Dolomite and Rome Formation near Austinville, Virginia. Section measured is marked by heavy bar. Q refers to quartzose lime sand unit (Taylor Marker). Modified from Barnaby and Read, 1990.

dal and oolitic dolomites (shallow subtidal shoal and peritidal platform); several quartz sand stringers are traceable off the shelf into dark "Taylor Marker" shaly carbonates. The quartzose Taylor Marker was formed from clastics being shed off the shelf during the deposition of the sandy portion of the middle part of the Austinville Member (Barnaby and Read, 1990). The Ivanhoe Member, (~20-30 m-thick) the upper unit of the Shady Dolomite, consists of a thin succession of interbedded peritidal limestones and dolomites. The Shady Dolomite is overlain by the Middle Cambrian Rome Formation, which is composed of cyclic peritidal and coastal plain redbeds and peritidal carbon-

ates (Fig. 3). Deposition was influenced by a combination of thermotectonic subsidence and eustasy (Barnaby and Read, 1990). Subsidence rates were estimated to be about 5 to 10 cm/k.y. (Barnaby and Read, 1990), but the new time scale of Gradstein et al. (2004) suggests higher rates of 10 to 15 cm/k.y. The Shady-Rome platform began as a ramp, and evolved into a rimmed shelf during the latest Early Cambrian (Barnaby and Read, 1990).

The age of the Shady-Rome is biostratigraphically constrained to be late Early Cambrian to Middle Cambrian. The formation contains *Bonnia-Olenellus* biozone trilobites (Willoughby, 1977; Barnaby and Read, 1990). The Patter-

son Member contains Early Cambrian *Salterella conulata.* Archaeocyathids in the Austinville Member are middle *Bonnia-Olenellus* biozone (Barnaby and Read, 1990). The Early Cambrian to Middle Cambrian boundary is marked by the transition of Early Cambrian trilobites to Middle Cambrian trilobites in the upper part of the Shady-Rome off-shelf sediments (Willoughby, 1977; Barnaby and Read, 1990).

METHODS

The Porters Crossroads section was logged bed-by-bed using a Jacob's staff, noting lithologies, contacts, color, grain size, sedimentary structures, and type of fossils present. The section starts in the Shady Dolomite within the Austinville Dolomite Member (above the non-cyclic portion), and was logged to the top of the outcrop within the Rome Formation. A stratigraphic column was constructed using the logged data, the column was computer-drafted and the lithologies color-coded. Parasequences were identified as upward-shallowing successions bounded by flooding surfaces. Cycle thicknesses were used to construct a Fischer plot, which is a plot that tracks changes in accommodation (sea level plus subsidence) through time (Read and Goldhammer, 1989). These track cumulative departure from average cycle thickness versus cycle number, such that a long-term sea level rise is manifested by the rising limb of the plot (thicker than average cycles) and a long-term fall is marked by a falling limb (thinner than average cycles). Fischer plots have previously shown their usefulness in defining short-duration (10 k.y. to 100 k.y) departures in relative sea-level as well as assessing magnitude of third-order (1 to 10 m.y.) fluctuations in sea-level which, assuming they can be correlated regionally, relate to eustatic events (Read and Goldhammer, 1998). The facies stacking patterns, in conjunction with the Fischer plot, were used to define cycle bundling, and larger scale sequences (Fig. 5). The cyclic character of the platform succession was then evaluated for any global climate signal.

FACIES AND INTERPRETATION

The facies in the upper Shady Dolomite and Rome formations at Porters Crossroads are shown on the column in Figure 5. They were described and interpreted by Pfeil (1977), although the section measured was relatively poorly exposed.

Mudrock

Description

These occur in 0.3-3 m-thick units mostly in the middle and upper parts of the section, and are gray to red, massive and microbially laminated, silt to fine-grained, well-sorted, siliciclastic mudrock with mudcracks, cross-laminations, ripple marks, some peds, and some interbedded silty seams.

Interpretation

The mudcracks, cross-laminations, ripple marks, peds and silty seams all indicate that this mudrock was formed in a terrestrial environment or intertidal mud-flat with periodic exposure (Reineck, 1975).

Sandstone

Description

These occur in 1-4 m-thick units mostly in the middle and upper parts of the section. They are tan, red, or yellow, massive or microbial and thickly laminated at parasequence caps, fine- to coarse-grained, well-sorted quartz sandstone with sand-filled mudcrack layers, rippled surfaces, burrows, and cross-laminations.

Interpretation

The mudcracks, cross-laminations, rippled surfaces, burrows and quartz sand indicate an intertidal sand-flat depositional environment (Reineck, 1975).

Microbially Laminated Dolomite

Description

This facies occurs in 0.3 to 6 m-thick units that are best developed in the lower and upper
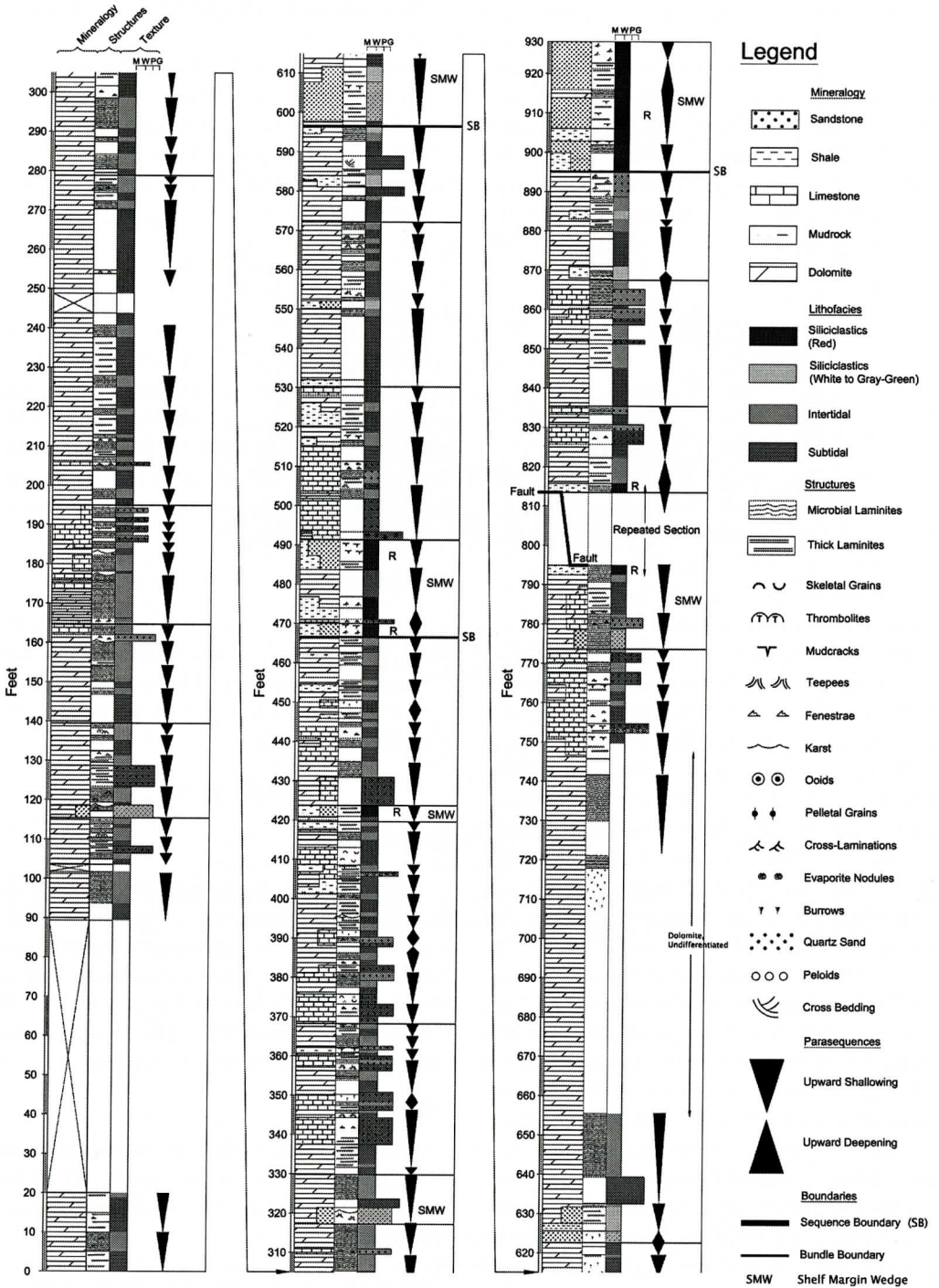
Figure 5. Stratigraphic column of logged section at Porters Crossroads, Virginia. Column measures 930 feet (approximately 300 m). It starts in the Austinville Member of the Shady Dolomite and ends in the Rome Formation. About 120 parasequences are present with bundles of 4-6 parasqeuences marked by thin, horizontal lines. Three sequence boundaries are marked by thick horizontal lines.

middle parts of the section, capping peritidal cycles. It is light to medium gray, microbially laminated dolomite with some planar laminations, some undulating tops, teepees, and rare domal laminations with some silica replacement, and is a fine- to medium-grained pelletal packstone and lime mudstone.

Interpretation

The laminites were formed from muds and pellets trapped and bound by microbial mats (Koerschner and Read, 1989), in low-energy tidal flats.

Thick-Laminated Dolomite

Description

This facies occurs in 0.3 to 4 m-thick units throughout the section, and is light to medium gray, thick-laminated, fine- to medium-grained dolomite with rare silica nodules after anhydrite.

Interpretation

The thick-laminated carbonates formed in low energy, lower intertidal environments. Laminations are probably mechanical, caused by the settling of pelletal silts and carbonate muds from low-energy tidal waters under the influence of microbial mats (Koerschner and Read, 1989). Silicified anhydrite nodules suggest a dry climate and tidal groundwater in the anhydrite field.

Fenestral Limestone and Thrombolites

Description

This facies occurs in 0.3 to 1 m-thick units in the lower and less commonly the middle part of the section. They are medium to dark gray, massive, locally capped by thick-laminated carbonate, and commonly have spherical calcite fenestrae and clotted fabrics. They generally are fine- to medium-grained, intraclastic pelletal grainstone or pelletal mudstone. Some units have undulating tops suggestive of thrombolite units.

Interpretation

The fenestrae and clotted fabrics formed in intertidal to shallow subtidal environments in which fenestrae formed by gas bubbles, mat decomposition, and shrinkage; clotted thrombolitic fabrics likely formed beneath pustular mats (Pfeil and Read, 1980).

Burrowed Dolomite/Limestone

Description

This facies occurs in 0.3 to 1.5 m-thick units in the middle part of the section. It is light to dark gray, massive with a burrowed, bioturbated/mottled texture, and composed of fine- to medium-grained intraclastic limestone or dolomite. There is a zebra dolomite overprint in places (Barnaby and Read, 1990).

Interpretation

The bioturbated carbonates formed in shallow subtidal, low-energy lagoons in which organisms burrowed the sediments, disrupting primary layering (Pfeil and Read, 1980).

SEQUENCE STRATIGRAPHY

Parasequences

Parasequences are 0.3 to 5 m-thick. Carbonate parasequences are characterized by low-energy subtidal to intertidal massive, burrowed, or locally fenestral and thrombolitic carbonates, shallowing up into microbially laminated caps. Mixed siliciclastic-carbonate parasequences consist of subtidal to intertidal laminated, mudcracked, or rippled sands or silts overlain by massive or laminated carbonate. Siliciclastic parasequences are composed of subtidal to intertidal shale or shaly sandstone, that is massive, rippled or laminated capped by mudcracked shaly sandstone.

Parasequence Sets or Bundles

Parasequences are typically bundled into units composed of 4 to 6 parasequences. Bundles are identified as groups of parasequences that thin upward, and contain successively shal-

lower water facies up-section. Bundles appear on Fischer plots as a rising limb of one or more thick cycles, followed by a falling limb of several thin cycles. About two-thirds of the siliciclastic-bearing cycles occur in lows on the Fischer plots, compatible with these being associated with intervals of low sea levels.

Sequences and Systems Tracts

The lower half of the measured section spans the falling limb of the Fischer plot, interrupted by a short-term rise, and then continued fall to the middle of the section. This suggests that this interval represents part of the highstand of the Shady Dolomite Sequence 1, on which is superimposed a smaller scale sea level rise and fall. The upper half of the section preserves the rising limb of the Fischer plot, suggestive of the transgressive systems tract of a second sequence in the Upper Shady-Rome Formation section. The top of the section may be the start of a second highstand, as the cycles form the onset of a falling pattern on the Fischer plot. Sequence 3 of the Shady-Rome succession (Brezinski et al., in press) is not exposed in the study area.

Highstand Systems Tract of Sequence 1

The highstand system tract (HST) consists of thinner than average cycles. The cycles are characterized by a thin, lower subtidal unit, and a relatively thick, very dolomitic, mechanically and microbially laminated carbonates and some capping quartz sands (Read, 1998).

Shelf Margin Wedge

The redbed interval in the middle of the measured section, in the trough of the Fischer plot, is suggestive of a shelf margin wedge or perhaps the updip part of a lowstand systems tract. It is possible that the redbeds at the top of the exposed section also are a shelf margin wedge, but they may be associated with a high frequency sea level fall, rather than a third-order sequence lowstand. The shelf margin wedge consists of thin cycles of quartz sandstone and mudrock, containing mudcracks, fenestrae, cross laminations, ripple marks and some microbial laminite caps. Locally, they contain basal upward-deepening units of thick-laminated mudrock at the bottom deepening upward to massive mudrock/sandstone.

Transgressive Systems Tract of Sequence 2

The transgressive systems tract (TST) consists of thicker than average cycles composed of thin, pelletal mudstone and microbial laminite capped parasequences at the bottom grading upwards into thicker, massive to thickly laminated dolomitic mudstones; siliciclastics are common, especially in upper parts of parasequence sets (lows on the Fischer plot; cf. Read, 1998).

DISCUSSION

The Shady-Rome succession is a second order supersequence (~ 8 m.y. duration) that contains three third-order depositional sequences (Brezinski et al., in press). The 300 m measured interval logged at Porters Crossroads, Virginia, spans the upper part of the Shady Dolomite and the lower Rome beds. The Fischer plot (Fig. 6) suggests that the measured interval includes the highstand of Sequence 1 and the transgressive and early highstand of Sequence 2. Sea level probably dropped below the shelf top during deposition of the sandy portion of the middle part of the Austinville Member (when clastics were shed off the shelf to form the quartzose Taylor Marker) during the latter part of Sequence 1. Sea level also falls off the shelf to form the major third-order lowstand evident at the base of Sequence 2, marked by the redbeds in the middle of the studied section. The deposition of clastics at the edge of the shelf is suggestive of Type I sequence boundaries, when sea level falls below the shelf top. However, there is little evidence of major unconformity development or long-term exposure and regolith development in the studied section. Much of the off-shelf section is highly condensed (Barnaby and Read, 1990), which could explain the lack of evidence of a major unconformity. It is not clear why the off-shelf section is highly
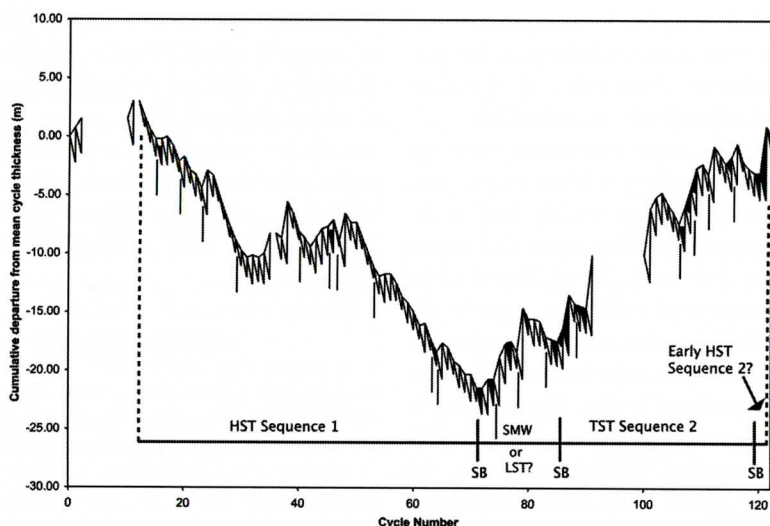
Figure 6. Fischer plot cycle number vs. thickness. Thin vertical lines are bundle boundaries. Thick vertical lines with SB are sequence boundaries. Dashed lines are unknown extent of systems tracts. The Fischer plot suggests that the measured interval includes the highstand (HST) of Sequence 1, shelf margin wedge (SMW) or updip lowstand (LST), and the transgressive (TST) and early highstand of Sequence 2.

condensed, but the presence of some anhydrites in other parts of the section suggests an arid climate. Therefore, an absence of fluvial sedimentation may be a factor.

Rapid thermotectonic subsidence and eustatic sea level rise (Barnaby and Read, 1990) led to high rates of accommodation increase (10 to 15 cm/k.y.). These values based on the new Gradstein et al. (2004) time scale are higher than the 5 to 10 cm/k.y. reported previously (Barnaby and Read, 1990). The high accommodation rates favored preservation of relatively complete peritidal successions once the interval had shoaled from the deep ramp facies of the Patterson Member and the overlying subtidal carbonate sand shoals of the lower Austinville Member (cf. Koerschner and Read, 1989; Goldhammer et al., 1990). The Shady-Rome succession spans approximately ~7 m.y. (based on Gradstein et al., 2004, time scale and apportioning the lower third of the *Bonnia-Olenellus* interval to the Chilhowee clastics). The measured section is roughly 25 to 33 percent of the total section, making it about 2 to 3 m.y. duration. Dividing the approximately 120 cycles (including cycles assigned to the non-differentiated intervals) into the 2 to 3 m.y. duration of

deposition suggests that the cycles are roughly 15 to 25 k.y. duration, compatible with a precessional signal. However, given the poor absolute time control these estimates are very tentative. The common bundling of the of 4 to 6 parasequences evident on the Fischer plot further supports the idea that the parasequences may be the product of precessional cycles (~20 k.y. duration or less), bundled into eccentricity cycles (~100 k.y. duration). It should be stressed that the duration of the Shady-Rome succession is very poorly constrained and these cycle durations should only be interpreted as falling within the fifth-order Milankovitch band. Although many of the cycles likely were driven by high frequency sea level changes as suggested by the meter scale (~5-25 m) accommodation changes on the Fisher plot, autocyclic shallowing also could have formed some of the cycles (cf. Wilkinson et al., 1997). It is possible that a few cycle boundaries may be absent. Non-recognition of one or two cycle boundaries has little effect on the large-scale curves defined by a Fischer plot, however it does affect the smaller scale departures (Read and Goldhammer, 1998). A few cycles may be missing due to exposure, however the low-amplitude sealevel

fluctuations evident on the Fischer plot suggest that few beats were missed on the peritidal portion of the platform. Correlation of cycles regionally could solidify this interpretation.

Previous studies show that fourth order cycles appear to be developed in the deeper subtidal facies of the lower Shady Dolomite, marked by shallowing of deep ramp into mound facies (Barnaby and Read, 1990). Fourth order bundling is also present within the upper Shady and Rome peritidal units, with parasequences bundled into what appear to be of fourth order (100 k.y.?) eccentricity cycles. Again, such estimates are very tentative and need geochronologic corroboration. Siliciclastics in the peritidal cycles appear to be best developed in (but not restricted to) the fourth order lowstands evident as lows between cycle bundles on the Fischer plots (Fig. 6).

The dominance of meter-scale cycles on the platform, the common microbially laminated caps suggestive of widespread tidal flat progradation, the lack of well developed subaerial regolith, caliche or other paleosol-like features, all are compatible with high frequency, small sea level changes typical of a relatively ice free earth (Read, 1998). The cycles are strikingly similar to Middle and Late Cambrian cycles described by Koerschner and Read (1991), Demicco (1985), Montanez and Osleger (1993), and interpreted as greenhouse platform cycles. Thus, the data from the Upper Shady Dolomite and Rome Formation, Virginia, suggests that at least the latest Early Cambrian was a greenhouse earth.

CONCLUSIONS

New data from a well-exposed road cut section of the Shady Dolomite-Rome succession, at Porters Crossroads, southwestern Virginia, shows that the succession consists of superbly developed peritidal parasequences. They occur within the highstand of Sequence 1 of the Shady dolomite (Austinville and Ivanhoe Members), and the transgressive systems tract of Sequence 2 (dominantly Rome Formation). The meter-scale parasequences, with subtidal bases and laminated dolomitic caps resemble those from

greenhouse platforms of slightly younger Cambrian age in North America, and appear to have formed under high frequency, low amplitude sea level fluctuations on an ice-free earth. The lithofacies, parasequences and stacking patterns indicate an ice-free greenhouse world (cf. Read, 1998) suggesting that onset of greenhouse conditions was at least as early as the late Early Cambrian.

REFERENCES

Barnaby, R.J. and Read, J.F., 1990, Carbonate ramp to rimmed shelf evolution: Lower to Middle Cambrian continental margin, Virginia Appalachians. Geological Society of America Bulletin, v. 102, p. 391-404.

Brezinski, D.K., Taylor, J.F., and Repetski, J.E., in press, Sequential development of platform and off-platform facies of the Great American Bank in the Central Appalachians: in Derby, J., editor, The Cambro- Ordovician Sauk Sequence of Laurentia – The Geology and Petroleum Potential of the Great American Carbonate Bank. American Association of Petroleum Geologists Special Volume.

Demicco, R.V., 1985, Platform and off-platform carbonates of the Upper Cambrian of western Maryland, U.S.A. Sedimentology, v. 32, issue 1, p. 1-22.

Goldhammer et al., 1990, Third order cycles, cyclostratigraphy, and sequence stratigraphy of Cambro-Ordovician carbonates of the central Appalachians. Appalachian Basin Industrial Associates, v. 15, p. 177-188.

Gradstein et al., 2004, A new geologic time scale, with special reference to Precambrain and Neogene episodes, v. 27, no. 2, p. 83-100.

Koerschner, W.F. and Read, J.F., 1989, Field modeling of Cambrian carbonate cycles, Virginia Appalachians. Journal of Sedimentary Petrology, v. 59, no. 5, p. 654-687.

Montanez, I.P., and Osleger, D.A., 1993, Parasequence stacking patterns, third-order accommodation events, and sequence stratigraphy of Middle to Upper Cambrian platform carbonates, Bonanza King Formation, southern Great Basin: in R.G. Loucks and J.F. Sarg, (eds.), Carbonate sequence stratigraphy: Recent developments and applications: American Association of Petroleum Geologists Memoir 57, p. 305-326.

Pfeil, R. W., Jr., 1977, Stratigraphy and sedimentology, Cambrian Shady Dolomite, Virginia, M.S. Thesis: Virginia Polytechnic Institute and State University, Blacksburg, VA, 137 p.

Pfeil, R.W., and Read, J.F., 1980, Cambrian platform margin facies, Shady Dolomite, southwestern, Virginia, U.S.A. Journal of Sedimentary Petrology, v. 50, no. 1, p. 0091-01116.

Read, J.F., 1998, Phanerozoic carbonate ramps from greenhouse, transitional, and ice-house worlds: Clues from

field and modeling studies. Geological Society, London, Special Publications, 149, p. 107-135.

Read, J.F., and Goldhammer, R.K., 1998, Use of Fischer Plots to define third-order sea-level curves in Ordovician peritidal cyclic carbonates, Appalachians. Geology, v. 16, p.895-899.

Reineck, Hans-Erich, 1975, German North Sea Tidal Flats. Tidal Deposits: A Casebook of Recent Examples and Fossil Counterparts. Springer-Verlag, New York, p. 5-20.

Wilkinson, B.W. et al., 1997, Stratal order in peritidal carbonate sequences. Journal of Sedimentary Petrology, v. 67, no. 6, p. 1068-1082.

Willoughby, R.H., 1977,Paleontology and Stratigraphy of the Shady Formation near Austinville, Virginia. Masters Thesis; Virginia Polytechnic Institute and State University.

Petrology of the Memphis Sand in the Northern Mississippi Embayment

Lumsden, D.N., Hundt, K.R., and Larsen, D.

Department of Earth Sciences
The University of Memphis
Memphis, TN 38152
dlumsden@memphis.edu

ABSTRACT

A field and petrologic study of the Memphis Sand, host to the regionally important Memphis Aquifer, was conducted to provide information about its porosity, origin, environment of deposition and possible hydraulic compartmentalization. Sample collection at six exposures, three wells, and two cores reveal that the Memphis Sand in the Northern Mississippi Embayment (NME) is a friable fine to coarse quartz wacke or quartz arenite. Primary intergranular porosity approached 40% and remains 25% to 35%. Although dominated by sharply angular monocrystalline quartz grains, rounded coarse sand polycrystalline quartz grains are abundant (30% to 55%) toward the east margin of the NME where they are associated with trace amounts of kyanite and zircon. We observed no glauconite. The grain size of sieved disaggregated samples varies from coarse sand near the embayment margin to fine sand near the center of the NME. Quartz cement is essentially absent. The weak coherence of the Memphis Sand is due to secondary kaolinite matrix, which shows meniscus texture and other petrographic signatures that indicate formation in a vadose environment. The clay mineralogy of Claiborne Group strata changes from kaolinite in the north of the NME through mixed kaolinite/smectite to smectite dominated composition south of the 35th parallel. Our results document the extraordinary porosity of the Memphis Sand and the partial occlusion of the porosity by vadose-zone kaolinite during early diagenesis. The results also support a scenario in which the Memphis Sand was deposited in braided and meandering fluvial environments north of the 35th parallel.

INTRODUCTION

The Eocene Memphis Sand hosts the Memphis Aquifer, the primary source of potable water for millions of people in the Northern Mississippi Embayment (NME) (Figure 1). Memphis alone withdraws more than 200 million gallons of water per day from the aquifer. Increasing population and irrigation in the "Fertile Crescent" of the NME has increased demand for water with concomitant problems related to water rights. Rational policy decisions about utilization and apportionment of this critical resource must transcend political boundaries. To this end, we must understand the regional lithologic variation of the Memphis Sand.

The Memphis Sand forms the bulk of the Claiborne Group (Table 1) in the Northern Mississippi Embayment. It is approximately 240 m thick beneath Memphis, thinning to zero meters approximately 100 km to east and west (Hundt, 2008; Parks and Carmichael, 1990).

In contrast to the substantial literature about the petrology and petrophysics of clastic petroleum reservoirs, there are very few similar studies of clastic fresh water aquifers with which to compare our findings. The only literature that addresses the petrology of the Memphis Sand is an abstract by Lumsden and others (2008) and the unpublished thesis of Hundt (2008). The Floridian Aquifer is largely carbonate and thus not a good analog. Studies of the Ogallala and Dakota Aquifers focus on hydrodynamics; we found no publications on their petrology. The Potomac Group hosts the Potomac Aquifer, a
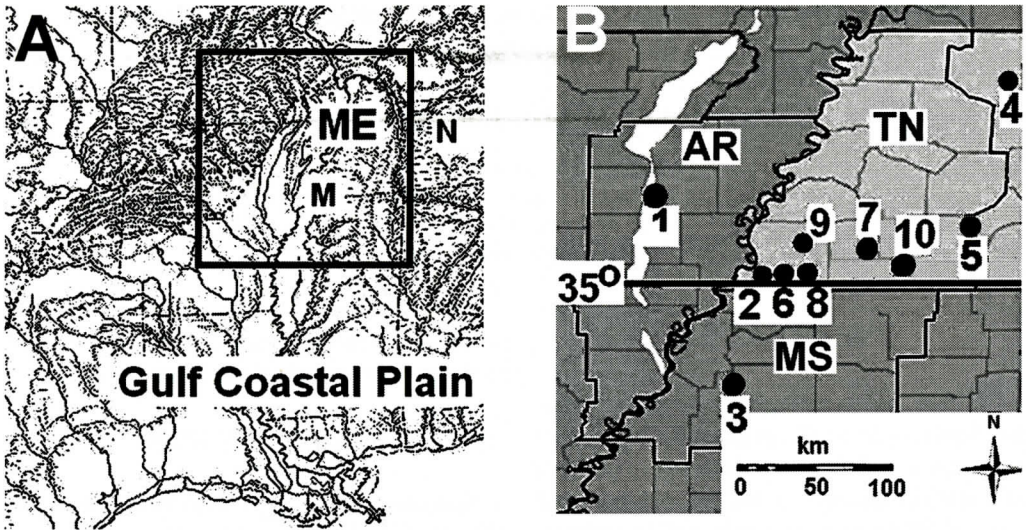
Figure 1. A - Memphis (M) is in the middle of the Mississippi Embayment (ME), a northern extension of the Gulf Coastal Plain. B - The 29 county study area is outlined in black and sample locations are numbered 1 to 10 (after Hundt, 2008). The 35th parallel, the Tennessee-Mississippi state line, coincides with an important transition in the depositional environment of the Memphis Sand.

major source of water to the population of the Chesapeake Bay area (McFarland and Bruce, 2006). Drobnyk (1965) discussed the mineralogy, granulometrics and environment of deposition of the Paleocene-Eocene Aquia Formation of the Potomac Group. However, he provided no information about porosity, matrix, or cement.

The interpretation of borehole log-based cross-sections and contour maps of the Memphis Sand is discussed elsewhere (Larsen and others, 2008 a, b; Hundt, 2008; Hundt and others, 2008). The purpose of the present investigation is to report grain composition, amount and origin of porosity, amount and origin of matrix, and amount and origin of cement. With these data we will address questions about the source of the sand, its environment of deposition, and the origin and occlusion of its porosity. The results will provide the basis for a better understanding of the origin, amount, and patterns of porosity in the Memphis Aquifer thereby contributing to a better understanding of its hydraulic compartmentalization, if any.

METHODS

The study includes 29 counties in east Ar-

kansas, west Tennessee and north Mississippi, an area of 42,500 sq km (Figure 1).

Samples were collected from six exposures, three mud-rotary boreholes, and two cores (Figure 1). Exposures provided sedimentary structure information (locations 1, 5, 7, 10). Locations 3 and 4 exposed the Cook Mountain confining unit but not the Memphis Sand. Samples from the three wells (locations 2, 6, and 8) provided grain composition and size data; however no information about porosity, matrix, or cement could be obtained from these disaggregated sands. Five samples were collected from a 20 m rotasonic core (UC-1) in Shelby Farms, Memphis, TN (location 9) (Garner and others, 2003; Gentry and others, 2006). The upper samples may be from a sand facies in the overlying Cook Mountain Formation, but the lower samples are from the Memphis Sand. Location 10 provided samples from a surface exposure and a 40 m deep sample from an auger core.

Petrographic analysis of 200 points was used to estimate bulk composition (percent grains, porosity, matrix, and cement) and grain composition. Samples were friable and impregnated with epoxy resin prior to thin section preparation. Grain surface texture of disaggregated samples was examined with a binocular micro-

Table 1. Cenozoic Era units in the western Tennessee portion of the Mississippi Embayment and their hydrologic relevance (based on Brahana and Broshears, 2001 and others).

CENOZOIC ERA
QUATERNARY PERIOD
       PLEISTOCENE AND MODERN ALLUVIUM –
           MISS. VALLEY ALLUVIAL AQUIFER AND EQUIVALENTS
       PLEISTOCENE LOVELAND, ROXANNA AND PEORIA LOESS – LEAKY CONFINING LAYER
       PLEISTOCENE TERRACE GRAVELS – LOCAL AQUIFER
       -----DISCONFORMITY ----------
TERTIARY PERIOD
       PLIOCENE-PLEISTOCENE EPOCH
          UPLAND COMPLEX – LOCAL AQUIFER
       -----DISCONFORMITY ----------
       EOCENE EPOCH
          JACKSON FORMATION – CONFINING LAYER
       Claiborne Group
          Cockfield Formation - confining layer, local aquifer
          Cook Mountain Formation - confining layer
          Memphis Sand – host to the Memphis Aquifer
     Paleocene Epoch
     Wilcox Group
          Flour Island Formation – confining unit
          Fort Pillow Sand – Fort Pillow aquifer
     Midway Group
          Old Breastworks Fm. – confining unit
          Porters Creek Clay – confining unit
----------------UNCONFORMITY (The K/T boundary) --------------------

scope and scanning electron microscopy.

Grain size was estimated by sieving disaggregated samples into half Phi size intervals (Boggs, 2001, p. 59 – 74). Samples were washed and fines (< 0.062 mm) decanted and weighed separately. Fines from water-wells samples (Locations 2, 6, and 8) were lost during the drilling process.

X-ray diffraction (XRD) was used to estimate the mineral composition of sandstone, sandstone matrix, and associated clay units.

RESULTS

Fresh hand specimens of the Memphis Sand are typically fine grained (mode 2 to 2.5 Phi, 0.25 to 0.177 mm), friable, quartz wacke or quartz arenite (Dott, 1964). Quartz wacke has 10% or more matrix, whereas quartz arenite contains less. Porosity in coherent samples is excellent; no cement is visible in hand samples.

Fresh outcrop sand, well samples, and core samples are very light gray (Munsell 8/1). Weathered outcrop samples are stained red from hematite with random centimeter-scale layers that are cemented by black limonite.

Memphis Sand grains are essentially 100% quartz present as single crystals, polycrystalline quartz, and chert (Table 2 and Figure 2A). The two easternmost samples (locations 5 and 10) have an abundance of coarse polycrystalline quartz grains. Trace amounts of feldspar, kyanite, and zircon occur with the polycrystalline grains. Muscovite is locally present in trace amounts. No glauconite was observed.

Monocrystalline quartz grains are well sorted, sharply angular to subangular, with some embayed grains (Figure 2B). Polycrystalline quartz grains are much larger than monocrystalline grains (typically 0.5 mm versus 0.2 mm) and are subrounded to rounded. The internal texture of polycrystal grains varies consider-

Table 2. Summary percent composition data for the Memphis Sand. ID numbers correspond to locations in figure 1. QA is quartz arenite, QW is quartz wacke.

ID	Grain composition						Bulk Composition				Class
	Mon Qtz	Poly Qtz	Cht	Total % Qtz	Feld	Rk Frag	% Grain	% Pore	% Matrix	% Cem	
1-L	83	15	2	100	0	0	59	35	6	0	QA
1-D	84	14	2	100	0	0	63	37	ND	ND	
2-1	84	13	3	100	0	0	ND	ND	ND	ND	
2-2	90	5	3	98	0	2	ND	ND	ND	ND	
2-3	88	4	2	94	0	6	ND	ND	ND	ND	
5	43	57	0	100	*	0	66	18	16	0	QW
6	91	8	1	100	0	0	ND	ND	ND	ND	
7a	90	10	0	100	0	0	53	10	0	37	QW
7b	89	11	0	100	0	0	46	26	8	20	QA
9, UC1-1a	90	6	2	98	0	2	51	29	20	0	QW
9, UC1-1b	79	11	10	100	0	0	55	22	23	9	QW
9, UC1-3	91	3	4	98	0	1	59	31	10	0	QW
9 UC1-4	84	10	4	98	0	2	58.5	23.5	18	0	QW
9, UC1-5a	89	7	2	100	0	0	60.5	22.5	17	0	QW
9, UC1-5b	82	12	6	100	0	0	63	18	19	0	QW
10 core	67	31	0	98	1**	0	79	17	4	0	QA
10 a	96	3	0	99	1	0	57			43***	
10 b	95	4	0	99	****		43	37	20	0	QW

1-L –Harrisburg, AR, weakly lithified by kaolinite matrix
1-D –Harrisburg, AR, disaggregated and washed of fines
2-1 - Allen Well 155A depth 220 to 253 ft, drill cuttings
2-2 - Allen Well 155A depth 565 to 597 ft, drill cuttings
5 – New Sand Pit, Chickasaw State Park, TN, kaolinite matrix with
meniscus texture
6 – South Campus well, U of M, drill cuttings,
7 a – Warren Road sample 4, cement is limonite
7 b – Warren Road sample 2, cement is limonite
8 – Johnson Road, Germantown, TN, well samples
9 – Shelby Farms, Memphis, TN, rotasonic core UC-1 top, UC -5,
bottom, a and b are different thin sections
10 core – LaGrange, TN, auger core
10 a – LaGrange, TN, weathered exposure sample, limonite cemented interval
10 b – LaGrange, TN, weathered exposure sample, not limonite cemented
* - trace feldspar, kyanite, and muscovite; ** - albite, ~ 0.5% kyanite, trace zircon
*** - limonite cement; **** - <1% zircon.

ably with equidimensional to elongated crystal domains, sharp and brush extinctions, and a range of crystal domain sizes (0.01 to 0.1 mm). Trace amounts of quartz grains are replaced carbonate; others have dust rims indicative of recycled detrital quartz or are vacuole-rich suggesting volcanic origin.

Grain luster is either vitreous or matte under the binocular microscope. A comparison of SEM images of grain surface textures of the Memphis Sand to a sample of the modern Mississippi River (Figure 3) showed both minor ce-
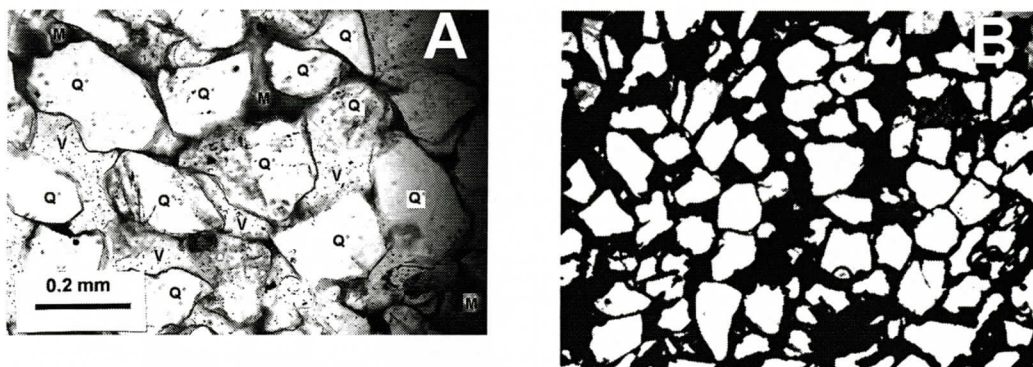
Figure 2. Thin section photomicrographs taken with plane polarized light. A. - Representative example of a coherent albeit friable sample showing quartz grains (Q), matrix (M), 35% void (V) but no cement. (Location 1, Harrisburg, AR, epoxy impregnated). B – Monocrystalline quartz grains, well sorted, sharply angular to subangular, some embayed, cemented by opaque limonite (47% of area) (Location 7, Warren Road).

ment overgrowths on some Memphis Sand grains (matte luster) whereas other grains had no overgrowths (vitreous luster).

No quartz cement was observed in any thin section (Table 2, Figure 2A). SEM images show partial and very thin quartz overgrowths (Figure 3). Centimeter-scale limonite-cemented layers are present at weathered exposures (locations 7 and 10). Limonite cemented samples do not have quartz cement (Figure 2B). Fewer and thinner limonite layers and some siderite layers are present in the UC-1 core (Gentry and others, 2006).

The weak coherence characteristic of the Memphis Sand is a result of 5 to 20% secondary kaolinite matrix (Table 2). Matrix commonly has a meniscus margin, color banding, and bulk crystal orientation perpendicular to the meniscus margin (results in a pseudoaxial cross under cross-polarized light). All of these characteristics are common features of post depositional clay precipitated in a vadose environment (Wilson and Pittman, 1977) (Figure 4A). In some samples "bridges" of matrix cross pores, (Figure 4B), whereas in other samples kaolinite "books" are visible in the matrix (Figure 4C). Both of these structures are characteristic of secondary matrix. Kaolinite postdates limonite where both are present (Figure 4B). In core samples, kaolinite also has a meniscus margin (locations 9 and 10) but a granular texture (Figure 4C) whereas outcrop samples have a fine fi-
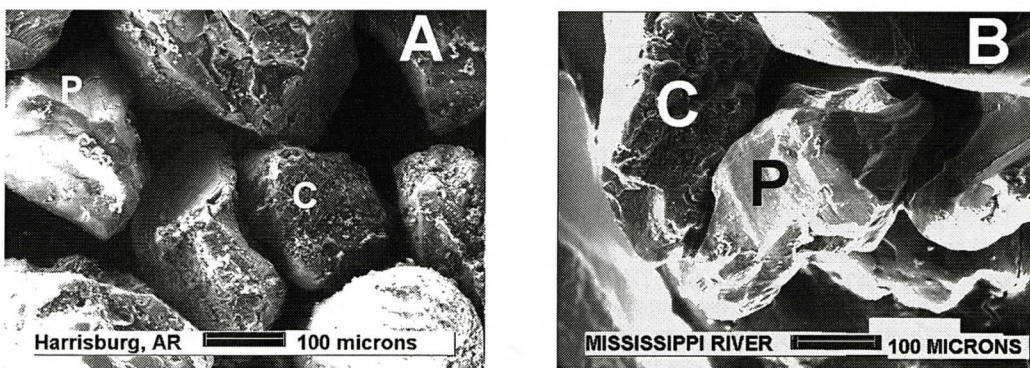
Figure 3. A comparison of SEM images of grain surface textures. A. - The Memphis Sand from Location 1. B. - Mississippi River sand. Both show both minor cement overgrowths (C) and pristine surfaces (P).
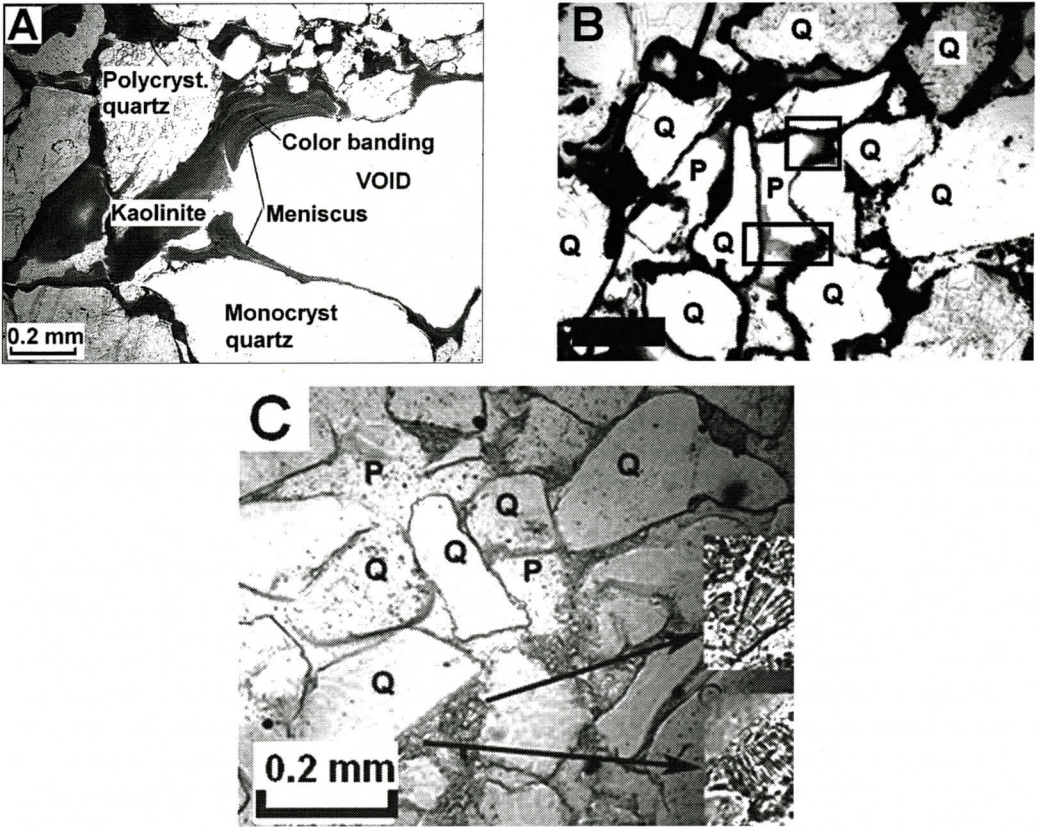
Figure 4. Photomicrographs of thin sections of epoxy impregnated Memphis Sand taken with plane polarized light. A - Thin section illustrating very fine secondary kaolinite matrix (Location 5, New Sand Pit). Note the meniscus contact and color banding. B. – Matrix with a meniscus boundary (light gray in the top black box) and a bridge (in the bottom black box). Note that kaolinite formed after the limonite cement (black) (Location 7, Warren Road). C. - Kaolinite matrix with a granular texture and meniscus boundary (around pore P) weakly binds quartz grains (Q) in sample UC1-4 from the rotasonic core, location 9, Shelby Farms. Enlarged kaolinite "books" are in inserts to the right.

brous texture (Figure 4A).

Primary porosity of 30 to 50 percent is partially filled by secondary matrix (and some limonite cement) (Table 2). Porosity is entirely intergranular; no secondary porosity was observed (Figures 2 and 4).

The Memphis Sand is fine grained and locally well sorted, with a mode 2.0 to 2.5 Phi (0.25 to 0.177 mm) (Table 3, Figures. 5 A, B). Polycrystalline grains are commonly 0.5 to 2.0 mm; much coarser than the 0.2 mm typical of monocrystalline grains (Figure 5 C). Locations 5 and 10 have a bimodal grain-size distribution with a coarse sand mode of polycrystalline

grains (Figure 5D, Table 3). Fines (< 0.062 mm) form a mode isolated from the bulk of the grains (Figure 5 A, C, D), an observation consistent with a post depositional origin for the matrix.

Cut-and-fill, tangential cross beds, and armored mud balls (centimeter-scale balls of clay coated with fine gravel) are present at location 5, and planar cross beds are present at locations 1, 5, 7, and 10 (Figure 6). Armored mud balls are common in high gradient streams subject to torrential flow (Pettijohn, 1975). Exposures near location 10, north of LaGrange, TN, show channel-structures with epsilon cross-bedding, clay rip-ups, and dispersed gravel.

Table 3. Summary of grain size data. The fine mode (<0.062 mm) was excluded from calculations as it is largely secondary.

Location number	Mean Φ	Mean mm	SD F	Sk Φ	Median Φ	Mode mid Φ	Coarse 1st % Φ
1	2.37	0.2	0.40	-0.07	2.30	2.25	1.25
2[1] 400 ft	1.69	0.31	0.70	-0.05	1.67	1.75	-1.25
2[1] 640 ft	2.03	0.24	0.67	-0.24	1.8	1.25 2.25	-0.25
5 -10	0.08	0.90	0.74	2.37	-0.55	-0.75	-1.25
5-11	0.35	0.80	0.72	1.33	0.2	-1.25 0.25	-1.25
6[1]	2.26	0.16	0.35	-0.41	2.0	2.25	1.25
7	1.51	0.35	0.46	1.13	1.45	1.25	-0.25
8[1]	1.95	0.26	0.70	-0.17	1.7	1.75	-0.25
9 UC1-1 55 – 65 ft	2.142	0.23	0.68	-1.84	2.2	0.25 2.25	-0.25
9 UC1-2	2.29	0.22	0.46	-0.41	2.35	2.25	-0.25
9 UC1-3	1.97	0.25	0.72	0.79	1.70	1.25 2.25	0.75
9 UC1-4	2.13	0.23	0.36	0.865	2.15	2.25	1.25
9 UC1-5 81 – 90 ft	2.01	0.25	0.38	0.76	2.00	1.75	1.25
10 Exposure	2.02	0.25	0.59	0.78	2.2	1.75	-0.25
10 Auger core	0.74	0.60	1.27	0.93	-0.1	-0.75 2.75	-1.25

1 - Well samples; Location 10 samples are from an exposure and an auger core. Location 9 data are from a rotasonic core UC-1 (Gentry et al., 2006).

SD is the standard deviation, Sk is skewness. The coarse 1st % is the midpoint of the coarsest mode that exceeds 0.1 percent.
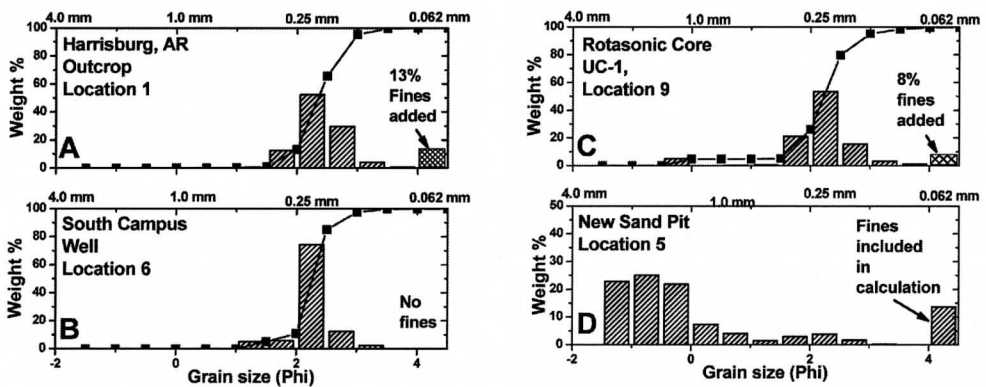
Figure 5. Representative grain-size data plotted as histograms and cumulative curves. Size was plotted using Krumbein's Phi scale with millimeter equivalents at the top of figures. Data for figures A, B, and C exclude fines to facilitate comparison between hand specimens (A and C) and wells (B). A bar for the excluded fine group was added to facilitate discussion of the role of fines. The New Sand Pit exposure figure (D) includes fines and a different Y scale.

Figure 6. A. Cut-and-fill, armored and unarmored mud balls, trough and planar cross-bedding at location 5. B. Planar cross-beds at location 7 are similar to those seen at location 1.

DISCUSSION

Interpretation of the lithologic variability of the Memphis Sand in the Northern Mississippi Embayment is constrained by the fact that six of the eight sample locations are in west Tennessee. Nevertheless we feel the data so far obtained provide important insights.

Regional Stratigraphy and Tectonics

The Gulf Coast is an Atlantic-type passive margin that evolved from a Triassic rift margin created by the breakup of Pangea (Gordon and Cox, 2008; Sawyer and others, 1991; Stearns and Marcher, 1962; Thomas, 1989, 2006). Punctuated and accelerating subsidence of the embryonic Mississippi Embayment was marked by Late Cretaceous transgressive-regressive cycles of fluvio-deltaic clastics and chalk/marl intervals (Salvador, 1991; Stearns, 1957). The Desha Basin in south Arkansas and adjacent Louisiana was the Mississippi Embayment depocenter during the Paleocene and Eocene (Cushing and others, 1964; Gordon and Cox, 2008; Onellion, 1956). During this time interval, fluvio-deltaic deposits of the Wilcox Formation (Early Eocene) were deposited on the marine Midway Shale (Paleocene). The Wilcox is overlain by an interbedded succession of alternating proximal and distal deltaic units and fluvial sands belonging to the Middle Eocene Claiborne Group (Cockfield, Cook Mountain, and Memphis Sand (e.g., Ahr, 1979; Berg, 1979). In the NME, north of the 35th par-

allel, the Memphis Sand consists dominantly of fluvial deposits that are difficult to correlate with shore-face strata farther south (Hundt, 2008; Russell and Parks, 1975). Marine conditions returned to the northern embayment with deposition of the clay and calcareous sand of the Late Eocene Jackson Formation (Wilbert, 1953).

Outcrop Scale Features

Massive to horizontal bedded and cross-stratified fine to coarse-grained sand dominates the Memphis Sand. Large planar cross bed sets, cut and fill structures, armored mud balls, and the relative lack of clay/shale beds in the Memphis Sand north of the 35th parallel are all consistent with braided river deposition (Galloway and Hobday, 1983; Hansen, 1969; Nanz, 1954). The SP log signature of the Memphis Sand commonly forms a cylinder pattern, a pattern often associated with braided river deposits (Hansen, 1969).

Lignite debris, kaolinite clay mudclasts (both armored and nonarmored), and siderite- and iron oxide laminations are common. Kaolinite clay beds associated with the sands are massive with locally incised channel-fill debris and brecciated intervals. The lithology and absence of any but plant fossils, suggest that the Memphis Sand is fluvial in origin. Sedimentary structures, channel sand with epsilon cross beds, moderate sorting, and cut-and-fill bedding, are consistent with both meandering and braided rivers. Similar observations favoring

both meandering and braided stream conditions were noted by Dilcher (1973).

Extensive meter-thick lignite beds are present north and south of the 35th parallel, but are more common in the south (Prior and others, 1985; Williamson, 2006). Lignite beds up to 1 m thick were observed in the confining units at locations 3 and 4 and are reported in the Memphis Sand of the Fort Pillow Test Well (Moore and Brown, 1969).

We suggest that the Memphis Sand records a depositional gradient from continental – fluvial environments north of the 35th parallel to transitional – marine environments immediately south of the 35th parallel. The shoreline migrated north and south with relative sea level rise and fall in the Gulf of Mexico Basin (e.g., Mancini and Tew, 1991).

The varied internal texture of polycrystalline grains, their coarse size, and their association with minor amounts of feldspar, kyanite, and zircon at locations 5 and 10 suggests a source area with granite, gneiss, and schist. The presence of embayed monocrystalline grains and the occasional presence of vacuole-rich grains suggest a volcanic source. Common chert (1 to 6%), occasional grains of quartz replaced carbonate, and grains with dust rims indicative of recycled quartz suggest that the source area included sedimentary rocks. The sharply angular and embayed morphology of the grains make it unlikely that the sand recycled from the Cretaceous Tuscaloosa Formation (Marcher and Stearns, 1962) or from the distant Appalachians (e.g., Stearns and Reesman, 1986). The closest source that combines massive igneous and metamorphic rocks, volcanic rocks, extensive chert and other sedimentary rocks is the Ozark Mountains of Missouri, approximately 150 km north and west of the NME. If the Ozarks were the source there should be some feldspar in the Memphis Sand, however only trace amounts are present. There is no evidence of secondary pores due to labile grain solution, so post depositional solution of feldspar is not likely. The Eocene was a time of overall warm humid conditions (Wing and others, 2003; Zachos and others, 2001). The Early Eocene in particular was a time of high global temperatures (the Paleo-cene-Eocene Temperature Maximum). We suggest that weathering in the source area dissolved the feldspar or altered it to kaolinite $(2KAlSi_3O_8 + H_2O + 2H+ \rightarrow Al_2Si_2O_5 (OH)_4 + 4SiO_2 + 2K+)$. Most of this fine kaolinite by passed the Northern Mississippi Embayment to transitional and marine environments south of the 35th parallel. The portion that went into solution supplied the ions needed for the post-depositional precipitation of the secondary kaolinite matrix.

The abundant matrix in the Memphis Sand (up to 20%) is a post-depositional kaolinite that formed in the vadose zone; i.e., essentially co-incident with deposition. The necessary ions were in the pore waters that percolated through the sand immediately after deposition.

Glauconite, a syndepositional mineral that forms only in a marine environment, was not observed in any samples.

The Memphis Sand is approximately 30 million years old and we expected some quartz cement, however it is essentially absent. Quartz cement in quartz sandstones may come from two sources: 1) internally by pressure solution when quartz grains interpenetrate during burial compaction and 2) precipitation from migrating fluids percolating through the pores. Burial compaction did not occur because of the less than one kilometer depth of the Memphis Sand. As for an external source, Memphis Aquifer water has 11 to 14 ppm SiO_2 (Moore and Brown, 1969; Parks and Carmichael, 1990), much less than the 40 ppm typical of soil water (Drever, 1997). Such low-silica water is consistent with negligible quartz cement. The syndepositional kaolinite coatings further inhibited cement overgrowths (Pittman and Lumsden, 1968).

The presence of fines (< 0.062 mm) clouds interpretation of grain size data. The fine mode stands isolated from the balance of the grain size distribution (Figure 5); a characteristic consistent with a post depositional matrix. Thus, further discussion of grain size is depends on data in which the fine modes are excluded.

Grain-size data from borehole samples are compromised by the loss of fines during sample recovery and mixing of grains from more than
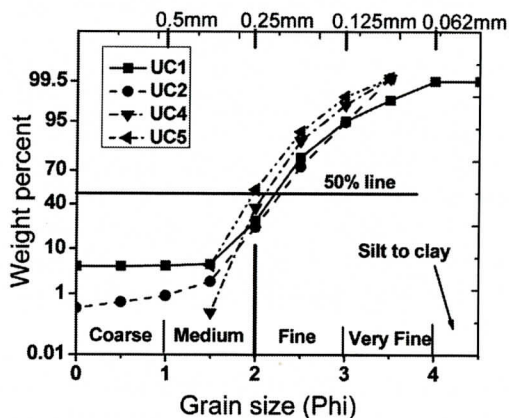
Figure 7. Cumulative weight percent curves (note probability scale) for four samples from the rotasonic core at location 9 (Shelby Farms). Sample UC1 is close to the top of the core, UC5 is close to the bottom.

one bed during drilling. When fines are excluded, the average grain size and grain size distributions in borehole samples are similar to those of outcrop and core samples (Figure 5). The bimodality in some borehole samples is likely a consequence of mixing from more than one sand unit. Some hand specimens have a small mode in the coarse sand range, a probable consequence of varying current strength in traction load.

The only continuous section from the Upper Claiborne is the rotasonic core taken at Shelby Farms (location 9) (Gentry and others, 2006). The top of the core may have included sand facies of the overlying Cook Mountain Formation rather than the Memphis Sand. However, the petrology data are consistent with data for the Memphis Sand from other locations (Table 2). Gentry and others (2006) obtained a mean size of approximately 0.25 mm, essentially the same as our estimates. The tail into the coarse fraction of two samples (Figure 7) suggests a mixed source, possibly the confluence of a tributary and a main channel or the mix of a coarse lag created by wind scouring of exposed sandbars. Grain size is essentially the same from top to bottom in the core (Figure 7) and is consistent with data from other locations.

Using data in table 3 we constructed CM

plots (cross plots of the coarsest one percent versus the median grain size (Passega, 1964), and cross plots of mean, standard deviation, and skewness statistics (Friedman, 1967). Probability-scale cumulative curves were also constructed (Figure 7). The patterns obtained here are consistent with fluvial deposition sandstones.

Petroleum geologists consider porosity of 20 to 25% in sandstone to be very good (Levorsen, 1967). In contrast, hydrologists and foundation engineers routinely anticipate that porosity will be in excess of 30 percent in sand (e.g., Todd, 1980). The different expectations are due to different sand body histories. Petroleum geologists exploit sandstone reservoirs that are very old (commonly hundreds of millions of years), are deeply buried (commonly 3 to 5 km), are lithified, and may have multiple generations of cement and porosity. Hydrologists deal with aquifers that are young in comparison to petroleum aquifers, have seldom been deeply buried, may be partially exposed at the surface, and are unconsolidated. Nevertheless, the large amount of initial and preserved porosity (35% to 50% and 15 to 35% respectively) of the Memphis Sand came as a surprise (Figure 2, Table 2). How was such great porosity formed and preserved?

Memphis Sand porosity at deposition was equal to the porosity of cubic packed spherical grains. Such great porosity occurs in other young sands. For example, Steckler and Watts (1978) used borehole logs of the CostB-2 well on the Atlantic continental shelf to estimate a shallow clastic porosity of 40 to 50%. Bond and Kominz (1984), in their development of quantitative tectonic subsidence curves, assumed initial sandstone porosities of 25 to 40%.

We suggest that the nearly 40% porosity of the Memphis Sand at deposition was a consequence of two factors. The angular grains provided an irregular, open, framework that was partially supported by fluid pressure. Before the grains could collapse into a stable (rhombohedral) packing, secondary kaolinite partially filled the original void spaces thereby preserving much of it. This same matrix prevented formation of quartz overgrowth cement (Pittman

and Lumsden, 1968). In sum, the Memphis Sand is relatively young, has sharply angular grains, is uncompacted, and has no cement; thus it has substantial porosity.

Formation of clay minerals commonly follows a trend from kaolinite in continental environments to smectite or illite in marginal marine and illite in marine environments (Chamley, 1989; Meunier, 2005; Weaver, 1958). Upper Claiborne clay units sampled in the NME transition from kaolinite in northwest Tennessee, through mixed kaolinite-smectite to largely smectite in northwest Mississippi (Jeffers, 1982; Kane, 1982; Hertzing, 1984; Williams, 1980; White, 1985; Moore and others, 2003). We interpret this to be a consequence of a transition in environments from non-marine in Tennessee to marine in the south. This is consistent with the regional change in environments of deposition in the Memphis Sand determined using borehole logs (Hundt, 2008; Larsen and others, 2008 a, b).

CONCLUSIONS

The Memphis Sand in the NME is a friable fine to coarse-grained quartz wacke or quartz arenite; it is well sorted locally. Grain size ranges from coarse sand in the eastern study area to fine sand toward the center of the NME. Polycrystalline quartz grains are abundant along the east margin of the NME where they are associated with traces of kyanite, and zircon. Only traces of quartz cement are present. The weak coherence of the Memphis Sand is due to a secondary matrix that consists of 5% to 20% kaolinite with vadose zone (meniscus) texture. Matrix reduces intergranular porosity that was originally 35% to 50% to present values of 15% to 35%.

The clay mineralogy in overlying fine-grained upper Claiborne Group strata changes from kaolinite in the north of the NME through mixed kaolinite/smectite to smectite dominated south of the 35th parallel.

Our results document the present substantial porosity of the Memphis Sand and its partial occlusion while the sand was still in the vadose zone. Data support a scenario in which the Memphis Sand was deposited in meandering and braided fluvial environments north of the 35 parallel. No evidence suggests regional hydraulic compartmentalization.

ACKNOWLEDGEMENTS

REFERENCES

Ahr, W.M., 1979, Depositional environments of the Claiborne Group: in Kersey, D.G., ed., Claiborne sediments of the Brazos Valley, southeast Texas, Houston Geological Society Guidebook, Houston, Texas, p. 12-13.

Berg, R.R., 1979, Stratigraphy of the Claiborne Group: in Kersey, D.G., ed., Claiborne sediments of the Brazos Valley, southeast Texas, Houston Geological Society Guidebook, Houston, Texas, p. 5-11.

Boggs, S., Jr., 2001, Principles of Sedimentology and Stratigraphy, 3rd ed.: Prentice Hall, Saddle River, New Jersey.

Bond, G.C. and Kominz, M.A., 1984, Construction of tectonic subsidence curves the early Paleozoic miogeocline, southern Canadian Rocky Mountains: Implications for subsidence mechanisms, age of breakup, and crustal thinning: Geological Society of America Bulletin, v. 95, p. 155-173.

Brahana, J.V. and Broshears, R.E., 2001, Hydrogeology and Ground-Water Flow in the Memphis and Fort Pillow Aquifers in the Memphis Area, Tennessee: U.S. Geological Survey Water-Resources Investigations Report 89-4131, 56 p.

Chamley, H., 1989, Clay Sedimentology: Springer-Verlag, Berlin and Heidelberg, 620 p.

Cushing, E.M., Boswell, E.H., and Hosman, R.L., 1964, General Geology of the Mississippi Embayment: U.S. Geological Survey Professional Paper 448-B, 28 p.

Dilcher, D.L., 1973, A paleoclimatic interpretation of the Eocene floras of southeastern North America: in A. Graham ed., Vegetation and vegetational history of

northern Latin America, Elsevier Publishing Co.: Amsterdam, London, New York. p. 39-59.

Dott, R.H., 1964, Wacke, graywacke and matrix – what approach to immature sandstone classification: Journal of Sedimentary Petrology, v. 34, p. 625-632.

Drobnyk, J.W., 1965, Petrology of the Paleocene-Eocene Aquia Formation of Virginia, Maryland, and Delaware: Journal of Sedimentary Research, v. 35, p. 626-642.

Drever, J.I., 1997, The Geochemistry of Natural Waters, Surface and Groundwater Environments: Prentice Hall, North Saddle River, New Jersey, 436 p.

Frederiksen, N.O., Bybell, L.M., Christopher, R.A., Crone, A.J., Edwards, L.E., Gibson, T.G., Hazel, J.E., Repetski, J.E., Russ, D.P., Smith, C.C., and Ward, L.W., 1982, Biostratigraphy and paleoecology of lower Paleozoic, Upper Cretaceous, and lower Tertiary rocks in U.S. Geological Survey New Madrid test wells, Southeastern Missouri: Tulane Studies in Geology and Paleontology, v. 17, no. 2, p. 23-45.

Friedman, G.M., 1967, Dynamic processes and statistical parameters compared for size frequency distribution of beach and river sands: Journal of Sedimentary Petrology, v. 37, p. 327-354.

Galloway, W.E. and Hobday, D.K., 1983, Terrigenous clastic depositional systems: Applications to petroleum, coal, and uranium explorations: Springer-Verlag, New York, 413 p.

Garner, C.B., Larsen, D., Carmichael, J. and Gentry, R., 2003, Hydrostratigraphy of a window through the Upper Claiborne confining unit, Memphis, Tennessee: Geological Society of America Abstracts with Programs, v. 35, no. 1, p. 37.

Gentry, R., McKay, L., Thonnard, N., Anderson, J.L., Larsen, D., Carmichael, J.K. and Solomon, K., 2006, Novel techniques for investigation recharge to the Memphis Aquifer: American Water Works Association, Denver, Colorado, 97 p.

Gordon, J. and Cox, R.T., 2008, Recurrent Mesozoic and Cenozoic Faulting along the Southern Margin of the North American Craton: Geological Society of America Abstracts with Programs, v. 40, no. 6, p. 147- 149.

Graham, D.D. and Parks, W.S., 1986, Potential for leakage among principal aquifers in the Memphis area, Tennessee: USGS Water Resource Investigation 85-4295, 46 p.

Hansen, H.J., 1969, Depositional environment of subsurface Potomac Group in southern Maryland; American Association of Petroleum Geologists Bulletin, v. 53, p. 1923-1937.

Hertzing, J.J., 1984, The Clay Mineralogy of the Claiborne Formation in Henry County, Tennessee: Unpublished MS Thesis, The University of Memphis, 51 p.

Hundt, K. R., 2008, Regional lithostratigraphic study of the Memphis Sand in the Northern Mississippi Embayment: Unpublished MS Thesis, The University of Memphis, 104 p.

Hundt, K.R., Lumsden, D.N., Larsen, D. and Waldron, B., 2008, Lithostratigraphy of the Memphis Sand (Eocene): the Northern Mississippi Embayment: Geological Society of America Abstracts with Programs, v. 40, no. 3, p. 38

Jeffers, W.L., 1982, The Clay Mineralogy of the Claiborne Formation in West Tennessee: Unpublished MS Thesis, The University of Memphis, 36 p.

Kane, D.G., 1982, The Clay Mineralogy of the Zilpha Formation in Panola County, Mississippi: Unpublished MS Thesis, The University of Memphis, 50 p.

Larsen, D., Hundt, K., Owen, A., Waldron, B., Van Arsdale, R., Lumsden, David N. and Csontos, R., 2008a, Hydrostratigraphic Relationships of the Wilcox and Claiborne Group in Northwestern Mississippi and Western Tennessee: Journal of the Mississippi Academy of Sciences, v. 53, no. 1, p. 65.

Larsen, D., Hundt, K., Waldron, B., Van Arsdale, R., Lumsden, D.N. and Csontos, R., 2008b, Detailed hydrostratigraphy of the Wilcox and Claiborne Group in northeastern Arkansas, northwestern Mississippi, and western Tennessee: Abstract Book,2008 Ground Water Summit, National Ground Water Association Press, Westerville, Ohio, p. 132-133.

Levorsen, A.I., 1967, Geology of Petroleum, W.H. Freeman and Company, 724 p.

Lumsden, D.N., Hundt, K.R., Larsen, D. and Waldron, B., 2008, Petrology Of The Memphis Sand (Eocene): the Northern Mississippi Embayment: Geological Society of America Abstracts with Programs, v. 40, n. 3, p. 9.

McFarland, E.R. and Bruce, T.S., 2006, The Virginia Coastal Plain Hydrogeologic Framework: U.S. Geological Survey Professional Paper 1731, 118 p.

Marcher, M.V. and Stearns, R.G., 1962, Tuscaloosa Formation in Tennessee: Geological Society of America Bulletin, v. 73, p. 1365-1386.

Mancini, E.A., and Tew, B.H., 1991, Relationships of Paleogene stage and planktonic foraminiferal zone boundaries to lithostratigraphic and allostratigraphic contacts in the eastern Gulf Coast Plain: Journal of Foraminiferal Research, v. 21, p. 48-66.

Moore, G.K. and Brown, D.L., 1969, Stratigraphy of the Fort Pillow test well, Lauderdale County, Tennessee: Tennessee Division of Geology Report of Investigations 26, 1 sheet.

Meunier, A., 2005, Clays: Berlin and Heidelberg, Springer, 472 p.

Nanz, R.H., 1954, Genesis of Oligocene sandstone reservoir, Seeligson Field, Jim Wells and Kleberg Counties, Texas; American Association of Petroleum Geologists Bulletin, v. 38, p. 96 - 119.

Onellion, F.E., 1956, Geology and ground water resources of Drew County, Arkansas: Arkansas Geological and Conservation Commission, Water Resources Circular 4, 43 p.

Parks, W.S. and Carmichael, J.K., 1990, Geology and ground-water resources of the Memphis Sand in Western Tennessee: U.S. Geological Survey Water Resources Investigation Report 88-4182, 30 p.

Passega, R., 1964, Grain size representation by CM patterns as a geological tool: Journal of Sedimentary Petrology, v. 34, p. 830-874.

Pettijohn, F.J., 1975, Sedimentary Rocks, 3rd ed.; Harper and Row, New York, 628 p.

Prior, W.L., Clardy, B.F. and Baber, Q.M., 1985, Arkansas lignite investigations: Arkansas Geological Commission Information Circular 28-C, 214 p.

Pittman, E.C. and Lumsden, D.N., 1968, Relationship between chlorite coatings of quartz grains and porosity, Spiro Sand, Oklahoma: Journal of Sedimentary Petrology, v. 38, p. 668-670.

Russell, E.E. and Parks, W.S., 1975, Stratigraphy and outcropping Upper Cretaceous, Paleocene, and Lower Eocene in Western Tennessee (including descriptions of younger fluvial deposits), State of Tennessee Department of Conservation, Division of Geology, Bulletin 75, 37 p.

Salvador, A., 1991, Origin and development of the Gulf of Mexico basin: in A. Salvador, (ed.), The Gulf of Mexico Basin: Geological Society of America, The Geology of North America, Vol. J, p. 389-444.

Sawyer, D.S., Buffer, R.T., and Pilger, R.H. 1991, The crust under the Gulf of Mexico basin: in A. Salvador (ed.), The Gulf of Mexico Basin: Geological Society of America, The Geology of North America, v. J, p. 53-72.

Stearns, R.G., 1957, Cretaceous, Paleocene, and Lower Eocene geologic history of the northern Mississippi Embayment: Geological Society of America Bulletin, v. 68, p. 1077-1100.

Stearns, R.G. and Marcher, M.V., 1962, Late Cretaceous and subsequent structural developments of the northern Mississippi Embayment area: Geological Society of America Bulletin, v. 73, p. 1387-1394.

Stearns, R.G. and Reesman, A.L., 1986, Cambrian to Holocene structural and burial history of Nashville Dome: American Association of Petroleum Geologists Bulletin, v. 70, p. 143-154.

Steckler, M.S. and Watts, A.B., 1978, Subsidence of the Atlantic-type continental margin off New York: Earth and Planetary Science Letters, v. 41, p. 1-13.

Thomas, W. A. 2006, Tectonic inheritance at a continental margin: GSA Today, v.16, p. 4-11.

Thomas, W. A., 1989, The Appalachian-Ouachita Orogen beneath the Gulf Coastal Plain between the outcrops in the Appalachian and Ouachita Mountains, in Hatcher, R. D., Jr., Thomas, W. A., and Viele, G.W., eds., The Appalachian-Ouachita Orogen in the United States: Boulder, Colorado, Geological Society of America, the Geology of North America, v. F-2.

Todd, D.K., 1980, Groundwater Hydrology, John Wiley and Sons Inc.

Weaver, C.E., 1958, The Origin and significance of clay minerals in sedimentary rocks: American Association of Petroleum Geologists Bulletin, v. 42, p. 254-271.

White, M.D., 1985, The Clay Mineralogy of the Claiborne Formation in Carroll and Weakley Counties, Tennessee: Unpublished MS Thesis, The University of Memphis, 44 p.

Wilbert, L.J., 1953, The Jacksonian Stage in Southeastern Arkansas: Arkansas Resource and Development Commission, Division of Geology, Bulletin 19, 125 p.

Williams, D.A., 1980, Geology and Paleoenvironment of the Zilpha Formation in North Central Mississippi: Unpublished MS Thesis, The University of Memphis, 51 p.

Williamson, D.R., 2006, An investigation of the Tertiary lignites of Mississippi: in Red Hills Mine Field Trip, Association of Environmental and Engineering Geologists, PO Box 22742, Jackson, Mississippi, 35 p.

Wilson, M.D. and Pittman, E.D., 1977, Authigenic clays in sandstones: Recognition and influence on reservoir properties and paleoenvironmental analysis: Journal of Sedimentary Petrology, v. 47, p. 3-31

Wing, S.L., Gingerich, P.D., Schmitz, B. and Thomas. E., 2003, Causes and consequences of globally warm climates in the Early Paleogene: Geological Society of America Special Paper 369.

Zachos, J.C., Pagani, M., Sloan, L.C., Thomas, E. and Billups, K., 2001, Trends, rhythms and aberrations in global climate 65 Ma to present: Science, v. 292, p. 686-693.

Geochemical Constraints on the Origin of Chloritoid-bearing Kyanite Quartzite at Hagers Mountain, North Carolina

Brent E. Owens and Shelbi E. Wilson

Department of Geology
College of William and Mary
Williamsburg, VA 23187

ABSTRACT

A distinctive chloritoid-bearing kyanite quartzite occurs at Hagers Mountain, North Carolina, within the Hyco Formation of the Carolina terrane. Apart from the presence of chloritoid, rocks here are similar to occurrences in Virginia, including Willis Mountain (the site of the only active kyanite mine in the United States). Based on geochemical evidence, we interpret the rocks at Hagers Mountain to represent metamorphosed hydrothermally altered Si-rich volcaniclastic rocks. Extent of alteration increases from quartz-sericite schist → chloritoid-sericite quartzite → kyanite-chloritoid quartzite → kyanite quartzite. Kyanite quartzites (without chloritoid) represent the most intensely altered protoliths, an interpretation supported by unusual U-shaped rare earth element patterns (a feature shared with the Virginia occurrences). Evaluation of mass losses indicates slight (~3%) to extensive (~32%) leaching of various elements. Our interpretations of precursor mineralogy in order of increasing degree of alteration are: 1) quartz + sericite; 2) quartz + sericite + chlorite; 3) quartz + kaolinite + chlorite; and 4) quartz + kaolinite. Such mineral assemblages are typical of advanced argillic (high-sulfidation) alteration. Hagers Mountain rocks are similar to other examples of quartz-rich rocks that also contain chloritoid plus an aluminosilicate mineral. Such rocks are commonly associated either with volcanic hosted massive sulfide deposits or epithermal gold deposits, but have in common severe leaching of all mobile constituents in hot, acidic fluids prior to metamorphism.

INTRODUCTION

Almost 50 years ago, Espenshade and Potter (1960) provided an extensive review of andalusite, kyanite, and sillimanite deposits in the southeastern United States, reporting on aspects of their field relations, mineralogy, and possible modes of formation. Their compilation included descriptions of nearly 40 occurrences, most in the Piedmont physiographic province (Fig. 1). Although known for many years, few occurrences have been described beyond the mapping and petrography stage. Recent interpretations of other highly aluminous rocks (pyrophyllite- rather than aluminosilicate-bearing in many cases) associated with gold deposits in the southeastern U.S. invoke reaction of acidic, hydrothermal fluids on volcanic rocks to produce Al- and Si-rich protoliths (Carpenter and Allard, 1982; Feiss, 1985; Schmidt, 1985; Schreyer, 1987; Klein and Criss, 1988; Ririe, 1990). Despite some consensus of interpretation, documentation and evaluation of the specific geochemical characteristics of this alteration have not been presented for most such areas.

Owens and Pasek (2007) recently reported on the mineralogy and geochemistry of numerous examples of kyanite quartzite in Virginia, including the deposit at Willis Mountain (Fig. 1). Willis Mountain is the site of the only active kyanite mine in the United States, with combined production of kyanite and mullite estimated at ~130,000 metric tons annually (USGS Mineral Commodity Summary, 2009). Previous investigations, particularly at Willis Mountain, suggested that these quartzites were derived from aluminous sedimentary rocks (Conley and Marr, 1980). However, Owens and Dickerson (2001) and Owens and Pasek (2007) argued on
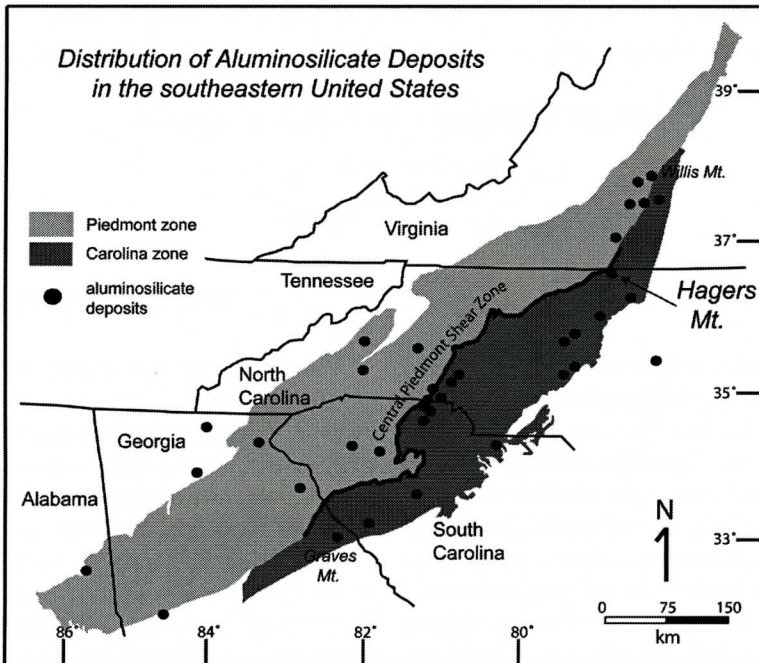
Figure 1. Distribution of aluminosilicate mineral deposits in the Piedmont and Carolina zones of the southeastern United States. Locations of the Willis Mountain, VA, Hagers Mountain, NC and Graves Mountain, GA are indicated. Modified from Espenshade and Potter (1960) and Hibbard and Samson (1995).

mineralogical and geochemical grounds for igneous protoliths that had been severely altered in a high-sulfidation (advanced argillic) hydrothermal setting, resulting in essentially quartz + kaolinite precursors.

The study of Owens and Pasek (2007) was regional in nature, and included data for only a few samples from each of the investigated localities. In this paper, we present a more detailed geochemical investigation of a single occurrence, including associated rocks, located at Hagers Mountain, North Carolina (Fig. 1). Although similar to occurrences in Virginia, some rocks at Hagers Mountain contain chloritoid, a mineralogical contrast to rocks in Virginia that in part prompted this study.

Most of the Virginia rocks occur within the middle Ordovician Chopawamsic (or correlative Milton) terrane (Coler et al., 2000) and are therefore younger than rocks in the Neoproterozoic to Cambrian Carolina terrane where Hagers Mountain is located. In addition, metamorphic grade reached as high as mid-am-

phibolite facies in the Chopawamsic terrane, but only greenschist grade across much of the Carolina terrane (e.g., Butler and Secor, 1991). Despite these contrasts, the overall mineralogical similarities suggest that the Virginia occurrences provide a useful framework for evaluation of the origin of the Hagers Mountain quartzites. The purposes of this study are to: 1) assess whether our Virginia model of hydrothermal alteration might apply at Hagers Mountain; and 2) evaluate more quantitatively chemical changes (mass gains and losses) during alteration by analyzing a more varied set of samples.

GEOLOGIC SETTING

Hagers Mountain (Fig. 1) occurs near the western margin of the Carolina zone of Hibbard and Samson (1995), as well as the Carolina terrane sensu-stricto (e.g., Horton et al., 1989). The Carolina zone consists of several distinct, predominantly metaigneous terranes that have
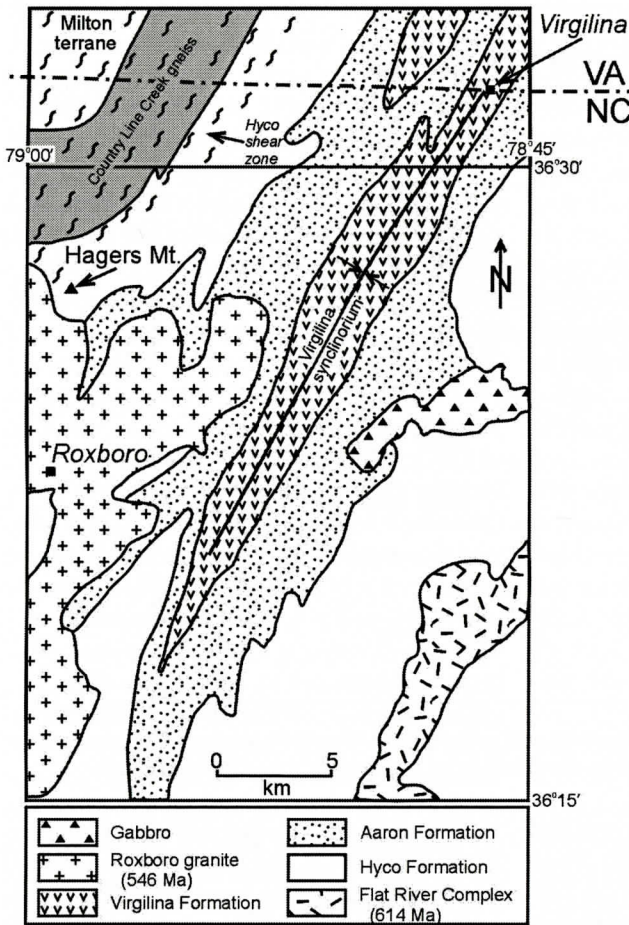
Figure 2. Geologic map of the Virgilina-Roxboro area showing the location of Hagers Mountain. Modified from Harris and Glover (1985) with additions based on Hibbard et al. (2006).

in common an exotic origin with respect to Laurentia (Hibbard and Samson, 1995). The location is also on the easternmost fringe of the Hyco shear zone (Fig. 2), which represents a tectonic boundary between the Carolina and Milton terranes and is a component of the larger Central Piedmont suture (Hibbard et al., 1998). Earlier geologic maps (e.g., Harris and Glover, 1985; Butler and Secor, 1991) place the Carolina-Milton (or Charlotte) boundary at the western margin of the Hyco Formation. However, Hibbard et al. (1998) recognized a distinct unit here termed the Country Line Creek gneiss (or complex), which they argued is part of the Carolina terrane. Regardless of these complications, proximity to the Hyco shear zone may have some bearing on rock textures at Hagers Mountain, as described in the Mineralogy section below.

Hagers Mountain occurs within the Hyco Formation of the Carolina terrane, along the westernmost periphery of the Virgilina district of southern Virginia and northern North Carolina (Laney, 1917; Glover and Sinha, 1973). Copper was produced extensively in the Virgilina district from 1890 until 1916 (Johnson et al., 1989), primarily from quartz veins in greenstones of the Virgilina Formation (Fig. 2). The district also contains several abandoned gold mines and prospects, including one located about 2 km north of Hagers Mountain (Lesure, 1993).

The Hyco Formation was originally called the Hyco Quartz Porphyry by Laney (1917), based on his interpretation that many of the rocks represent metamorphosed felsic lavas. Subsequent investigations by Glover and Sinha (1973), Hadley (1973) and Kreisa (1980)

137
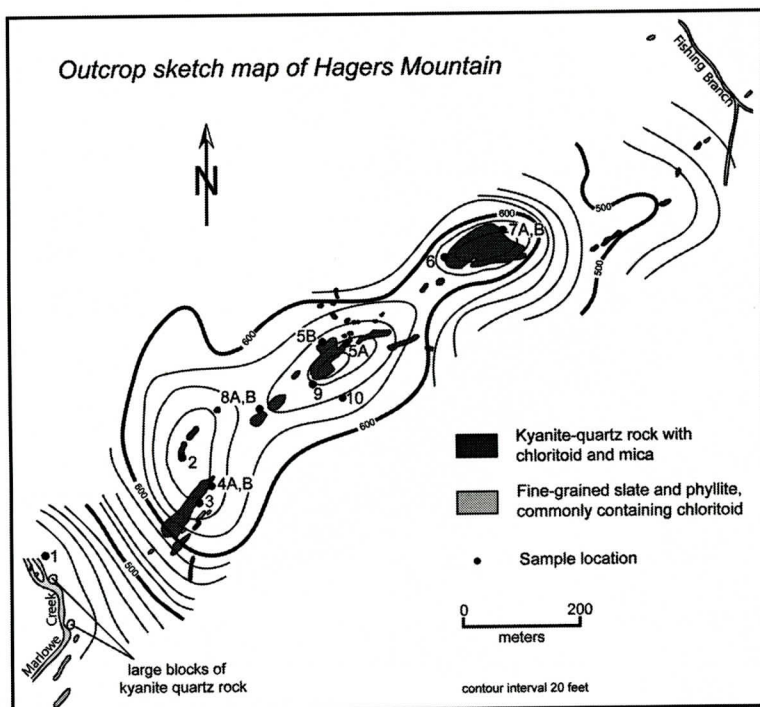
Figure 3. Sketch map of outcrop locations on and near Hagers Mountain and sample locations of this study. HM06 prefix omitted for clarity. Modified from Espenshade and Potter (1960).

showed a more diverse range of rock types that in many cases were of pyroclastic origin. Thus, Kreisa (1980) renamed the unit the Hyco Formation. The formation primarily consists of metamorphosed crystal- and crystal-lithic tuffs, now largely converted to quartz-feldspar-sericite schists. Metamorphic grade is primarily in the greenschist facies. Relict pyroclastic textures are well-preserved east of the study area, but the degree of deformation and recrystallization increases to the west such that volcanic features are no longer recognizable. Wortman et al. (2000) reported U-Pb zircon ages of 616 ± 3 and 620 ± 4 Ma for two crystal tuffs in the western part of the Hyco Formation.

PREVIOUS WORK

Stuckey (1932) showed the Hagers Mountain locality on a map illustrating kyanite deposits in North Carolina, but provided no information about the occurrence. He later reported both kyanite and pyrophyllite in quartz veins that cut "schistose acid tuff" on a cliff face (Stuckey, 1935). Espenshade and Potter (1960) included Hagers Mountain in their compilation of aluminosilicate deposits in the southeastern U.S. (Fig. 1), and their report provides the only previous detailed description of this locality. In addition to quartz and kyanite, Espenshade and Potter (1960) identified variable amounts of chloritoid, white mica (muscovite and paragonite, but not pyrophyllite), rutile, ilmenite(?), chlorite, and zircon. Based on field relations and mineralogy, Espenshade and Potter (1960) suggested two possible protoliths for these rocks: 1) quartz-rich sediments; or 2) hydrothermally altered volcanic rocks. They noted that the fine-grained nature of the quartz is similar to quartz textures in pyrophyllite deposits of hydrothermal origin found farther south, and thus favored a hydrothermally altered volcanic protolith.

Lesure (1993) reported semiquantitative trace element data for numerous samples across the region, focusing primarily on the Virgilina

district to the east. His study included about a dozen rock samples from the vicinity of Hagers Mountain, as well as three stream sediment samples from Fishing Branch (Fig. 3) at the north end of the mountain. Five of the rock samples contained trace amounts of Au (0.02 to 0.04 ppm), and similar amounts were found in the stream sediment samples.

In their investigation of Virginia kyanite quartzites, Owens and Pasek (2007) argued for hydrothermally altered protoliths based on both mineralogical and geochemical evidence. The mineralogy of all Virginia rocks is dominated by quartz and kyanite, with accessory white mica and rutile. In addition, pyrite, topaz, and lazulite occur locally. This mineralogy suggests protoliths dominated by quartz and kaolinite (± pyrophyllite), with rutile reflecting breakdown of pre-existing Ti-bearing oxides or silicates. Concentrations of CaO, MgO, K_2O, Na_2O, and many trace elements (Ga in particular) are typically below the limits of detection, reflecting severe leaching of all soluble elements. Finally, chondrite-normalized rare earth element (REE) patterns show unusual shapes, with relative depletions in the middle- to heavy-REE. Such U-shaped patterns occur in other examples of hydrothermally altered rocks in advanced argillic (high-sulfidation) settings (e.g., Huston, 2001). Owens and Pasek (2007) argued that low pH, sulfate-bearing fluids are the best candidates for complexation and mobility of the REE. Owens and Pasek (2007) further suggested that these pattern shapes resulted from initial destruction of REE-bearing phases (primarily phosphates), followed by preferential retention of the light-REE in newly precipitated phosphates, while the heaviest-REE were retained in zircon.

METHODS

We collected 14 hand samples, including three of associated sericite schist, from exposures near the base and along Hagers Mountain (Figure 3). The remaining 11 samples are kyanite quartzite (± chloritoid), and a single example of quartz-chloritoid-sericite rock. Nine samples were selected for whole-rock chemical analysis. Approximately 500 g portions of each sample

were ground to a fine powder prior to analysis using methods similar to those described by Dymek and Owens (2001). Samples were analyzed for whole-rock major element oxides and trace elements by X-ray fluorescence (XRF) at Washington University in St. Louis, using techniques described by Couture et al. (1993) and Couture and Dymek (1996). The rare earth elements (REE) and selected other trace elements were determined by inductively coupled plasma – mass spectrometry (ICP-MS) methods by Activation Laboratories, Ltd., Ontario. The method involves a lithium metaborate and/or tetraborate fusion of the sample prior to digestion, to ensure dissolution of resistate phases. The agreement between XRF and ICP-MS methods for elements that were analyzed by both techniques is excellent. Trace element values reported here include V, Co, Ni, Zn, Ga, Rb, Sr, Y, Nb, Ba, and Pb (by XRF), and the REE, Cr, Zr, Cu, Ge, Sn, Sb, Cs, Hf, Ta, W, Tl, Th, and U (by ICP-MS). The ICP-MS values for Zr were chosen to ensure that Zr and Hf were determined on the same sample aliquot, and the ICP-MS values yield more consistent Zr/Hf values for the sample set as a whole. Values for some trace elements (As, Mo, Ag, In, Bi) determined by ICP-MS that are below the limits of detection are not reported.

FIELD OBSERVATIONS

Hagers Mountain forms a rugged ridge about one km long that rises about 50 meters above its surroundings (Figure 3). Exposure is extensive along the main part of the ridge, with most outcrops consisting of quartz-rich rock. Surrounding rocks are primarily fine-grained, white to gray sericite schists. Typical fresh kyanite quartzite is fine-grained and remarkably white in color, and the white color of the kyanite makes it difficult to recognize in hand sample. This uncommon kyanite color is a feature these rocks share with many occurrences in Virginia, and probably reflects a very low Fe-content (Owens and Dickerson, 2001). Espenshade and Potter (1960) estimated that some rocks contain up to 30% kyanite, but also noted that many rocks contain much less. Chloritoid can locally

Table 1. Estimated modal mineralogy of chemically analyzed samples (based on a single thin section for each)

Sample	HM06-2	HM06-6	HM06-8B	HM06-3	HM06-4A	HM06-5A	HM06-5B	HM06-7B	HM06-10
Rock type	KQ	KQ	KQ	KQ	KQ	KQ	KQ	CSQ	QSS
quartz	75	80	60	56	70	70	70	88	50
kyanite	24	20	40	40	25	30	29	--	--
chloritoid	--	--	--	2	2	tr	1	2	--
white mica	--	--	tr	1	tr	tr	tr	10	48
opaques	1	tr	--	1	1	tr	tr	--	2
rutile	tr	--	tr	--	tr	tr	tr	tr	--
zircon	tr	tr	tr	tr	tr	tr	tr	tr	tr

* Rock type abbreviations: KQ (kyanite quartzite); CSQ (chloritoid-sericite quartzite); QSS (quartz-sericite schist) tr = trace amount

be recognized in hand sample as small (≤ 0.2 mm across) dark green grains. One area (near our sample locations HM06-8A and 8B) consists of highly iron-stained kyanite quartzite that is somewhat vuggy. Sample HM06-7A from the northeast portion of the ridge is brecciated, a feature also noted locally by Espenshade and Potter (1960). Quartz veins ranging from a few cms to a meter in thickness occur throughout the ridge. Stuckey (1935) and Espenshade and Potter (1960) reported one quartz vein that also contains kyanite crystals oriented perpendicular to the edge of the vein.

MINERALOGY

The rocks at Hagers Mountain can be roughly grouped into three rock types, including kyanite ± chloritoid quartzite, chloritoid-sericite quartzite, and quartz-sericite schist. We use the term sericite here to refer to all varieties of fine-grained white mica, recognizing that muscovite and paragonite are probably both present. Estimated modes for the chemically analyzed samples are listed in Table 1, although these are based on only one thin section for each sample. Thus, these modes are not necessarily representative of the bulk sample that was analyzed, but do provide some indication of overall mineralogy.

Quartz is the dominant mineral in all sam-

ples. It is typically fine-grained and polygonal, ranging from 0.01 to 0.1 mm across. In the kyanite quartzites, kyanite ranges in texture from typical bladed, elongate grains (locally with abundant quartz inclusions) to highly irregularly-shaped masses of fine-grained kyanite and quartz. In some cases, larger bladed grains are partially to completely surrounded by these aggregates of kyanite and quartz, reflecting some degree of recrystallization as a consequence of deformation (Fig. 4A). These textures and grain sizes for quartz and kyanite contrast strongly with occurrences in Virginia, which contain blocky kyanite (up to 4 cm long) and much larger (up to 10 mm across) quartz grains. These textural contrasts may be due to the location of Hagers Mountain on the fringes of the Hyco Shear Zone (Fig. 2).

In kyanite quartzites with chloritoid (HM06-3, HM06-4A, HM06-5A, HM06-5B), the chloritoid typically forms small (<0.04 to 0.1 mm across) stubby to equant grains that are weakly pleochroic from pale yellow to pale greenish blue. Chloritoid occurs both in contact with kyanite and as isolated grains (Fig. 4B). In the chloritoid-sericite quartzite, chloritoid forms slightly larger grains, but these also are somewhat ragged around the edges. Chloritoid is not abundant in any sample, ranging from trace amounts only up to a few percent (Table 1).

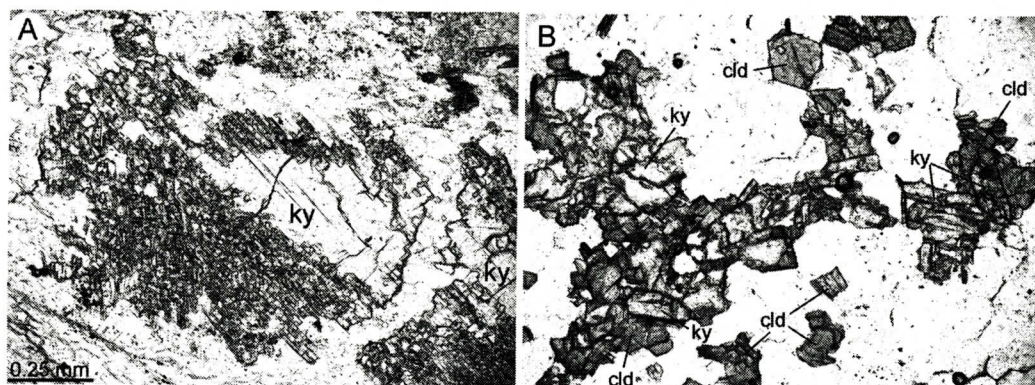Sericite (or larger grains of white mica) is on-

Figure 4. Photomicrographs of textures in Hagers Mountain kyanite quartzites, both in plane-polarized light. (A) Kyanite (ky) grain partially surrounded by a fine-grained aggregate of kyanite and quartz (sample HM06-8B). (B) Small grains of kyanite and chloritoid (cld) in sample HM06-5B. Scale in both photomicrographs is the same.

ly present in significant amounts in the chloritoid-sericite quartzite (HM06-7B) and quartz-sericite schists (HM06-1, HM06-9, HM06-10). The mica forms small individual flakes <0.01 up to 0.1 mm long or in multi-grain clusters.

Opaque grains occur in trace to minor amounts in most samples, locally decorating quartz grain boundaries. We have not evaluated these grains in reflected light, but suspect that most are hematite given that none of the samples are magnetic and there is no correlation between Fe and Ti content in the whole-rock data (which would indicate ilmenite). Rutile is a common accessory positively identified in more than half of the samples, including quartz-sericite schist (HM06-9) and chloritoid-sericite quartzite (HM06-7B). It typically occurs as small (<0.01 to 0.4 mm across) isolated grains. Trace amounts of zircon occur in most samples.

WHOLE-ROCK COMPOSITIONS

Nine samples (seven kyanite quartzites, one chloritoid-sericite quartzite, and one quartz-sericite schist) were analyzed for major and trace elements, and results are listed in Table 2. Also included for comparison in Table 2 are three previously published major element analyses of metarhyolites from the Hyco Formation (Laney, 1917; Kreisa, 1980). All three sample locations are in Virginia, approximately 15 km northeast of Hagers Mountain.

Major Elements

All kyanite ($\pm$ chloritoid) quartzites are dominated by SiO_2 (72-82 wt%) and Al_2O_3 (14-27 wt.%), the two oxides together accounting for 95-99% of the major element totals. Concentrations of $Fe_2O_3(T)$ are variable, but crudely correlate with the amount of chloritoid ($\pm$ hematite). For example, the lowest-iron samples HM06-2 and HM06-6 lack chloritoid, but chloritoid is most abundant in higher-iron samples HM06-3 and HM06-4A. Concentrations of TiO_2 range from 0.34 to 0.65 wt%, and probably reflect variable amounts of rutile. Concentrations of all other oxides are low, below the limits of detection in many cases. Where detectable, Na_2O and K_2O are probably present in minor amounts of white mica.

Although the chloritoid-sericite quartzite and quartz-sericite schist are also dominated by SiO_2 and Al_2O_3, they differ from kyanite quartzites in containing higher Na_2O (1.3-1.6 wt%) and K_2O (1.0-2.2 wt%), consistent with greater amounts of white mica. Amounts of $Fe_2O_3(T)$ reflect the presence of chloritoid in HM06-7B and probable hematite in HM06-10. The major element compositions of these two samples are similar to those of Hyco Formation rhyolites (Table 2), but differ in containing slightly less K_2O and Na_2O, as well as negligible MgO and CaO.

Owens and Pasek (2007) showed that the

Table 2. Whole-rock major and trace element compositions of Hagers Mt. samples, and major element compositions of three metarhyolite samples of the Hyco Formation (HF) from Laney (1917) and Kreisa (1980). [major elements in wt.%, trace elements in ppm; bd = below detection limit; nd = not determined; rock type abbreviations as in Table 1.]

Sample	HM06-2	HM06-6	HM06-8B	HM06-3	HM06-4A	HM06-5A	HM06-5B	HM06-7B	HM06-10	Laney	Kreisa, 1	Kreisa, 2
Rocktype	KQ	KQ	KQ	KQ	KQ	KQ	KQ	CSQ	QSS	HF	HF	HF
SiO$_2$	79.36	79.95	76.30	71.64	80.98	81.80	70.87	79.06	77.50	77.78	73.16	73.42
TiO$_2$	0.34	0.34	0.46	0.52	0.34	0.43	0.65	0.47	0.34	0.28	0.40	0.27
Al$_2$O$_3$	19.44	17.76	21.35	24.64	13.95	16.71	27.35	13.89	14.50	12.78	13.42	13.97
Fe$_2$O$_3$(T)	0.02	0.06	0.34	2.02	3.26	0.23	0.35	1.56	2.34	2.43	2.19	2.06
MnO	0.01	bd	bd	0.01	bd	bd	0.01	0.06	bd	trace	0.06	0.06
MgO	bd	bd	0.01	0.01	bd	bd	bd	bd	bd	0.77	0.53	0.51
CaO	bd	bd	bd	0.01	bd	bd	bd	0.15	0.04	0.24	1.67	0.64
Na$_2$O	bd	bd	0.30	0.21	bd	0.20	bd	1.58	1.30	0.54	2.40	3.10
K$_2$O	0.10	bd	0.15	0.16	0.05	0.06	bd	1.02	2.20	3.63	3.06	3.53
P$_2$O$_5$	0.06	0.18	0.10	0.63	0.05	0.04	0.02	0.01	0.02	0.66	nd	nd
LOI	0.50	0.19	0.46	0.63	1.04	0.31	0.86	1.75	1.83	1.66	3.11	2.46
Total	99.67	99.20	99.46	100.48	99.66	99.74	99.91	99.50	100.30	100.74	100.00	100.02
V	<7	10.2	5.4	23.4	16.5	14.3	30.6	24.3	16.7			
Cr	<20	<20	<20	<20	<20	<20	<20	<20	<20			
Co	<1	<5	<5	<8	<5	<8	<5	<4	<5			
Ni	<7	<7	<4	<6	<5	<6	<7	<8	<7			
Cu	<10	10	<10	<10	<10	<10	<10	<10	<10			
Zn	<2	<2	<2	13.3	9.3	<2	<2	2	<3			
Ga	11.7	19.6	23.1	20.5	15.6	23.5	31.4	17.9	15.9			
Ge	0.9	1.4	0.6	0.9	0.6	0.6	0.8	1	0.6			
Rb	<3	<2	3.4	9.2	<3	<2	<2	24.4	53.3			
Sr	<3	3	21.7	3.9	10.6	19.5	4.7	219.1	195.4			
Y	22.3	17.1	41.2	28.8	65.7	10.6	13.2	27.1	34.3			
Zr	326	338	378	383	264	323	370	302	255			

| Sample	HM06-2	HM06-6	HM06-8B	HM06-3	HM06-4A	HM06-5A	HM06-5B	HM06-7B	HM06-10	Laney	Kreisa, 1	Kreisa, 2
Rocktype	KQ	KQ	KQ	KQ	KQ	KQ	KQ	CSQ	QSS	HF	HF	HF
Nb	14.5	15.4	16.6	17.7	11.1	15.8	22.5	12.6	11.9			
Ba	<22	<25	83.1	34.4	74.1	170	<21	1036.1	2013			
Cs	0.1	<0.1	0.1	<0.1	<0.1	<0.1	<0.1	0.9	1.3			
Sn	1	2	2	2	<1	<1	2	2	1			
Sb	2.3	2.5	2	4	2.9	5.4	2	3.4	4.5			
La	59.1	16.7	164	13.3	33	37	46.1	42.8	16.5			
Ce	114	30.5	293	30.9	63.2	81.1	94.2	85.5	43.9			
Pr	11.1	2.91	19.7	3.27	6.51	8.75	9.72	8.93	5.04			
Nd	28.1	8.91	33	12.3	24.5	27	27.7	28.8	19.5			
Sm	3.53	1.66	3.95	2.83	5.25	5.11	4.38	5.61	4.65			
Eu	0.744	0.366	1.09	0.591	1.51	0.726	0.642	0.973	0.917			
Gd	2.42	1.65	2.03	3.7	7.22	3.07	2.57	4.55	4.53			
Tb	0.48	0.4	0.59	0.75	1.52	0.37	0.38	0.78	0.95			
Dy	3.54	3.15	5.52	4.89	10.2	1.98	2.13	4.65	6.31			
Ho	0.9	0.75	1.51	1.11	2.28	0.42	0.47	0.97	1.38			
Er	3.27	2.59	5.68	3.79	7.3	1.44	1.69	3.11	4.41			
Tm	0.59	0.466	0.984	0.639	1.12	0.253	0.297	0.49	0.716			
Yb	4.35	3.45	7	4.32	7.35	1.88	2.21	3.23	4.81			
Lu	0.7	0.562	1.12	0.701	1.14	0.325	0.38	0.509	0.74			
Hf	8.2	8.7	9.7	10	6.8	8.5	9.6	7.6	6.5			
Ta	1	0.97	1.14	1.36	0.84	1.11	1.41	0.88	0.85			
W	2.1	3.5	1.9	1.9	1.4	1.5	2	1.2	<0.5			
Tl	<0.05	<0.05	<0.05	<0.05	<0.05	<0.05	<0.05	0.27	0.41			
Pb	<6	<5	<5	<5	<5	<5	<5	4.7	17.3			
Th	15.6	16.6	17.7	10.2	9.37	12.3	11.7	9.52	9.43			
U	3.6	4.56	3.2	3.03	2.24	2.43	2.66	2.5	1.93			
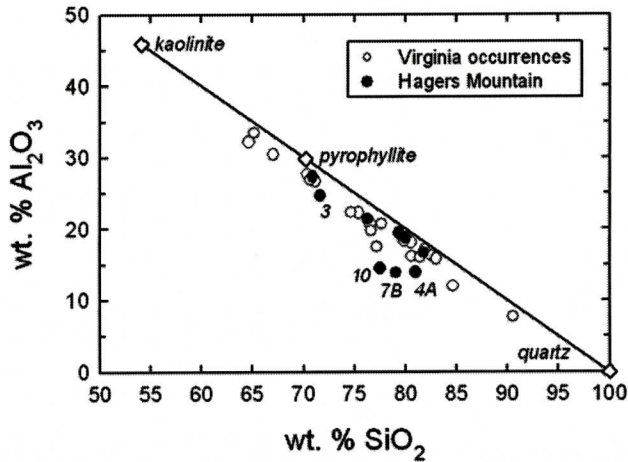
Figure 5. A plot of wt.% SiO_2 vs. wt.% Al_2O_3 in whole-rock samples of this study (black symbols). Open circles are the compositions of occurrences from Virginia (Owens and Pasek, 2007). Samples that plot further away from the quartz-kaolinite line are labeled. Included for reference are the compositions of quartz, pyrophyllite, and kaolinite (plotted on an anhydrous basis).

compositions of most kyanite quartzites in Virginia form a linear array when plotted on a graph of wt% SiO_2 vs. wt% Al_2O_3, and that this array closely parallels a line connecting the compositions of quartz, pyrophyllite, and kaolinite. Figure 5 shows a similar plot for Hagers Mountain samples, and includes the Virginia occurrences for comparison. Samples with higher Fe_2O_3(T) or alkalis are more displaced from the line, but overall the Hagers Mountain rocks yield an array similar to the Virginia samples.

Trace Elements

Rb, Ba, Sr

Concentrations of these elements are extremely low to modest in all kyanite quartzites (Rb <10 ppm, Ba <170 ppm, Sr <20 ppm), but significantly higher in chloritoid-sericite quartzite and quartz-sericite schist. Higher concentrations in the quartz-sericite schist correlate with higher alkalis, implying that these elements reside primarily in white mica.

Cr, Ni, Co, Zn, Cu

None of these ferromagnesian trace elements are present in concentrations above the limits of detection in any of the samples, with the exception of slightly higher Zn (9-13 ppm) in kyanite quartzite samples HM06-3 and HM06-4A.

Sn, V, Nb, Ta

Tin concentrations are uniformly low (<2 ppm) in all samples. Levels of V, Nb, and Ta are also low, but show a crude correlation with TiO_2, suggesting that these elements are primarily in rutile or an Fe-Ti oxide. Niobium and Ta are well-correlated, yielding an average Nb/Ta value of 14.4, slightly higher than the average upper crustal value ~11 (Taylor and McLennan, 1985).

Zr, Hf, Pb

Concentrations of Zr range from 255 to 383 ppm and correlate well with Hf concentrations (6.5-10 ppm). The average Zr/Hf value for the sample set is 39, again slightly higher than the upper crustal value of 33 (Taylor and McLennan, 1985). Concentrations of Pb are below detection limits in the kyanite quartzites, and only slightly higher (5-17 ppm) in chloritoid-sericite quartzite and quartz-sericite schist.

Ga

Owens and Pasek (2007) reported anomalously low Ga (below detection limits in some cases) in many kyanite quartzites from Virginia,
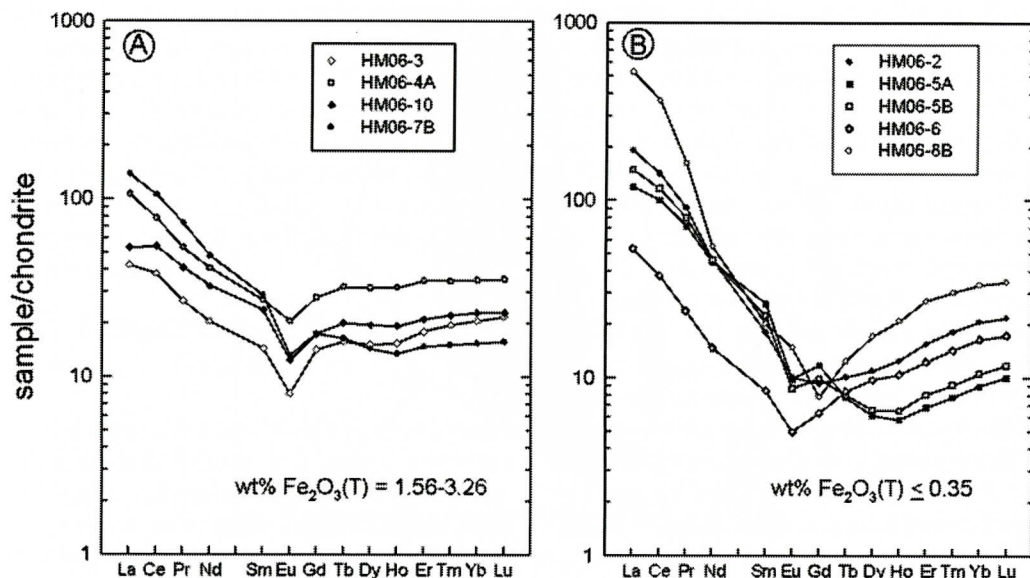
Figure 6. Chondrite-normalized concentrations of the rare earth elements (REE) in whole-rock samples of this study. Chondrite values from Boynton (1984). (A) Samples that contain higher amounts of Fe, which have similar light-REE-enriched patterns, prominent negative Eu-anomalies, and flat heavy-REE patterns. (B) Samples with negligible Fe, which have steeper light-REE patterns, and relative depletions in the middle- to heavy-REE.

and correspondingly low Ga/Al values compared to typical continental crust. Owens and Pasek (2007) evaluated this anomaly using thermodynamic principles, and showed that effective fractionation of Ga from Al can only occur in highly acidic (pH <2.5), sulfate-bearing fluids. The Hagers Mountain samples do not show this anomaly, i.e., Ga concentrations (12-31 ppm) and Ga/Al values are in the typical range for crustal rocks.

Rare earth elements (REE) and Y

Chondrite-normalized REE patterns for all samples are shown in Figure 6, where it can be seen that they fall into two groups with contrasting patterns. One group (Fig. 6A) shows similar light-REE-enriched patterns ($La_N/Sm_N = 2\text{-}5$), with relatively flat heavy-REE slopes and prominent negative Eu-anomalies. These four samples include the quartz-sericite schist, chloritoid-sericite quartzite, and the two kyanite quartzites with the most abundant chloritoid. The other five samples (Fig. 6B) typically display even more fractionated light-REE patterns ($La_N/Sm_N = 5\text{-}26$), and an unusual U-shape

overall, with relative depletions from the middle- to heavy-REE. As shown on the diagrams, the contrasting pattern shapes of the two groups can be correlated with Fe-content, with the most Fe-poor samples belonging to the second group. The unusual patterns displayed by the low-Fe group are similar to those reported by Owens and Pasek (2007) for kyanite quartzites from four separate localities in Virginia. As a final observation, Y concentrations show an excellent correlation with Ho ($r^2 = 0.99$), confirming that Y behaves similarly to the heavy REE.

DISCUSSION

Conditions of metamorphism

All kyanite quartzites at Hagers Mountain are low in alkalis, MgO, and CaO, therefore the $FeO\text{-}Al_2O_3\text{-}SiO_2\text{-}H_2O$ (FASH) system is appropriate for evaluating the conditions of metamorphism for this locality. Figure 7 shows a P-T diagram illustrating mineral stabilities in a portion of the FASH system.

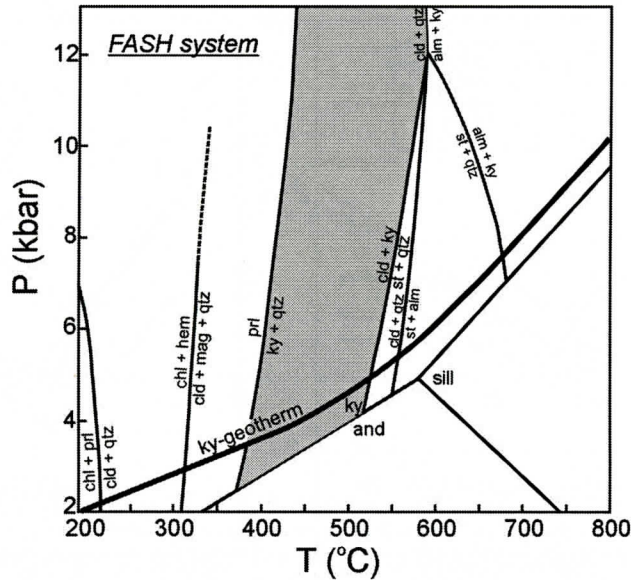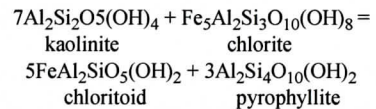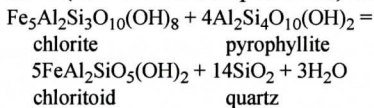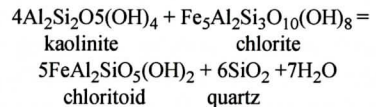The typical chloritoid-producing reaction in

Figure 7. Phase equilibria in the system FeO-Al$_2$O$_3$-SiO$_2$-H$_2$O (FASH), simplified from Bucher and Frey (2002). Shaded region indicates those conditions under which chloritoid and kyanite are stable together, as at Hagers Mountain. Mineral symbols from Kretz (1983).
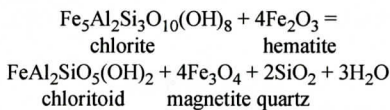
this system (for Al-rich compositions) is:

$$Fe_5Al_2Si_3O_{10}(OH)_8 + 4Al_2Si_4O_{10}(OH)_2 =$$
chlorite   pyrophyllite
$$5FeAl_2SiO_5(OH)_2 + 14SiO_2 + 3H_2O$$
chloritoid   quartz

This reaction occurs at temperatures ≤ 250°C, although the precise T is not well known according to Spear (1993). Regardless, Spear (1993) pointed out that chloritoid and pyrophyllite are known to coexist, so the reaction precedes pyrophyllite breakdown. Additional chloritoid may also be produced at ~300°C by the reaction:

$$Fe_5Al_2Si_3O_{10}(OH)_8 + 4Fe_2O_3 =$$
chlorite   hematite
$$FeAl_2SiO_5(OH)_2 + 4Fe_3O_4 + 2SiO_2 + 3H_2O$$
chloritoid   magnetite quartz

Some Hagers Mountain rocks appear to contain hematite, but lack magnetite, suggesting that this reaction probably played only a minor role in the formation of chloritoid (probably because all chlorite was consumed in the initial reaction above).

A number of additional chloritoid-producing reactions are possible (Zhou et al., 1994), including:

$$7Al_2Si_2O5(OH)_4 + Fe_5Al_2Si_3O_{10}(OH)_8 =$$
kaolinite   chlorite
$$5FeAl_2SiO_5(OH)_2 + 3Al_2Si_4O_{10}(OH)_2$$
chloritoid   pyrophyllite

and

$$4Al_2Si_2O5(OH)_4 + Fe_5Al_2Si_3O_{10}(OH)_8 =$$
kaolinite   chlorite
$$5FeAl_2SiO_5(OH)_2 + 6SiO_2 + 7H_2O$$
chloritoid   quartz

In addition, Luptak et al. (2000) suggested the involvement of ilmenite in chloritoid production via a generalized reaction that also produces rutile:

ilmenite + chlorite(1) + quartz = chloritoid + chlorite(2) + rutile + H$_2$O
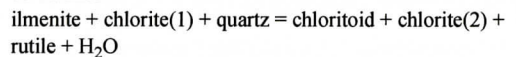
The specific reaction that produced chloritoid at Hagers Mountain is unknown, but each of the above reactions includes chlorite as a reactant phase. Thus, we infer that chlorite was present in the hydrothermally altered protolith of all chloritoid-bearing samples.

Kyanite is produced via pyrophyllite breakdown at ~375°C along the typical kyanite geotherm (Fig. 7). Chloritoid and kyanite are then stable together up to ~525°C, the precise T dependent on P. At higher temperatures, chloritoid reacts to produce either staurolite or garnet, nei-

ther of which occur at Hagers Mountain. Thus, metamorphic temperatures can be broadly constrained to the range 375-525°C. This result is consistent with other evidence from the Carolina terrane for metamorphic conditions primarily in the greenschist facies. The shaded region on Figure 7 represents those P-T conditions where chloritoid and kyanite are stable together, as at Hagers Mountain.

Comparisons with Virginia Occurrences

The rocks at Hagers Mountain share several mineralogical features with kyanite quartzites in Virginia, but also display some key differences. Quartz-kyanite-rutile-white mica is the characteristic mineral assemblage in all Virginia occurrences (Owens and Pasek, 2007), and the same is true for Hagers Mountain rocks with the obvious addition of chloritoid in some samples. Pyrite is widespread and locally abundant in Virginia rocks, but appears to be absent at Hagers Mountain. Its absence, coupled with the possible presence of hematite in some rocks, may reflect an overall higher fO_2 during hydrothermal alteration. Trace amounts of several other minerals have been reported locally from Virginia rocks, including topaz, lazulite, trolleite, barite, apatite, and garnet (Espenshade and Potter, 1960; Mitchell and Fordham, 1987; Owens and Pasek, 2007).

The major element compositions of kyanite-bearing rocks at Hagers Mountain are virtually indistinguishable from Virginia kyanite quartzites. Trace element concentrations are also similar, particularly strong depletions in many elements, e.g., Rb, Ba, Sr, Cr, Ni, Co, Zn, and Cu. Furthermore, the odd U-shaped REE patterns of the low-Fe samples are also shared by the Virginia rocks. A potentially significant difference is the striking Ga-depletion shown by many Virginia rocks versus normal Ga levels at Hagers Mountain.

Evaluation of chemical alteration

The range of rock types and whole-rock compositions at Hagers Mountain suggests that they represent variably altered protoliths. Sample HM06-10, the quartz-sericite schist, appears to be the least altered sample in that its major element composition most closely resembles those of other Hyco Formation rhyolites (Table 2). However, MgO and CaO are below detection in this sample, and the alkalis (especially K_2O) are typically lower than in the unaltered rhyolites. We have no way of assessing whether the original composition of HM06-10 matched those of the other rhyolites, but its less altered character suggests that it makes a plausible reference composition for evaluating the extent of alteration of the other Hagers Mountain samples. The chloritoid-sericite-quartzite (HM06-7B) is similar in composition to HM06-10, but contains only half as much K_2O. The two kyanite quartzites with more than trace amounts of chloritoid (HM06-3 and HM06-4A) have lost most of their alkalis, but are not depleted in Fe. Based on their similar and normal REE patterns (Fig. 6A), these four samples are the least altered of the group, but nonetheless show a progression in degree of alteration.

Assuming a Hyco rhyolite protolith, the remaining five kyanite quartzite samples represent intensely altered rocks that have lost most or all MgO, CaO, Na_2O, K_2O, Fe_2O_3(T), and many trace elements. Compared with the less altered samples, particularly HM06-10, their REE patterns reflect LREE enrichment coupled with depletion in the middle- to heavy REE. Considering the sample set as a whole, the rocks vary in extent of alteration in the sequence quartz-sericite schist → chloritoid-sericite quartzite → kyanite-chloritoid quartzite → kyanite quartzite.

We had originally hoped to evaluate quantitatively mass losses (or gains) in this sequence using the isocon approach of Gresens (1967) and Grant (1986), comparing in this case the compositions of all samples to HM06-10. However, this approach requires that all samples be related to a common unaltered (or less altered) sample, and this does not appear to be true for these rocks as illustrated in the diagrams of Figure 8. Concentrations of Zr are plotted vs. TiO_2 (Fig. 8A) and Al_2O_3 (Fig. 8B), and these graphs thus utilize three elements that are generally
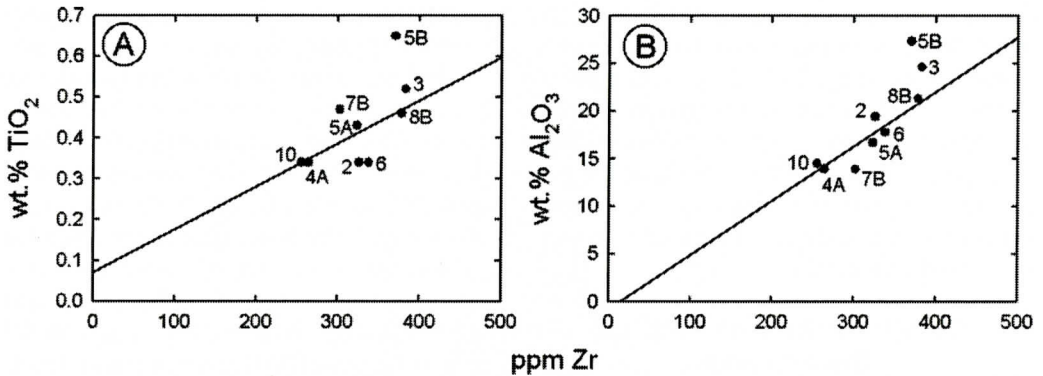
Figure 8. Plots of ppm Zr vs. (A) wt.% TiO₂; and (B) wt.% Al₂O₃ in whole-rock samples of this study. The regression lines apply only to samples 10, 4A, 5A, and 8B.

considered immobile during alteration (or metamorphism). If a sample suite can be related by variable degrees of mass loss or gain, such plots should yield good linear trends that are highly correlated ($r^2 > 0.9$) and ideally pass through the origin (MacLean and Barrett, 1993). The Hagers Mountain sample set as a whole does not meet this requirement, yielding r^2 values of 0.4 (Zr vs. TiO₂) and 0.7 (Zr vs. Al₂O₃), and regression lines (not plotted) that do not intersect the origin. In addition, some samples plot in different positions on the two diagrams, e.g., relative to HM06-10, HM06-2 has gained Al₂O₃, but not TiO₂. The lack of correlation can be interpreted in two ways: 1) these elements did not remain immobile during alteration; or 2) the samples represent alteration from precursors that were originally somewhat heterogeneous, i.e., they cannot all be related by simple mass gain or loss from a common parent rock. We consider the latter interpretation to be more plausible, given the well-documented immobility of Zr and Ti in many other studies.

Despite the overall scatter of points in Figure 8, a subset of the data does meet the above criteria reasonably well. Specifically, samples HM06-10, HM06-4A, HM06-5A, and HM06-8B yield regression lines with r^2 values of 0.95 on both graphs, and the lines pass close to the origin. When compared to HM06-10, the other three samples yield excellent isocon lines defined by 8 to 11 elements (Fig. 9), which include those that are typically immobile (e.g.,

Al, Zr, Hf, Ti, Nb, Ga, Ta, Th, Sm, Yb, Lu). Using the approach of Grant (1986), these lines correspond to calculated mass losses ranging from 3 to 32%. Elements that plot to the right of the regression line have been lost from the sample, whereas those plotting to the left have been gained.

Sample HM06-4A (Fig. 9A) shows only a slight net mass loss, primarily the alkalis, Sr, and Ba, coupled with a modest gain in Fe. All REE plot to the left of the nearly 1:1 isocon line, consistent with the parallel but slightly higher chondrite-normalized REE pattern compared to HM06-10 (Fig. 6A). In contrast, HM06-5A (Fig. 9B) shows significantly greater mass loss (23%), including Fe, alkalis, Sr, Ba, middle- to heavy-REE, and some SiO₂ (despite the higher weight percentage). Concentrations of La and Ce have increased, consistent with the steeper light-REE slope of this sample relative to HM06-10. Finally, HM06-8B (Fig. 9C) shows an overall distribution of data points similar to that of HM06-5A, but with a steeper isocon line corresponding to a greater mass loss of 32%. The significant displacement of La, Ce, and Pr from the isocon line matches the much steeper light-REE slope for this sample compared to all others (Fig. 6B).

Although the other samples are not amenable to strict application of the isocon approach, the overall similarity of their whole-rock compositions to those of either HM06-4A (HM06-3 and HM06-7B), or HM06-5A and 8B (HM06-2, HM06-5B, and HM06-6) suggests that mass
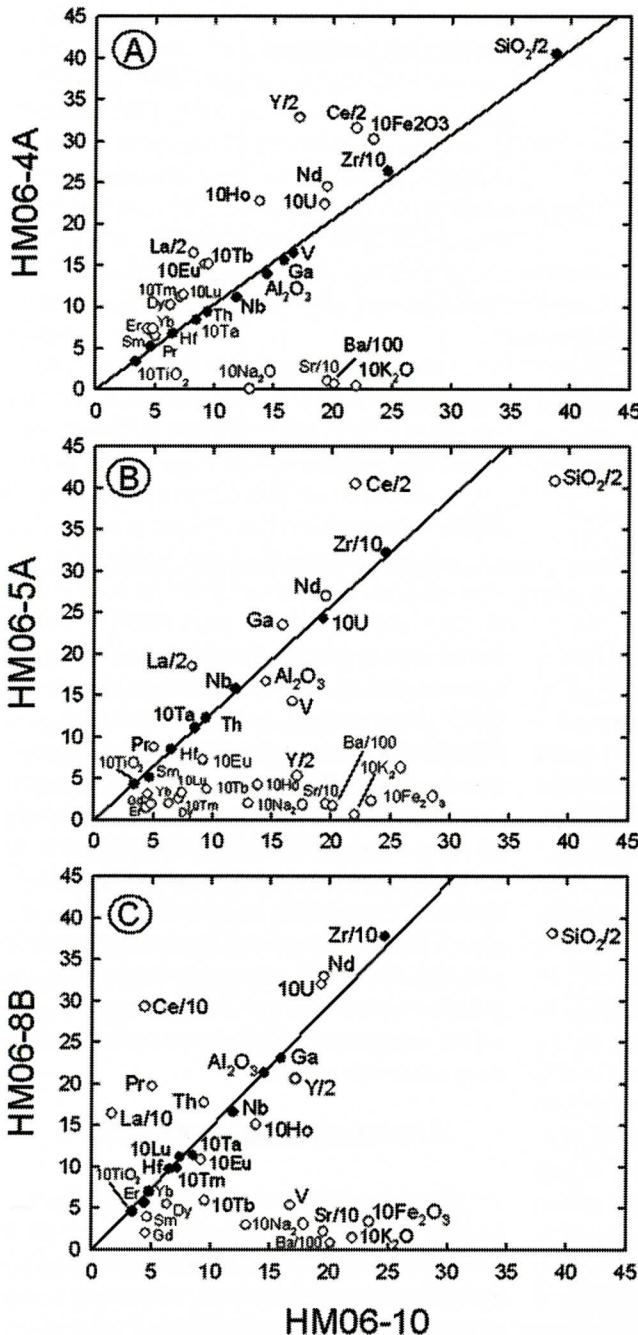
Figure 9. Isocon diagrams (Grant, 1986) for samples HM06-4A, HM06-5A, and HM06-8B compared to HM06-10. Only those elements plotted with black symbols were used in calculating the isocon line in each case. Scaling factors for each element are indicated on the graphs.

losses of similar magnitude affected them. Relative to unaltered rhyolite, HM06-10 probably experienced only slight mass loss, primarily of alkalis and CaO reflecting destruction of feldspar.

Protolith considerations

The ultimate protoliths for all rocks at Hagers Mountain prior to hydrothermal alteration were probably felsic volcanic rocks of the Hyco Formation. This interpretation is supported by: 1) the location near the western mapped extent of the formation; 2) the similarity in major element composition of quartz-sericite schist sample HM06-10 to other Hyco Formation rhyolites; and 3) the REE patterns of the less-altered samples, which are typical of felsic volcanic rocks (i.e., light REE-enriched, flat heavy-REE slopes, and negative Eu-anomalies). Furthermore, all samples plot in the more-evolved portion (rhyodacite to rhyolite) of the Nb/Y vs. Zr/TiO_2 classification diagram of Winchester and Floyd (1977), designed to deal with altered or metamorphosed rocks (Fig. 10).

The current mineralogy and chemical composition of the rocks provide key clues regarding the mineralogy of hydrothermally altered precursor rocks. The quartz-sericite schist was probably derived from a mineralogically similar rock. Chlorite was an additional mineral in what is now the chloritoid-sericite quartzite, as well as in kyanite quartzites with chloritoid. Based on the distribution of data points on Figure 5, kyanite quartzites that lack chloritoid originally contained variable amounts of quartz and kaolinite, perhaps with
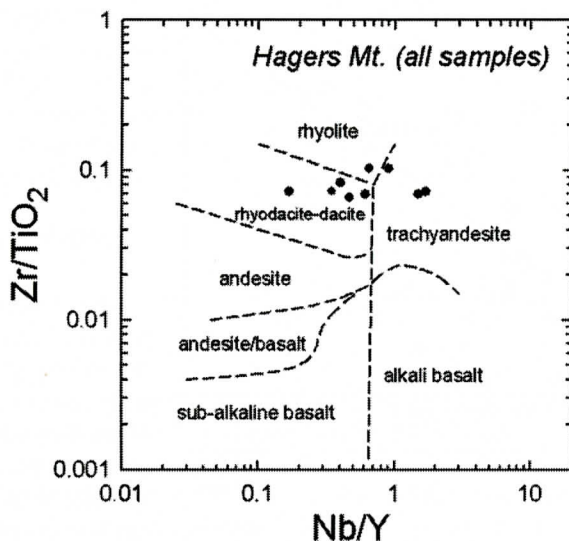
Figure 10. Whole-rock samples of this study plotted on the Nb/Y vs. Zr/TiO$_2$ volcanic rock classification diagram of Winchester and Floyd (1977).

additional pyrophyllite. Thus, our interpretations of precursor mineralogy in order of increasing degree of alteration are: 1) quartz + sericite; 2) quartz + sericite + chlorite; 3) quartz + kaolinite + chlorite; and 4) quartz + kaolinite. In all rocks, rutile was produced via the breakdown of other Ti-bearing silicates or oxides.

This precursor mineralogy is typical of that produced during advanced argillic (high-sulfidation) alteration, i.e., as a consequence of intense leaching of all mobile components in hot, acidic fluids. The evidence for hydrothermally altered igneous protoliths is compelling for the Virginia occurrences (Owens and Pasek, 2007), as outlined in our Previous Work section, and we suggest that the same arguments apply here. Some of the contrasts between Hagers Mountain and the Virginia rocks may reflect differences in protolith rock type and the specific conditions of alteration. Based on the associated rock types and the classification diagram of Figure 10, the Hagers Mountain protoliths were probably more-evolved than those for the Virginia rocks, which were primarily mafic to intermediate in composition (Owens and Pasek, 2007). Chloritoid occurs in rocks which are less-intensely altered, and no equivalent rocks have yet been recognized in Virginia (although

metamorphic grade is higher). Based on the thermodynamic analysis of Owens and Pasek (2007), the normal levels of Ga at Hagers Mountain indicate slightly different initial alteration conditions. Owens and Pasek (2007) showed that the pH-pSO$_4$ conditions necessary for the preferential leaching of Ga relative to Al are fairly restricted, and slightly less acidic conditions or lower pSO$_4$ could result in no Ga removal. Nonetheless, the unusual U-shaped REE patterns of the more-intensely altered Hagers Mountain rocks match those of the Virginia rocks, suggesting that alteration conditions were otherwise similar.

Analogous rocks elsewhere

Quartz-rich rocks that also contain chloritoid plus an aluminosilicate have been described from several other examples of metamorphosed hydrothermal alteration zones elsewhere. Many of these occurrences are associated with volcanogenic-hosted massive sulfide (VHMS) deposits, including Mattabi, Ontario (Franklin et al., 1975), Bousquet, Quebec (Valliant et al., 1983), Headway-Coulee, Ontario (Osterberg et al., 1987), and Gossan Hill, Australia (Sharpe and Gemmell, 2001). Other examples include

the Helen, Ontario, siderite deposit (Morton and Nebel, 1984) and the Campbell, Ontario, epithermal Au-As-Sb-Zn-(Hg) deposit (Penczak and Mason, 1997). Thus, aluminous hydrothermal alteration zones can be produced in a variety of settings ranging from submarine (VHMS; cf. Sillitoe et al., 1996; Dubé et al., 2007) to subaerial (high-sulfidation epithermal gold deposits; cf. Cooke and Simmons, 2000), and are not necessarily unique to any particular type of mineralization.

One feature of the Hagers Mountain rocks that can potentially discriminate between these two alteration settings is the REE pattern displayed by the most altered rocks. Specifically, Huston (2001) noted that the distinctive concave upward patterns and overall steeper slopes are more characteristic of altered rocks associated with acid-sulfate epithermal deposits rather than VHMS deposits. In addition, many of the gold deposits elsewhere in the Carolina terrane appear to have formed in epithermal rather than VHMS settings (e.g., Spence et al., 1980; Scheetz et al., 1991; Bierlein and Crowe, 2000). Although beyond the scope of this study, the apparent paucity of gold mineralization at Hagers Mountain can be explained in several ways, including: 1) inadequate exploration (with possible mineralization at depth); 2) tectonic dismemberment of alteration and ore zones, perhaps as a consequence of shearing along the Hyco shear zone; or 3) by the formation of a hydrothermally altered, but otherwise barren region.

ACKNOWLEDGMENTS

REFERENCES

Bierlein, F.P., and Crowe, D.E., 2000, Phanerozoic orogenic lode gold deposits: Reviews in Economic Geology, v. 13, p. 103-109.

Boynton, W.V., 1984, Geochemistry of the rare earth elements: meteorite studies, in Henderson, P., ed., Rare Earth Element Geochemistry: Elsevier, p.63-114.

Bucher, K., and Frey, M., 2002, Petrogenesis of Metamorphic Rocks: Germany, Springer-Verlag, Berlin, Germany.

Butler, J.R., and Secor, D.T., Jr., 1991, The Central Piedmont, in Horton, J.W., Jr., and Zullo, V.A., eds., The Geology of the Carolinas, Carolina Geological Society Fiftieth Anniversary Volume: The University of Tennessee Press, Knoxville, TN, p. 59-78.

Carpenter, R.J., and Allard, G.O., 1982, Aluminosilicate assemblages; an exploration tool for metavolcanic terrains of the Southeast, in Exploration for Metallic Resources in the Southeast Conference, University of Georgia Department of Geology and Center for Continuing Education, p. 1-4.

Coler, D.G., Wortman, G.L., Samson, S.D., Hibbard, J.P., and Stern, R., 2000, U-Pb geochronologic, Nd isotopic, and geochemical evidence for the correlation of the Chopawamsic and Milton Terranes, Piedmont Zone, Southern Appalachian orogen: Journal of Geology, v. 108, p. 363-380.

Conley, J.F., and Marr, J.D., Jr., 1980, Evidence for the correlation of the kyanite quartzites of Willis and Woods mountains with the Arvonia Formation: Virginia Division of Mineral Resources Publication 27, p. 1-11.

Cooke, D.R., and Simmons, S.F., 2000, Characteristics and genesis of epithermal gold deposits: SEG Reviews, v. 13, p. 221-244.

Couture, R.A., Smith, M.S., and Dymek, R.F., 1993, X-ray fluorescence analysis of silicate rocks using fused glass discs and a side window Rh tube: Accuracy, precision and reproducibility: Chemical Geology, v. 110, p. 315-328.

Couture, R.A., and Dymek, R.F., 1996, A reexamination of absorption and enhancement effects in X-ray fluorescence trace element analysis: American Mineralogist, v.81, p. 639-650.

Dubé, B, Mercier-Langevin, P., Hannington, M., Lafrance, B., Gosselin, G., and Gosselin, P., 2007, The LaRonde Penna world-class Au-rich volcanogenic massive sulfide deposit, Abitibi, Québec: mineralogy and geochemistry of alteration and implications for genesis and exploration: Economic Geology, v. 102, p. 633-666.

Dymek, R.F., and Owens, B.E., 2001, Chemical assembly of Archean anorthosites from amphibolite- and granulite-facies terranes, SW Greenland: Contributions to Mineralogy and Petrology, v. 141, p. 513-528.

Espenshade, G.S., and Potter, D.B., 1960, Kyanite, sillimanite, and andalusite deposits of the southeastern states: U.S. Geological Survey Professional Paper 336, 121 p.

Feiss, P.G., 1985, Volcanic-hosted gold and high alumina rocks of the Carolina slate belt: Field Trip Guidebook,

1985 Annual Meeting of the Geological Society of America and Society of Economic Geologists, 217 p.

Franklin, J.M., Kasarda, J., and Poulsen, K.H., 1975, Petrology and chemistry of the alteration zone of the Mattabi sulfide deposit: Economic Geology, v. 70, p. 63-79.

Glover, L., III, and Sinha, A.K., 1973, The Virgilina deformation, a Late Precambrian to Early Cambrian(?) orogenic event in the central Piedmont of Virginia and North Carolina: American Journal of Science, v. 273-A, p. 234-251.

Grant, J.A., 1986, The isocon diagram – a simple solution to Gresens' equation for metasomatic alteration: Economic Geology, v. 81, p. 1976-1982.

Gresens, R.L., 1967, Composition-volume relationships of metasomatism: Chemical Geology, v. 2, p. 47-55.

Hadley, J.B., 1973, Igneous rocks of the Oxford area, Granville County, North Carolina: American Journal of Science, v. 273-A, p. 217-233.

Harris, C.W., and Glover, L., III, 1985, The Virgilina deformation: Implications of stratigraphic correlation in the Carolina slate belt: Field trip guidebook, Carolina Geological Society, Durham, North Carolina, 16-17 Nov. 1985, and Blacksburg, Virginia Polytechnic Institute and State University, Department of Geological Sciences, 59 p.

Hibbard, J.P., and Samson, S.D., 1995, Orogenesis exotic to the Iapetan cycle in the southern Appalachians, in Hibbard, J.P., van Staal, C.R., and Cawood, P.A., eds., Current Perspectives in the Appalachian-Caledonian Orogen: Geological Association of Canada Special Paper 41, p. 191-205.

Hibbard, J.P., Shell, G.S., Bradley, P.J., Samson, S.D., and Wortman, G.L., 1998, The Hyco shear zone in North Carolina and southern Virginia: implications for the Piedmont Zone-Carolina Zone boundary in the Southern Appalachians: American Journal of Science, v. 298, p. 85-107.

Hibbard, J.P., van Staal, C.R., Rankin, D.W., and Williams, H., 2006, Lithotectonic map of the Appalachian orogen, Canada–United States of America: Geological Survey of Canada, Map 2096A, scale 1:1 500 000.

Horton, J.W., Jr., Drake, A.A., Jr. and Rankin, D.W., 1989, Tectonostratigraphic terranes and their Paleozoic boundaries in the central and southern Appalachians, in Dallmeyer, R.D., ed., Terranes in the Circum-Atlantic Paleozoic orogens. Geological Society of America Special Paper 230, p. 213-245.

Huston, D.L., 2001, Geochemical dispersion about the Western Tharsis Cu-Au deposit, Mt. Lyell, Tasmania: Journal of Geochemical Exploration, v. 72, p. 23-46.

Johnson, N.E., Craig, J.R., and Rimstidt, J.D., 1989, Vein mineralization of the Virgilina district, Virginia and North Carolina: in Evans, N.H., ed., Contributions to Virginia Geology – VI, Virginia Division of Mineral Resources Publication 88, p. 1-16.

Klein, T.L., and Criss, R.E., 1988, An oxygen isotope and geochemical study of meteoric-hydrothermal systems at Pilot Mountain and selected other localities, Carolina

Slate Belt: Economic Geology, v. 83, p. 801-821.

Kreisa, R.D., 1980, Geology of the Omega, South Boston, Cluster Springs, and Virgilina quadrangles: Virginia Division of Mineral Resources Publication 5, 22 p.

Kretz, R., 1983, Symbols for rock-forming minerals: American Mineralogist, v. 68, p. 277-279.

Laney, F.B., 1917, The geology and ore deposits of the Virgilina district of Virginia and North Carolina: Virginia Geological Survey Bulletin 14, 176 p.

Lesure, F.G., 1993, Reconnaissance geochemistry in the southern part of the Virgilina district, North Carolina and Virginia: U.S. Geological Survey Miscellaneous Field Studies Map, MF-2203, 1 sheet, scale 1:48,000.

Luptak, B., Janak, M., Plasienka, D., Schmidt, S., and Frey, M., 2000, Chloritoid-kyanite schists from the Veporic Unit, western Carpathians, Slovakia: implications for Alpine (Cretaceous) metamorphism: Schweizerische Mineralogische und Petrographische Mitteilungen, v. 80, p. 213-223.

MacLean, W.H., and Barrett, T.J., 1993, Lithogeochemical techniques using immobile elements: Journal of Geochemical Exploration, v. 48, p. 109-133.

Mitchell, R.S., and Fordham, O.M., Jr., 1987, Trolleite and some associated minerals in kyanite quartzites, Willis Mountain, Virginia: Southeastern Geology, v. 28, p. 81-86.

Morton, R.L., and Nebel, M.L., 1984, Hydrothermal alteration of felsic volcanic rocks at the Helen siderite deposit, Wawa, Ontario: Economic Geology, v. 79, p. 1319-1333.

Osterberg, S.A., Morton, R.L., and Franklin, J.M., 1987, Hydrothermal alteration and physical volcanology of Archean rocks in the vicinity of the Headway-Coulee massive sulfide occurrence, Onaman area, northwestern Ontario: Economic Geology, v. 82, p. 1505-1520.

Owens, B.E., and Dickerson, S.E., 2001, Kyanite color as a clue to contrasting protolith compositions for kyanite quartzites in the Piedmont Province of Virginia: Southeastern Geology, v. 40, p. 285-298.

Owens, B.E., and Pasek, M.A., 2007, Kyanite quartzites in the Piedmont Province of Virginia: evidence for protolith production in a high-sulfidation hydrothermal system: Economic Geology, v. 102, p. 495-509.

Penczak, R.S., and Mason, R., 1997, Metamorphosed Archean epithermal Au-As-Sb-Zn-(Hg) vein mineralization at the Campbell mine, northwestern Ontario: Economic Geology, v. 92, p. 696-719.

Ririe, G.T., 1990, A comparison of alteration assemblages associated with Archean gold deposits in western Australia with Paleozoic gold deposits in the southeast United States: Canadian Journal of Earth Sciences, v. 27, p. 1560-1576.

Scheetz, J.W., Stonehouse, J.M., and Zwaschka, M.R., 1991, Geology of the Brewer gold mine in South Carolina: Mining Engineering, v. 43, p. 38-42.

Schmidt, R.G., 1985, High-alumina hydrothermal systems in volcanic rocks and their significance to mineral prospecting in the Carolina Slate Belt: U.S. Geological Sur-

vey Bulletin 1562, 59 p.

Schreyer, W., 1987, Pre- or synmetamorphic metasomatism in peraluminous metamorphic rocks, *in* Helgeson H. C., ed., Chemical Transport in Metasomatic Processes: NATO ASI Series, Series C. Mathematical and Physical Sciences, v. 218, p. 265-296.

Sharpe, R., and Gemmell, J.B., 2001, Alteration characteristics of the Archean Golden Grove Formation at the Gossan Hill deposit, western Australia: induration as a focusing mechanism for mineralizing hydrothermal fluids: Economic Geology, v. 96, p. 1239-1262.

Sillitoe, R.H., Hannington, M.D., and Thompson, J.F.H., 1996, High sulfidation deposits in the volcanogenic massive sulfide environment: Economic Geology, v. 91, p. 204-212.

Spear, F.S., 1993, Metamorphic Phase Equilibria and Pressure-Temperature-Time Paths. Mineralogical Society of America Monograph, Mineralogical Society of America, Washington, D.C.

Spence, W.H., Worthington, J.E., Jones, E.M., and Kiff, I.T., 1980, Origin of the gold mineralization at the Haile mine, Lancaster County, South Carolina: Mining Engineering, v. 32, p. 70-73.

Stuckey, J.L., 1932, Cyanite deposits of North Carolina: Economic Geology, v. 27, p. 661-674.

Stuckey, J.L., 1935, Origin of cyanite: Economic Geology, v. 30, p. 444-450.

Taylor, S.R., and McLennan, S.M., 1985, The Continental Crust: Its Composition and Evolution: Oxford, Blackwell Scientific Publications, 312 pp.

U.S. Geological Survey, 2009, Mineral commodities summaries 2009: U.S. Geological Survey, 195 p.

Valliant, R.I., Barnett, R.L., and Hodder, R.W., 1983, Aluminum silicate-bearing rock and its relation to gold mineralization; Bousquet Mine, Bousquet Township, Quebec: CIM Bulletin, v. 76, p. 81-90.

Winchester, J.A., and Floyd, P.A., 1977, Geochemical discrimination of different magma series and their differentiation products using immobile elements: Chemical Geology, v. 20, p. 325-343.

Wortman, G., Samson, S., and Hibbard, J., 2000, Precise U-Pb zircon constraints on the earliest magmatic history of the Carolina Terrane: Journal of Geology, v. 108, p. 321-338.

Zhou, T., Dong, G., and Phillips, G.N., 1994, Chemographic analysis of assemblages involving pyrophyllite, chloritoid, chlorite, kaolinite, kyanite, and quartz: application to metapelites in the Witwatersrand gold fields, South Africa: Journal of Metamorphic Geology, v. 12, p. 655-666.

EXTREME RARE-ELEMENT ENRICHMENT IN A MUSCOVITE-RARE-ELEMENT CLASS GRANITIC PEGMATITE: A CASE STUDY OF THE SPODUMENE-AMAZONITE MCHONE PEGMATITE, SPRUCE PINE, NORTH CAROLINA

MICHAEL A. WISE

wisem@si.edu

CATHLEEN D. BROWN

brownc@si.edu
Department of Mineral Sciences
National Museum of Natural History, Smithsonian Institution
Washington, D.C., 20560, U.S.A.

ABSTRACT

The McHone pegmatite is one of a limited number of mineralogically diverse and chemically evolved dikes located in the Spruce Pine pegmatite district, North Carolina and is unusual in two respects: (1) the presence of spodumene + pollucite with amazonite + fluorite is extremely atypical of pegmatites from either LCT (lithium, cesium, tantalum) or NYF (niobium, yttrium, fluorine) granite-pegmatite suites and (2) the highly fractionated nature is uncharacteristic of pegmatites belonging to the muscovite - rare-element class. Primary assemblages show LCT-like rare-element mineralization in the form of microlite and manganocolumbite (Nb, Ta), schorl (B), beryl (Be), spodumene (Li), and rare pollucite (Cs). Late stage enrichment in F, as indicated by the crystallization of fluorite, and the presence of amazonite are consistent with NYF-like mineralization. Amazonitization of microcline-perthite apparently postdates the crystallization of primary assemblages.

The McHone pegmatite exhibits levels of trace-element enrichment similar to pegmatites of both NYF- and LCT-family populations. The high levels of Rb (maximum of 5789 ppm in microcline-perthite and Cs (maximum of 37020 ppm in beryl) encountered in the McHone pegmatite are more typical of LCT-affiliated systems than NYF family or muscovite – rare-element class pegmatites. By comparison, the enrichment of Pb in the McHone microcline-perthite (maximum of 2109 ppm) and Zn in muscovite (maximum of 3949 ppm) and beryl (maximum of 2222 ppm) is more characteristic of pegmatites with a NYF geochemical signature. The enrichment patterns of rare alkalis, Pb and Zn in the pegmatite and the resultant mixed geochemical signature appear to be the product of magmatic fractionation rather than contamination by exterior sources or overprinting by hydrothermal fluids.

INTRODUCTION

The Spruce Pine pegmatite district encompasses one of the largest populations of granitic pegmatites in the southern Appalachian region. Pegmatites in this area have been mined primarily for economic-grade feldspar, muscovite and quartz for nearly a century (Olson, 1944). Despite a long history of production, the area has been the subject of only a modest number of modern scientific studies (e.g., Wood, 1996; Tappen and Smith, 2003; Veal, 2004). According to the classification criteria of Černý and Ercit (2005), the Spruce Pine pegmatites best fit the muscovite–rare-element (MS-REL) class of granitic pegmatites that are emplaced in kyanite- to sillimanite-grade metamorphic rocks which attained peak metamorphism at ~5-8 kb and ~580-650°C. Rare-element-bearing granitic pegmatites are widely dispersed throughout the district, but of the several hundred exposed pegmatites, only two are known to carry Li and/or Cs mineralization. The McHone and Ray
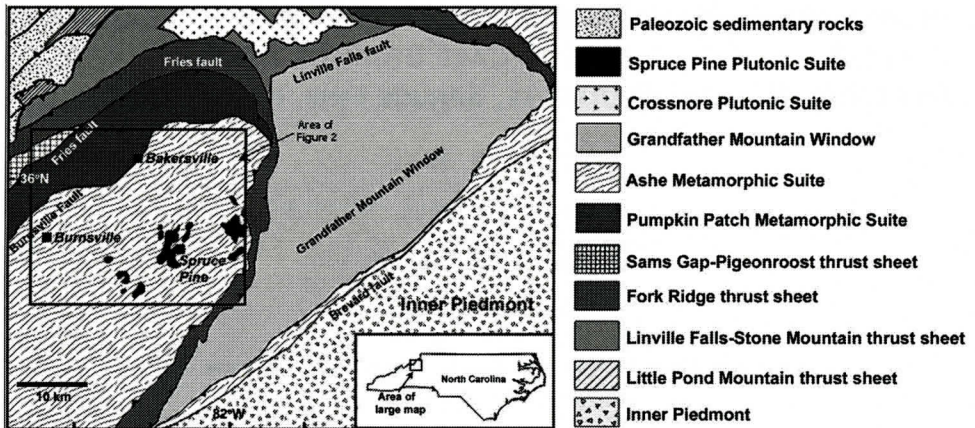
Figure 1. General tectonic map of western North Carolina showing the location of the Spruce Pine pegmatite field. Modified from Trupe et al. (2003).

pegmatites both contain amazonitic microcline-perthite, elbaitic schorl and minor quantities of pollucite and fluorite, while spodumene only occurs in the McHone pegmatite.

The presence of spodumene and pollucite in granitic pegmatites generally implies an origin consistent with fractional crystallization from a peraluminous, S- or I-type parental granite with enriched levels of Be, Nb, Ta (with Ta>Nb), Sn, P, Rb, Cs, Li and B (Černý's *LCT* family; 1991a; London, 2005; London, 2008). By comparison, the presence of amazonite, with or without fluorite, is more commonly found in pegmatites generated by A-type granites with compositions that display a geochemical signature characterized by enrichment in Nb>Ta, Y, REE, Sc, Ti, Zr, Be, Th, U, F (Černý's *NYF* family; 1991a). Although granitic pegmatites that display both NYF and LCT characteristics have been recognized, they are uncommon compared to the worldwide occurrences of purely NYF or LCT affiliated pegmatites. In light of the unusual mineral assemblage (spodumene + pollucite + amazonite + fluorite) in the McHone pegmatite, this paper presents new chemical data on mineral species known to be recorders of pegmatite evolution and discusses the behavior of rare-elements leading to the development of a mixed NYF-LCT geochemical signature.

REGIONAL GEOLOGY

The Blue Ridge thrust complex of western North Carolina consists of a stack of crystalline thrust sheets that record multiple tectonothermal events (Goldberg et al., 1986, 1989, 1992a; Butler et al., 1987; Fig. 1). The Blue Ridge has been divided into three provinces: the eastern (EBR), central (CBR) and western (WBR) Blue Ridge (Hatcher, 1978; Berquist et al., 2005). The EBR, which hosts the pegmatite population examined here, is separated from the Inner Piedmont to the southeast by the Brevard Fault Zone, a major structure with a multiphase history of displacement (Hatcher, 1978), and the WBR from the Valley and Ridge province by the Blue Ridge fault system to the west. The CBR lies between the EBR and WBR (Berquist et al., 2005).

The structurally complex EBR records a prolonged and complex period of subduction, arc accretion, and continental collision interpreted to be in response to the closing of the Iapetus Ocean that occurred prior to the collision of the Piedmont arc with Laurentia during the middle Ordovician. The EBR contains large bodies of high-T (>750°C) Ordovician-age eclogite and other high-pressure metamorphic rocks, immature clastic metasedimentary rocks, and amphibolite that are locally intruded by Paleozoic felsic plutons (Rankin, 1975; Hatcher, 1978). Rocks exposed within the Grandfather Moun-
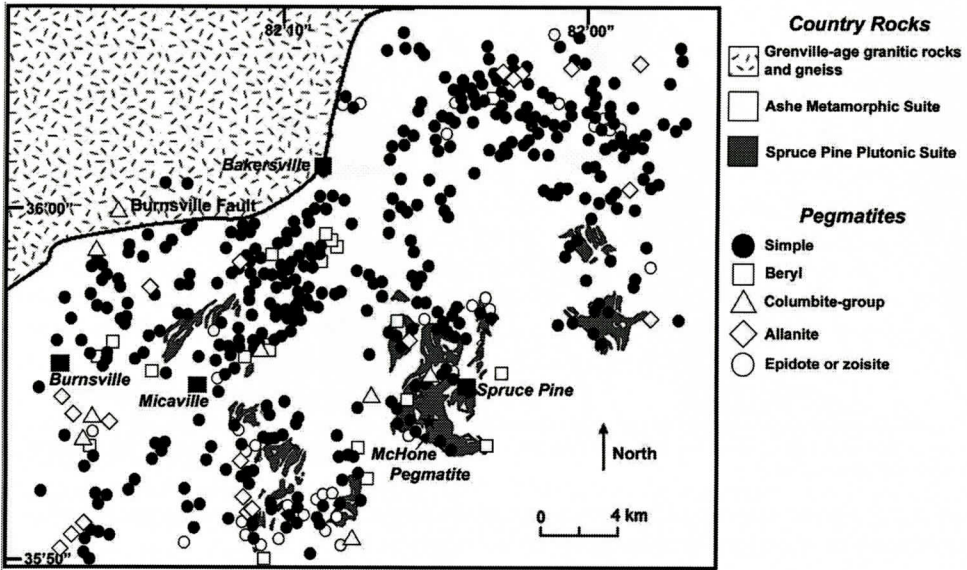
Figure 2. The Spruce Pine pegmatite field showing the distribution of pegmatites (symbols) with granodiorite (gray). Star marks the location of the McHone pegmatite. Pegmatite data modified from Lesure (1968).

tain Window are thought to represent 1.1 Ga Grenville basement consisting of the Blowing Rock and the Wilson Creek gneisses. It has been suggested that these rocks represent rifted Laurentian basement (Hatcher, 1989) or accreted suspect terranes from Gondwana (Stewart et al., 1997). Overlying the basement is a thick sequence of Cambrian age clastics (sandstones, mudstones, and conglomerates) and volcanic rocks (basalts, rhyolites, and tuffaceous rocks) that were all deformed and metamorphosed during the Ordovician and early Devonian. Thrusting events followed in the Late Devonian and lasted until the Late Triassic.

Granitic plutons are relatively sparse in the eastern Blue Ridge and are mineralogically and geochemically akin to the K-poor TTG association (tonalite-trondhjemite-granodiorite) (Miller et al., 1997). Plutonism was thought to be related to three tectonothermal events: Taconian (Ordovician), Acadian (Devonian-Silurian) and Alleghanian (Carboniferous-Permian) (Miller et al., 2006). All plutons intrude schists, paragneisses and amphibolite and postdate at least some regional fabric development. Although all are overprinted by deformation and metamorphism, most do retain some magmatic

textures. Mafic complexes in the region are generally interpreted to be older than the plutons, but none is well-dated. Peak metamorphism occurred during the Taconian orogeny in the EBR and ranged from middle amphibolite to granulite facies (650-800°C) (Goldberg and Dallmeyer, 1997; Miller et al., 1998).

The McHone pegmatite is one of numerous pegmatites known to occur in the 777 km^2 Spruce Pine pegmatite district spread across Avery, McDowell, Mitchell and Yancey counties (Lesure, 1968). The pegmatite district is underlain by Precambrian, amphibolite grade, metamorphosed sedimentary rocks of the northeast-southwest trending Ashe Metamorphic Suite (Brobst, 1962; Rankin et al., 1973; Wood, 1996; Fig. 2). The Ashe Metamorphic Suite consists of intimately interlayered muscovite-biotite gneiss and mica schist, amphibolite and metagraywacke. Estimated P-T conditions for prograde metamorphism of the Ashe Metamorphic Suite are 640-700°C and 7-9 kb (Goldberg et al., 1992b). The Ashe Metamorphic Suite is intruded by numerous granodiorite plutons, dikes, sills and associated granitic pegmatites collectively known as the Spruce Pine Plutonic Suite. The Chalk Mountain pluton is the largest

Biotite schist

Unit 1: Kfs, qtz, mus, plg

Unit 2: Qtz, mus, plg, (tur)

Unit 3: Kfs (amz), qtz, mus

Unit 4: Kfs (amz), qtz, spd

Unit 5: Kfs (amz), qtz, spd, byl tur, fl, (mic, pol)

Fracture fill: qtz, plg, mus

Spodumene

Beryl

Fluorite

Unit 6: plg, qtz, mus (mic, ct, fl)

Abbreviations: amz - *amazonite*, **byl** - *beryl*, **ct** - *columbite*, **fl** - *fluorite*, **Kfs** - *microcline-perthite*, **mic** - *microlite*, **mus** - *muscovite*, **plg** - *plagioclase*, **pol** - *pollucite*, **qtz** - *quartz*, **spd** - *spodumene*, **tur** - *tourmaline*. **Parentheses represent minor phases.**
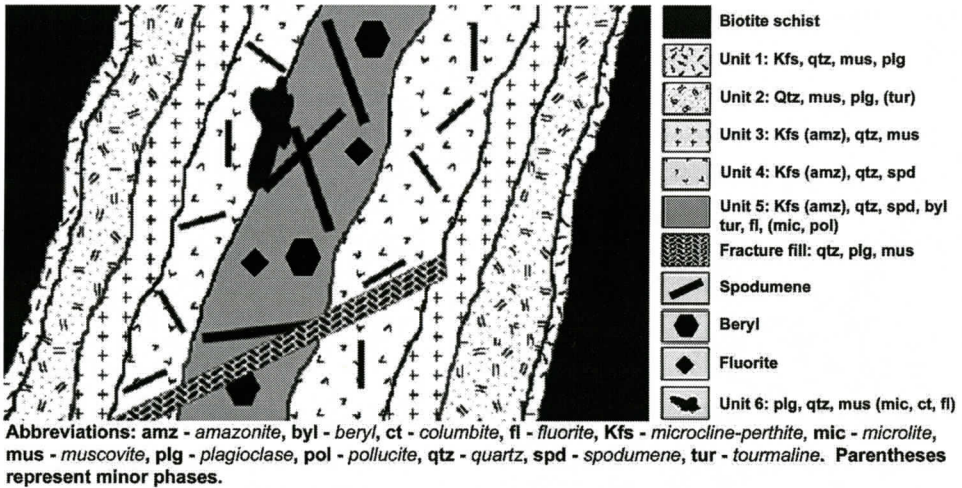
Figure 3. Schematic diagram of the internal zonation of the McHone pegmatite showing the spatial relationships of pegmatite units. Diagram not drawn to scale.

granitic intrusion in the district and U-Pb zircon ages place its time of crystallization at 377.7 ± 2.5 Ma (Miller et al., 2006). The Chalk Mountain pluton is granodioritic in composition, variably foliated and locally displays pegmatitic textures. It has been interpreted to be syntectonic with respect to Acadian amphibolite-facies metamorphism and deformation (Waters et al., 2000; Johnson et al., 2001).

Pegmatites occur in both the granodiorite and metamorphic rock with contacts that vary from sharp to gradational (Wood, 1996; Veal, 2004). Granitic pegmatites that intrude the Ashe Metamorphic Suite are concordant to discordant to the main foliation. The origin of the Spruce Pine pegmatites remains unresolved; some workers have proposed that the pegmatites are differentiates of a granodiorite magma (Olson, 1944; Lesure, 1968; Wood, 1996) while others suggest that the pegmatites were derived by the anatexis of metasedimentary rocks (Kish, 1989; Feiss et al., 1991). The majority of pegmatites in the Spruce Pine district are mineralogically simple (i.e., containing mostly quartz, microcline-perthite, albite-oligoclase and muscovite) and lack complex internal zonation as defined by Cameron et al. (1949). Biotite, garnet and apatite are the most common accessory minerals present. Overall, rare-element mineralization is generally uncommon

(Fig 2.) and when present is limited to variable but generally very low amounts of tourmaline, beryl, columbite-group minerals, zircon and allanite. Sulfide mineralization may be locally abundant (Heinrich, 1950) while epidote, clinozoisite, zoisite, calcite, uraninite, microlite, spodumene and pollucite are rare (Olson, 1944; Lesure, 1968).

INTERNAL STRUCTURE OF THE MCHONE PEGMATITE

Limited excavation of the McHone pegmatite has exposed only a modest portion of the dike and therefore the internal lithologic units presented here may not be entirely representative of the whole body. The pegmatite is mapped as being hosted by the Chalk Mountain granodiorite (Olson, 1944), but Wood (1996) observed that the pegmatite is situated within a screen of kyanite-bearing, muscovite-biotite schist that lies within the granodiorite. Tourmalinization of the schist is sporadic and may extend up to 20 cm away from the pegmatite contact. Examination of the present pegmatite exposure revealed six lithologic units distinguished by mineral assemblages and textures (Fig. 3). The outermost unit defined here as the "wall zone" (Unit 1) consists of medium-grained subhedral crystals of microcline-perthite, quartz, musco-

vite and plagioclase. Unit 2 is texturally similar to Unit 1, but lacks microcline-perthite and contains minor quantities of tourmaline. Unit 3 contains subhedral, white to green (amazonite) blocky microcline-perthite (up to 10 cm in length), quartz and crystals of muscovite that rarely reach 2 cm in their largest dimension. The color of the McHone amazonite is noticeably different from the classic blue-green color from other amazonite localities (e.g., Pikes Peak, Colorado; Morefield mine, Virginia). Individual crystals of amazonite display mottled to patchy pale, sea-green to grass-green coloration. The intensity of the green color shows no correlation with position in the pegmatite; however, the most intense green color generally occurs along the edges of white microcline-perthite crystals and along cleavage planes and fractures that crosscut the crystals. Unit 4 consists largely of medium- to coarse-grained, white to green microcline-perthite, blebby gray quartz and spodumene crystals up to 12 cm in length. Muscovite is uncommon and tourmaline is rare.

The central "core" (Unit 5) is comprised predominantly of very coarse-grained white microcline-perthite (up to 35 cm) with local green domains, masses of quartz, and spodumene crystals up to 4 cm in length. Much of the spodumene is altered, but when fresh it displays a pale green color. Tourmaline crystals up to 4 cm in length occur singularly and in radiating aggregates in microcline-perthite and quartz. Crystals of white to pale blue beryl, up to 1.3 cm thick and 6 cm across, are also typical of this unit and are tabular perpendicular to the c-axis. Muscovite is typically found as 2-5 mm sized euhedral to subhedral crystals in quartz and less frequently in microcline-perthite. Accessory green to blue fluorite is present as anhedral masses in microcline-perthite and quartz. The fluorite displays thermoluminescence changing from a gray-blue color to vivid blue-green when heated. Rare pollucite occurs as colorless, transparent masses with spodumene in Unit 5.

Unit 6 consists primarily of fine-grained saccharoidal albite, and medium-grained quartz and muscovite with disseminated, rare octahedral crystals of brown to orange microlite and dark red-brown manganocolumbite. Rare pur-

ple fluorite is found as interstitial grains and thin films with microlite and manganocolumbite. This unit replaces microcline-perthite throughout the pegmatite, but is most prevalent in Units 2 and 3. Quartz-plagioclase-microcline-perthite-muscovite veins locally crosscut Units 3 and 4. The veins vary from 2 to 9 cm wide and contain rods of quartz and microcline-perthite crystals that are oriented perpendicular to the length of the veins. Fine-grained muscovite occurs as sparse crystals in quartz and microcline-perthite.

ANALYTICAL METHODS

The following discussion on mineral chemistry is limited to primary phases that are routinely used to characterize the geochemical evolution of granitic pegmatites. Microcline-perthite and micas were sampled from blocky microcline-perthite + quartz rich pods. Beryl, Nb-Ta oxides, and tourmaline were collected from all texturally distinct units where available.

Unaltered and inclusion-free microcline-perthite and muscovite were hand-separated from pegmatite samples for trace-element analysis. Samples were pulverized, sieved to 100 mesh, made into pressed pellets and analyzed using an automated Phillips X-ray fluorescence spectrometer (model PW1480). Microcline-perthite, mica-group minerals and beryl were analyzed for Ba, Cs, Ga, Ni, Nb, Pb, Rb, Sn, Sr, Ta, Tl, Zn and Zr.

Fragments and crystals of microcline-perthite, muscovite, beryl, manganocolumbite, tourmaline and microlite were analyzed using a JEOL Model JXA-8900R electron microprobe in the wavelength-dispersion mode. Four to six spots per grain were analyzed using an accelerating voltage of 15 kV and beam current of 20 nA. Counting time for background and peak determinations were 5-10 s and 15-40 s, respectively. Crystals were analyzed using the $K\alpha$ lines of Si, Al, Na, K, Ca, Mg, Fe, Mn, Ti, Zn, P, F, Cl with the following standards: hornblende, garnet, ilmenite, gahnite, apatite, scapolite and synthetic $ScTiO_5$. $NbL\alpha$, $TaM\alpha$, $SnL\alpha$ were analyzed using synthetic standards
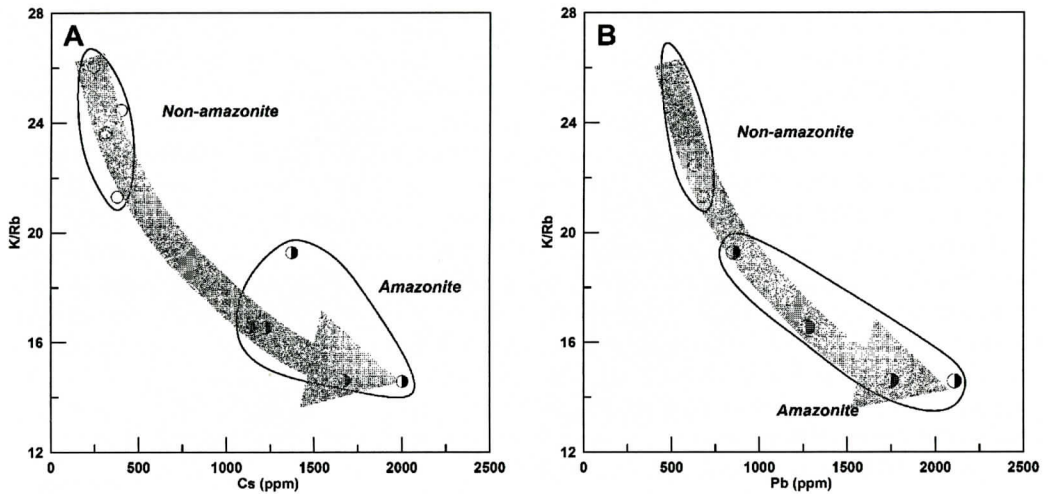
Figure 4. Fractionation trends (shaded arrow) for (a) K/Rb vs Cs and (b) K/Rb vs Pb in microcline-perthite from the McHone pegmatite.

$MnNb_2O_6$, $CaTa_4O_{11}$, and SnO_2, respectively. Data reduction was done using a conventional ZAF correction. The structural formula of tourmaline was calculated on the basis of 31 anions, assuming stoichiometric amounts of B_2O_3 as $(BO_3)^{-3}$ [B=3 *apfu*], H_2O as $(OH)^-$ [i.e. OH+F=4 *apfu*] and Li=3-ΣY *apfu*. Atomic contents of manganocolumbite were calculated on the basis of 24 atoms of oxygen per formula unit.

MINERAL CHEMISTRY

Microcline-perthite

Microcline-perthite from the McHone pegmatite is fairly homogeneous ranging from $Or_{97}Ab_3$ to $Or_{92}Ab_8$. The concentration of Na_2O varies from 0.29 to 0.77 wt.%. Negligible amounts of P (0.0 to 0.26 wt.% P_2O_5) are typical of the McHone K-feldspars. Microcline-perthite attains a maximum concentration of Rb up to 5789 ppm (Table 1) and displays K/Rb values (14.6 to 26.0) much lower than the rest of the Spruce Pine pegmatite population (51.8 to 290.0; Wood, 1996). Cesium values are in the range of 215 to 2003 ppm with the highest values occurring in microcline-perthite from Unit 5. However, the maximum Tl (< 20 ppm) and Ga (27 ppm) values are well below that expect-

ed for evolved lithium-rich pegmatites (cf., Černý et al., 1985; Černý, 2005). McHone microcline-perthite consistently shows elevated Pb concentrations that range from 458 to 2109 ppm and exceed that generally found in most Li-rich pegmatites. White microcline-perthite contains lower Cs and Pb contents and lower K/Rb ratios than green microcline-perthite (Fig. 4).

Muscovite

The limited data set of the McHone muscovite show considerable Fe (4.0 to 5.2 wt.% total Fe as FeO) and MgO (0.30 to 1.46 wt.%) contents. Li_2O calculated from electron microprobe data following the method of Tischendorf et al. (1997) estimate Li contents at less than 0.25 wt.% which is consistent with Li contents from muscovite–class pegmatites (Černý and Burt, 1984). Enrichment in Rb (439 to 3230 ppm), Cs (54 to 352 ppm) and Ga (52 to 131 ppm) is variable, but Rb and Cs are within the range observed from other spodumene-bearing pegmatites (Černý and Burt, 1984; Zhu et al. 2006). Muscovite in the McHone pegmatite is distinctly enriched in Zn (252 to 3949 ppm) relative to most of the pegmatites in the Spruce Pine pegmatite field (55 to 1094; Wood 1996). Muscovite from the late primary units shows el-

Table 1. Representative composition of selected silicates from the McHone pegmatite, North Carolina.

Tourmaline

	Country rock	Unit 5
SiO_2	35.06	35.75
TiO_2	1.27	0.26
B_2O_3	10.19	10.59
Al_2O_3	27.81	36.46
ZnO	0.00	1.26
FeO	12.82	4.78
MnO	0.13	1.32
MgO	5.39	0.54
CaO	1.17	1.07
Na_2O	2.22	2.14
K_2O	0.07	0.03
Li_2O	0.07	1.39
H_2O	3.52	3.32
F	0.00	0.71
O=F	0.00	-0.30
Total	99.72	99.32

T-site	Si	5.979	5.869
	Al	0.021	0.131
	Σ	6.000	6.000
B-site	B	3.000	3.000
Z-site	Al	5.609	5.968
	Ti	0.163	0.032
	Mg	0.228	0.000
	Σ	6.000	6.000
Y-site	Al	0.000	0.955
	Zn	0.000	0.153
	Mg	1.142	0.132
	Mn	0.019	0.184
	Fe^{2+}	1.828	0.656
	Li	0.048	0.918
	Σ	3.037	2.998
X-site	Na	0.734	0.681
	Ca	0.214	0.188
	K	0.015	0.006
	□	0.037	0.125
	Σ	1.000	1.000
	F	0.000	0.369
	OH	4.000	3.631
	Σ	4.000	4.000

Microcline-perthite

	MH-37 (white)	MH-18 (green)
SiO_2	64.32	64.75
TiO_2	0.02	0.02
Al_2O_3	19.04	19.16
FeO	0.03	0.00
MnO	0.01	0.01
MgO	0.00	0.00
CaO	0.01	0.00
Na_2O	0.69	0.57
K_2O	15.25	14.68
P_2O_5	0.06	0.08
Total	99.42	99.28

		MH-37	MH-18
Cs, ppm		242	2006
Rb		3318	5789
Ga		18	35
Pb		518	2109

T-site	Si	2.976	2.985
	Ti	0.001	0.001
	Al	1.038	1.041
	P	0.002	0.003
	Σ	4.017	4.030
M-site	Fe2+	0.001	0.000
	Mn	0.000	0.001
	Mg	0.000	0.000
	Ca	0.000	0.000
	Na	0.062	0.051
	K	0.900	0.864
	Σ	0.963	0.916
	An	0.05	0.00
	Ab	6.43	5.57
	Or	93.52	94.43

Muscovite

	MH-1	MH-42
SiO_2	49.71	48.67
TiO_2	0.20	0.20
Al_2O_3	34.25	34.31
FeO	5.07	4.34
MnO	0.33	0.08
MgO	0.31	1.37
CaO	0.03	0.03
Na_2O	0.23	0.40
K_2O	5.57	6.75
F	0.47	0.33
Total	95.05	95.50
O=F	0.20	0.14
Total	94.86	95.36

		MH-1	MH-42
Cs, ppm		293	54
Rb		3230	440
Zn		3949	252
Ga		126	52
Pb		24	21
Nb		507	96
Ta		35	27

T-site	Si	6.469	6.345
	^{IV}Al	1.531	1.655
	Σ	8.000	8.000
M-site	^{VI}Al	3.722	3.616
	Ti	0.020	0.020
	Fe^{2+}	0.552	0.473
	Mn	0.036	0.009
	Mg	0.060	0.266
	Σ	4.370	4.384
I-site	Ca	0.004	0.004
	Na	0.058	0.101
	K	0.925	1.122
	Σ	0.987	1.227
	Cl	0.000	0.000
	F	0.193	0.136
	Σ	0.193	0.136

B_2O_3, Li_2O, and H_2O for tourmaline calculated based on stoichiometry (31 anions). Muscovite formula calculated on 22 anions.
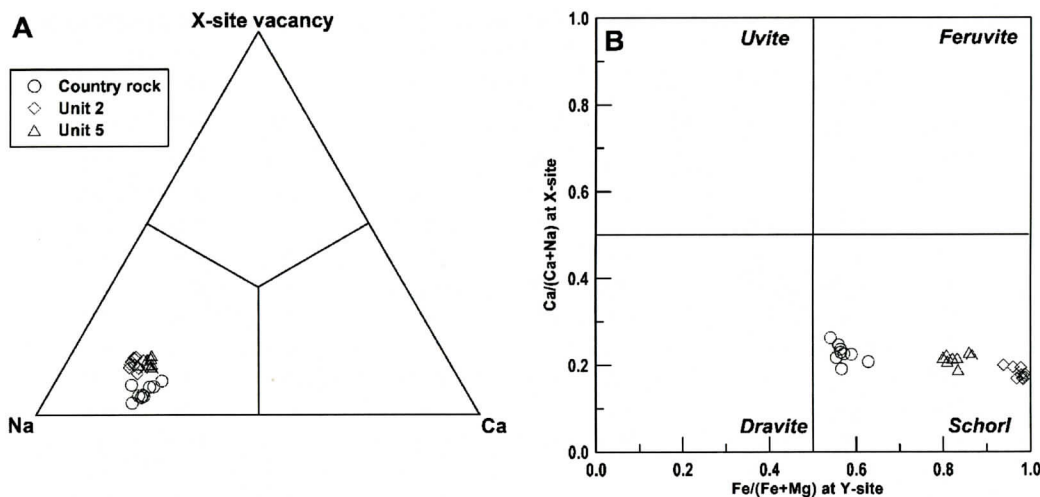
Figure 5. Composition of McHone tourmaline. (A) *X*-site occupancy, (B) Ca/(Ca+Na) *versus* Fe/(Fe+Mg) at the *Y*-site.

evated Nb contents (up to 500 ppm) while Ta contents are low (< 30 ppm) and Sn is absent.

Beryl

Beryl from the McHone pegmatite contains high concentrations of Cs, Rb, and Zn. Cs and Rb values range from 6377 to 37020 ppm and 430 to 532 ppm respectively. Zn concentrations are unusually high for pegmatitic beryl and range from 1058 to 2222 ppm. FeO is low reaching approximately 0.1 wt.% while Na_2O values range between 1.0 and 2.0 wt.%. Cr was analyzed for but not detected. Calculated channel water content ranges from 2.31 to 2.79 wt.% and is typical of beryl from granitic pegmatites (e.g., $1.20 < H_2O^+ < 2.55$ wt.% Deer et al., 1986; Taylor et al., 1992).

Tourmaline

Tourmaline from the McHone pegmatite shows only modest variation in its chemical composition. Most of the variation in composition is due to changes in the Fe/(Fe+Mg) ratio. All compositions plot within the schorl field of the uvite-feruvite-dravite-schorl composition quadrilateral (Selway et al., 1998; Fig. 5). Compositions of tourmaline from the country rock are significantly more Mg-rich [Fe/(Fe+Mg) =

0.54 to 0.63] than tourmaline from the pegmatite [Unit 2: Fe/(Fe+Mg) = 0.94 to 0.99; Unit 5: Fe/(Fe+Mg) = 0.80-0.87]. The *X*-site is dominated by Na cations with limited vacancies (0.03 to 0.16 *apfu*). Schorl from the country rock is typically F-deficient compared to schorl from the pegmatite which contains 0.31 to 0.43 *apfu* F. The maximum calculated Li varies from 0.84 to 0.94 *apfu* in Unit 2 tourmaline and is slightly higher in tourmaline from Unit 5 (up to ~1.03 *apfu*).

Nb, Ta-Minerals

Only two specimens of columbite-group minerals were available for microprobe study and the analyses indicate enrichment in Mn and Nb relative to Fe and Ta (Table 2). The data plot within the manganocolumbite field of the columbite quadrilateral with Mn/(Mn + Fe) values of 0.77 to 0.92 and Ta/(Ta+Nb) of 0.10 to 0.22 (Fig. 6). The analyzed crystals show low amounts of Ti (0.48 to 0.85 wt.% TiO_2) and W (0.48 to 1.34 wt.% WO_6), but no Sc. Sn is erratically distributed throughout the crystals studied and varies from 0 to 0.85 wt.% SnO_2.

Electron-microprobe analyses of microlite are given in Table 2. Oxide totals vary between 88 and 94 wt.% and the low sums suggest the presence of structural H_2O. Because of the pos-

Table 2. Representative composition of manganocolumbite and microlite from the McHone pegmatite, North Carolina.

	Manganocolumbite				Microlite		
	McHone 5b	McHone 31			McHone 39	McHone 5	McHone 25
Na_2O	0.02	0.00		Na_2O	4.31	2.78	3.84
CaO	0.15	0.41		CaO	12.84	11.45	12.82
FeO	1.60	4.11		FeO	0.03	0.07	0.04
MnO	17.03	14.86		MnO	0.17	0.45	0.28
MgO	0.00	0.00		MgO	0.00	0.00	0.00
TiO_2	0.62	0.56		TiO_2	2.06	2.10	2.33
Nb_2O_5	55.38	66.16		Nb_2O_5	20.30	19.72	24.36
Ta_2O_5	24.02	12.22		Ta_2O_5	51.04	49.48	44.07
SnO_2	0.11	0.85		SnO_2	0.00	0.00	0.00
WO_3	1.24	0.32		WO_3	0.00	0.00	0.00
UO_2	0.01	0.00		UO_2	1.07	1.10	2.17
Total	100.18	99.49		F	2.73	2.00	2.47
					94.54	89.14	92.38
				O=F	1.15	0.84	1.04
				Total	93.39	88.30	91.34

Cations based on 24 oxygens					Normalized on B-site occupancy=2		

|								
A-site	Na	0.00	0.00	A-site	Na	0.68	0.46	0.60
	Ca	0.04	0.12		Ca	1.12	1.05	1.11
	Fe	0.32	0.80		U	0.02	0.02	0.04
	Mn	3.56	3.00		Fe	0.00	0.00	0.00
	Mg	0.00	0.00		Mn	0.01	0.03	0.02
					Mg	0.00	0.00	0.00
B-site	Ti	0.12	0.12					
	Nb	6.20	7.08	B-site	Ti	0.13	0.14	0.14
	Ta	1.64	0.80		Nb	0.74	0.76	0.89
	Sn	0.00	0.08		Ta	1.13	1.16	0.97
	W	0.08	0.04		Sn	0.00	0.00	0.00
	U	0.00	0.00		W	0.00	0.00	0.00
	Total	12.00	11.96					
					F	0.70	0.55	0.63
					Total	4.53	4.18	4.41
	Mn/(Mn+Fe)	0.92	0.79					
	Ta/(Ta+Nb)	0.21	0.10		Mn/(Mn+Fe)	0.85	0.87	0.86
					Ta/(Ta+Nb)	0.60	0.60	0.52
	A site	3.92	3.92					
	B site	8.04	8.08		A site	1.83	1.56	1.77
					B site	2.00	2.00	2.00
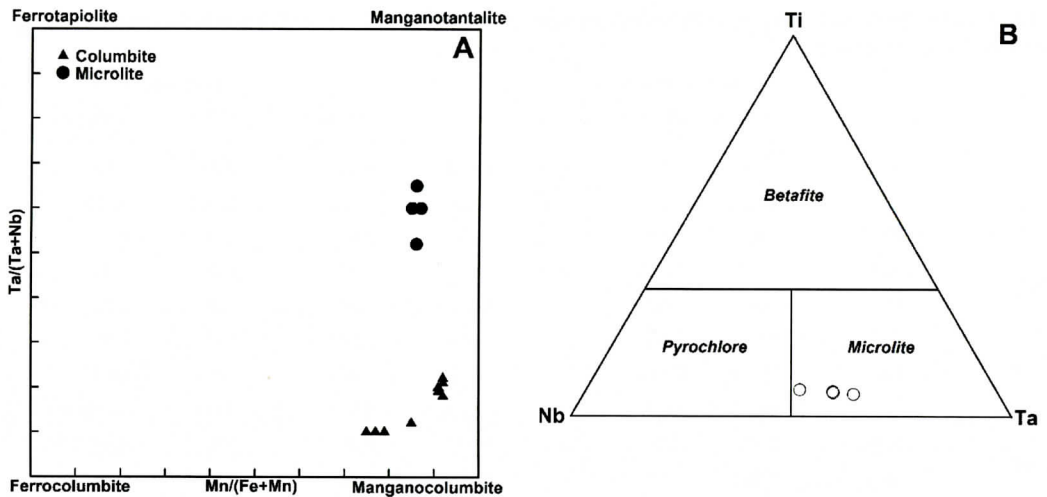
Figure 6. (a) Columbite quadrilateral and (b) microlite ternary diagram.

sible occurrence of X-site vacancies, formula calculations are based on the normalization of the fully occupied B-site to 2 cations per formula unit. The major cations occurring at the A-site are Ca and Na, with Ca always greater than Na. Most analyses show a modest enrichment in U (up to 2.17 wt.% UO_2) and typically very little Pb. The B-site chemistry is dominated by Ta and Nb with limited substitution by Ti, but all contain Ta>Nb and 2Ti < (Nb+Ta) (Fig 6). Ta/(Ta+Nb) values are consistently higher in microlite than in manganocolumbite.

RARE-ELEMENT ENRICHMENT IN THE MCHONE PEGMATITE

The present study reveals a level of Rb and Cs enrichment in the McHone pegmatite that is unmatched by most pegmatites of the Spruce Pine district. The McHone amazonite attains Rb and Cs values that approach those of some of the most fractionated LCT pegmatites known (e.g., Tanco, Manitoba; Varuträsk, Sweden). This is noteworthy since in most instances high Rb and Cs contents are generally not encountered in microcline-perthite (including the amazonite variety) from NYF pegmatites. Examples of microcline-perthite from NYF pegmatites that contain exceptionally high Rb contents include some pegmatites from the Pikes Peak batholith with maximum Rb content

of 5315 ppm, but only 30 ppm Cs (Foord and Martin, 1979) and blocky K-feldspar from the Falun pegmatite field, Sweden with 810 to 1687 ppm Rb, and low Cs (up to 61 ppm; Smeds 1994). The Rb and Cs contents of microcline-perthite from the REE-enriched Landsverk pegmatite were comparable to the Falun field (Taylor et al., 1960).

Muscovite from the McHone pegmatite is also enriched in Rb and Cs, although its overall concentration is considerably lower than anticipated for lithium-rich pegmatites. Little data exist on the Rb and Cs contents of muscovite from NYF pegmatites largely due to the fact that muscovite is generally absent in pegmatites from this geochemical family. Smeds (1994) reports Cs contents in muscovite up to 714 ppm in the Falun pegmatites, but most have less than 50 ppm. A single ferroan muscovite from a miarolitic pegmatite in the Pikes Peak batholith contained approximately 1000 ppm Cs (Foord et al., 1995). The Rb and Cs concentrations of the McHone muscovite are more typical of values reported for muscovite-class pegmatites than those from the LCT affiliation (Černý and Burt, 1984). The high Cs values observed in the McHone beryl are consistent with Cs values found in beryl from highly evolved LCT pegmatites. Extreme Cs enrichment in beryl from NYF pegmatites is rarely known to occur above 1000 ppm (e.g., Pezzotta et al., 2005). On the

other hand, "mixed" NYF+LCT type pegmatites such as the Sakavalana pegmatite, Madagascar, display extreme Cs enrichment in the form of the Cs mineral pezzottaite (Laurs et al., 2003).

Pb is a prominent, but highly variable element that frequently resides in the structure of pegmatitic K-feldspar. In comparing the Pb content of K-feldspar from different pegmatite types, Pb concentrations in K-feldspar from LCT pegmatites are generally low relative to those from NYF pegmatites. In LCT pegmatites, Pb values in microcline-perthite are often < 200 ppm, even for the most evolved spodumene-bearing pegmatites (e.g., Black Hills district, South Dakota [4 to 80 ppm] - Shearer et al., 1985; Yellowknife field, NWT [3 to 91 ppm] - Meintzer, 1987; Little Nahanni group – [22 to 122 ppm] – Mauthner, 1996; Sebago group, Maine [3 to 89 ppm] – unpublished data of M. Wise). Little data exist for the Pb contents of K-feldspar from muscovite – rare-element class pegmatites although Wood (1996) reported 148 to 233 ppm Pb in K-feldspar from selected pegmatites of the Spruce Pine district. Heier (1962) noted that Pb was enriched in K-feldspars from the most evolved NYF pegmatites in southern Norway, contrary to being captured early in the fractionation process. Larsen (2002) observed Pb concentrations within K-feldspar from the Evje-Iveland and Froland pegmatite fields, Norway up to 350 ppm. By comparison, microcline-perthite from the NYF pegmatite field at Falun, Sweden contained maximum Pb concentrations of 56 (Smeds (1994). Foord and Martin (1979) reported a general enrichment trend in Pb contents from core to rim in some microcline-perthite-amazonite crystals. Amazonitic K-feldspar of NYF affiliation typically contains the highest amount of Pb ranging up to 13500 ppm (Foord and Martin, 1979). Extremely high Pb concentrations (up to 18000 ppm) were measured in a green orthoclase from anatectic pegmatites at Broken Hill, Australia (Stevenson and Martin, 1986). The high Pb content of the McHone microcline-perthite is atypical of pegmatites affiliated with LCT systems and appears to be more like granitic pegmatites that were generated by the A-nitic pegmatites that were generated by the A-type granite-NYF pegmatite association.

Muscovite and beryl from the McHone pegmatite are enriched in Zn relative to other Spruce Pine pegmatites (unpublished data of M. Wise) and other muscovite class pegmatites (e.g., Černý and Burt, 1984; Cocker, 1992). Zn values of the McHone muscovite are more typical of micas from anorogenic pegmatites with NYF-type signatures (Černý and Burt, 1984). The accumulation and behavior of Zn in beryl in granitic pegmatites is more difficult to characterize due to the fact that its normal concentrations are very low, and because the element is typically not sought after during routine analysis. The Zn values of the McHone beryl far exceed that from any reported beryl, especially those from LCT pegmatites. Beryl from beryl-columbite, beryl-columbite-phosphate and spodumene-bearing pegmatites of the LCT Sebago Pegmatite group collectively shows Zn values of 11 to 575 ppm (unpublished data of the authors) but no systematic trends were observed. Tappen and Smith (2003) found Zn values ranging from 79 to 140 ppm in beryl from the Crabtree pegmatite in the Spruce Pine district. Zn values comparable to those found in the McHone pegmatite have been reported from only a few localities. Red beryl occurring in anorogenic, rift-related rhyolite from the Wah Wah Mountains, Utah (Christiansen et al., 1986) was reported to contain up to 700 ppm Zn by Shigley and Foord (1984) and pegmatitic beryl associated with anorogenic granites in the Eastern Desert of Egypt gave Zn values of 747 to 1122 ppm (Surour et al., 2002).

The compositions of Nb,Ta oxide minerals in the McHone pegmatite indicate a high degree of Ta enrichment in the later stage of pegmatite consolidation. The high Ta/Nb values exhibited by microlite are consistent with data of Nb-Ta minerals found in highly evolved LCT pegmatites. Furthermore, the data for manganocolumbite are consistent with F-rich, lepidolite-bearing pegmatites of the LCT association. However, it should be noted that Mn, Nb-dominant members of the columbite group are also known to characterize some NYF pegmatites and extreme Ta enrichment has been observed in some MSREL-REE type pegmatite popula-

tions such as the Mattawa pegmatite district (Ercit 1992).

GENESIS OF MIXED NYF-LCT SIGNATURE

The mineralogy of the McHone pegmatite combines features of both LCT and NYF rare-element pegmatites. The presence of spodumene, beryl and pollucite suggest an affiliation with the LCT geochemical family of granitic pegmatites, whereas the occurrence of amazonite and fluorite is more typical of pegmatite populations associated with NYF suites. The juxtaposition of LCT and NYF mineralization within a single pegmatite body does not allow for an unambiguous genetic classification of the McHone pegmatite. Moreover, the derivation of the mixed NYF-LCT geochemistry in granitic pegmatites on the whole has not been thoroughly investigated due in part to the lack of a suitable number of well-documented examples in which to develop meaningful generalizations. Few pegmatites are known to exhibit such dramatic "mixed" type geochemical signature [e.g., Heftejern pegmatite, Tørdal, Norway: Bergstøl and Juve (1988); O'Grady batholith, NWT, Canada: Ercit et al. (2003); Anjanabonoina and Sakavalana pegmatites and the Ambositra district, Madagascar: De Vito et al., (2006); Hawthorne et al. 2004; Pezzotta (2001)]. Černý (1991b), Černý and Ercit (2005), and Martin and De Vito (2005) discuss possible scenarios for the genesis of "mixed" or "hybrid" NYF-LCT pegmatites and speculate that the mixed signature may have originated from: (i) the contamination of a NYF pegmatite melt by digested supracrustal rocks, (ii) a partially depleted crustal protolith, (iii) a mixed range of depleted and undepleted protoliths that were affected by anatexis, and (iv) the overprinting of a NYF assemblage by an LCT assemblage during a hydrothermal stage.

The chemical composition of a pegmatite melt may be modified by the introduction of metasomatic fluids from an outside source, but this style of component exchange is somewhat difficult to prove. Taylor et al. (1979) noted that the isotopic signature of the host rock is pre-served in the border zone of pegmatites that experienced an influx of metasomatic fluids. Thomas and Spooner (1988) documented the occurrence of methane in fluid inclusions from the border zone of the Tanco pegmatite and attributed its presence to the influx of fluids from the host amphibolite. Evidence for the proposed infiltration of Mg- and Fe-bearing fluids derived from country rock is exhibited by the lengthwise perpendicular growth of tourmaline (*comb structure*) in the outermost pegmatite zones (London, 1992). In a similar manner, the infiltration of Fe-, Cr- and/or V-enriched fluids derived from mafic host rocks into a Be-enriched pegmatite melt may produce emeralds near the contact (Laurs et al., 1996, Tappen and Smith, 2003). In spite of the occurrence of tourmaline and beryl in the McHone pegmatite, no comb structure texture or emerald was observed which implies that there was no influx of components from the schist into the pegmatite. On the other hand, there does appear to be some evidence to support the migration of components out of the pegmatite and into the host rocks. Some B clearly escaped the pegmatite resulting in the crystallization of dravitic schorl in the schist immediately near the pegmatite contact. The unaltered country rock shows considerable enrichment in some "pegmatophile" elements, most notably Rb and Cs. However, both elements show a decrease in concentration with increasing distance from the pegmatite contact suggesting that Rb and Cs probably migrated from the pegmatite into the host rock. Thus it appears that the movement of components via fluid migration was largely unidirectional.

The incorporation and digestion of host rocks may be viable mechanisms for modifying the original bulk composition of the McHone pegmatite melt, a scenario that has been documented in the Tørdal granite pegmatite veins and used to explain the enrichment of Sn and Sc and its mixed NYF-LCT signature (Bergstøl and Juve, 1988). Small remnants of country rock (the largest approximately 65 x 30 cm) are present in the McHone pegmatite and show modest degrees of assimilation. The assimilated schist should contribute significant amounts of Fe and Mg in addition to rare alkalis (e.g., Cs)
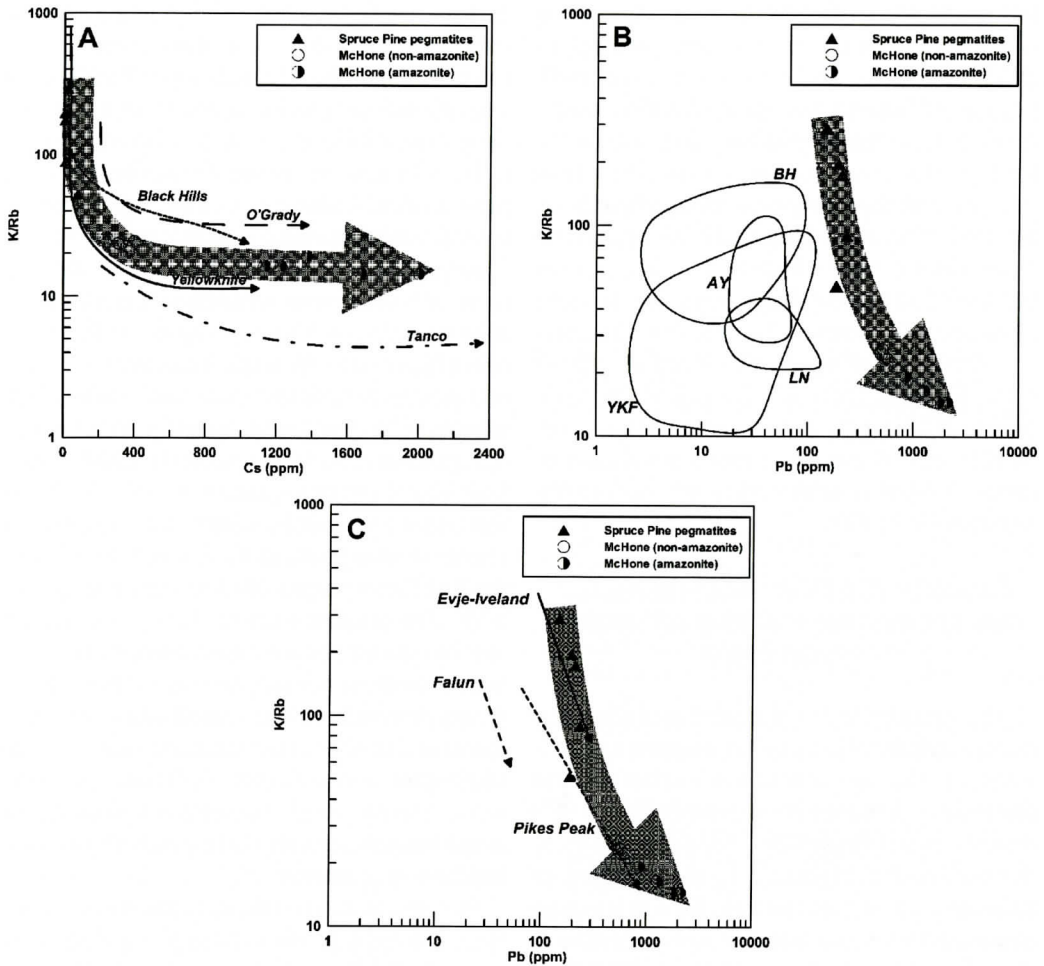
Figure 7. Cs and Pb contents of microcline-perthite from spodumene-bearing LCT-family pegmatites (a and b) and NYF-affiliated pegmatites (c). Data for LCT microcline-perthites: Black Hills pegmatite field (BH), South Dakota - Shearer et al., 1985; Yellowknife field (YKF), Northwest Territories, Canada – Meintzer, 1987; Aylmer Lake field (AY), Northwest Territories, Canada – Tomascak, 1991; Little Nahanni field (LN), Northwest Territories, Canada – Mauthner, 1996; and Tanco, Manitoba, Canada – Černý, 1994. Arrows in (c) indicate fractionation trend for microcline-perthite. Evje-Iveland and Falun, Norway trends derived from the data of Larsen (2002) and Smeds (1994), respectively. Pikes Peak, Colorado trend from unpublished data of M.Wise. Symbols: triangles – Spruce Pine pegmatites, circles – McHone pegmatite.

as a result of the breakdown of biotite. This is obviously not the case, as the mineralogy of the pegmatite is mostly devoid of ferromagnesian minerals. We conclude therefore, that the trace element chemistry of the host rock and fluids derived from it probably had minimal effect on the original melt composition of the pegmatite and in all probability did not impart a LCT or NYF signature on a previously pristine melt.

In the course of this study, it became clear to us that none of the above scenarios could adequately explain the mixed NYF-LCT signature of the McHone pegmatite. In fact, our data suggest an alternative mechanism that has been considered for the development of mixed type geochemistry: magmatic fractionation. The majority of geochemical studies of granitic pegmatites have focused on those of LCT affiliation

and the behavior of many trace elements during pegmatite evolution has been well established (cf. Černý et al., 1985). By comparison, NYF pegmatites have not been studied with the same detail and we know relatively little about the fractionation trends of rare alkalis, high-field strength and light lithophile elements in NYF systems. It has been noted that NYF pegmatites do exhibit LCT-style fractionation (e.g., Černý and Ercit 2005) and in some cases may be quite advanced in this respect (Smeds, 1994; Foord et al., 1995). Whether an NYF-type pegmatite melt can fractionate to give rise to an "end-member" LCT-type mineral assemblage is debatable, nevertheless the process should not be arbitrarily dismissed as a viable process of NYF pegmatite evolution.

CLASSIFICATION AND GENETIC IMPLICATIONS OF THE MCHONE PEGMATITE

The Spruce Pine pegmatite population carries a weak but distinct REE signature as evident by the occurrence of allanite and samarskite as prominent accessory phases in a number of the pegmatites. Niobium is locally enriched and is expressed by the presence of columbite rather than tantalite. Be and B mineralization is widespread but not particularly abundant, whereas, P, Li and Cs enrichment is nearly absent throughout the field. With the exception of the McHone pegmatite, F concentrations are low as demonstrated by the general absence of fluorite, topaz, lepidolite and amblygonite. The Spruce Pine field is best characterized as a member of the REE-enriched subclass of the muscovite - rare-element class (MSREL-REE) of pegmatites which may carry a modest NYF-like signature (Černý and Ercit, 2005).

The McHone pegmatite is an anomaly compared to the rest of the Spruce Pine pegmatites. The occurrence of Be-, Li- and B-minerals in the McHone pegmatite establishes it as a member of the MSREL-Li subclass which tends to have LCT-like characteristics. On the other hand, the occurrence of fluorite and amazonite in the pegmatite is consistent with granitic peg-

matites displaying NYF-like tendencies and thus the pegmatite could be considered belonging to the MSREL-REE subclass. The McHone pegmatite is unique in its mixed geochemical signature within the Spruce Pine pegmatite field. The mineral chemistry of the McHone pegmatite indicates an advanced degree of rare-element fractionation compared to other Spruce Pine pegmatites. In particular, blocky microcline-perthite shows considerable enrichment in rare alkalis, as illustrated by the K/Rb vs Cs plot (Fig. 7) and displays fractionation levels that are comparable to spodumene-bearing pegmatites belonging to LCT-family granite-pegmatite suites. The behavior of Pb in K-feldspar from the McHone pegmatite is very similar to fractionation patterns observed in other NYF systems and suggests that chemical evolution of the Spruce Pine pegmatites may be more akin to NYF-like systems than LCT (Fig. 7). Rb, Cs and Zn data for Spruce Pine muscovite also correlates well with mica chemistry from NYF family pegmatites. Although the absolute abundances of the above trace elements may indicate levels consistent with both NYF and LCT systems, their overall behavior during pegmatite evolution most closely corresponds to the NYF family of pegmatites.

In consideration of the tectonic affiliation of NYF and LCT systems, there is a general tendency for LCT systems to be syn- to late-tectonic, and for NYF systems to be largely post- to anorogenic in character (Martin 1989; Martin and DeVito, 2005; Černý and Ercit, 2005). However, exceptions do exist and caution must be exercised when attempting to make any genetic connection between tectonic setting and pegmatite geochemistry. The Chalk Mountain granodiorite that is parental to the Spruce Pine pegmatites, crystallized within a syntectonic setting and its peraluminous chemistry might lead one to expect pegmatites with a LCT geochemical signature (Černý, 1991b; Černý and Ercit, 2005).

Wood (1996) has determined that the Spruce Pine pegmatites were derived from the differentiation of magma of granodiorite composition. Normative analyses indicate that the granodiorite is peraluminous and the chemical data plot within

the volcanic arc granite field on the widely used tectonic-discrimination plots of Pearce et al. (1984). McSween et al. (1991) considered the peraluminous nature of the Spruce Pine Plutonic Suite group to indicate an origin, in, or contaminated by, continental crust and that the granodiorites were comparable to subduction-related magmas. Miller et al. (2006) advocated a tectonic model that involves input from upwelling hot asthenosphere and subsequent melting of deep-crustal accretionary wedge rocks during subduction to form the Acadian plutons, such as the Chalk Mountain granodiorite, in the Eastern Blue Ridge Province. The crustal source rocks for these plutons were presumably similar to rocks of the Ashe Metamorphic Suite. If, as suggested above, the Chalk Mountain pluton was generated in a subduction-related setting, then partial melts may have possibly been modified by enrichment in Na, B, Li, Rb and Cs that was inherited from seawater, chlorite and clay minerals released from the subducted slab. This plus input from a mantle-derived magma might result in a magma with both S- and A-type imprints. At this time, detailed petrologic and isotopic studies on the Chalk Mountain pluton and neighboring Spruce Pine Plutonic Suite granitoids are not available and are not within the scope of this study.

The parental granodiorite magma probably derived its mixed character via the melting of lower crust comprised of a mixed range of depleted and undepleted protoliths. In light of the tectonic model for Acadian plutonism in the Eastern Blue Ridge Province proposed by Miller et al. (2006), the general geochemical signature of the granodiorite-pegmatite system of the Spruce Pine pegmatite district and the trace element evolution of the McHone pegmatite, we propose that the mineralogy of the McHone pegmatite reflects advanced fractionation from a parental melt with a more-or-less original mixed NYF-LCT signature.

ACKNOWLEDGEMENTS

REFERENCES

Bergstøl, S., Juve, G., 1988. Scandian ixiolite, pyrochlore and bazzite in granite pegmatite in Tørdal, Telemark, Norway: a contribution to the mineralogy and geochemistry of scandium and tin. Mineral. Petrol. 38, 229-243.

Berquist, P.J., Fisher, C.M., Miller, C.F., Wooden, J.L., Fullagar, P.D., Loewy, S.L., 2005. Geochemistry and U-Pb zircon geochronology of Blue Ridge basement, western North Carolina and eastern Tennessee: Implications for tectonic assembly. in Hatcher, R.D., Jr., and Merschat, A.J., eds., Blue Ridge Geology Geotraverse East of the Great Smoky Mountains National Park, Western North Carolina. North Carolina Geol. Surv., Carolina Geol. Soc. Ann. Field Trip Guidebook, p. 33-44.

Brobst, D.A., 1962. Geology of the Spruce Pine district, Avery, Mitchell and Yancey Counties, North Carolina. U.S. Geol. Surv. Bull. 1122-A, 26 p.

Butler, J.R., Goldberg, S.A., Mies, J.W., 1987. Tectonics of the Blue Ridge west of the Grandfather Mountain window, North Carolina and Tennessee. Geol. Soc. Am. Abstracts with Programs, v. 19, p. 77.

Cameron, E.N., Jahns, R.H., McNair, A.H., Page, J.J., 1949. Internal structure of granitic pegmatites. Econ. Geol. Monogr 2.

Černý, P., 1991a. Rare-element granitic pegmatites, Part 1: Anatomy and internal evolution of pegmatite deposits. Geosci. Can. 18, 49-67.

Černý, P., 1991b. Fertile granites of Precambrian rare-element pegmatite fields: is geochemistry controlled by tectonic setting or source lithologies? Precambr. Res. 51, 429-468.

Černý, P., 1994. Evolution of feldspars in granitic pegmatites. In I.Parsons, ed., *Feldspars and Their Reactions*. NATO ASI Series C, 421, 501 40.

Černý, P., 2005. The Tanco rare-element pegmatite deposit, Manitoba; regional context, internal anatomy, and global comparisons. In: Linnen, R.L. & Samson, I.M. (eds.) Rare-element Geochemistry and Mineral Deposits. Short Course Notes, Geol. Assoc. Can. 17, 127-158.

Černý, P., Burt, D.M., 1984. Paragenesis, crystallochemical characteristics, and geochemical evolution of micas in granite pegmatites: In: Bailey, SW (ed) Reviews in mineralogy, vol 13, Micas. Mineralogical Society of America, 257-297.

Černý, P., Ercit, T.S., 2005. The classification of granitic pegmatites revisited. Can. Mineral. 43, 2005-2026.

Černý, P., Meintzer, R.E., Anderson, A.J., 1985. Extreme fractionation in rare-element granitic pegmatites: selected examples of data and mechanisms. Can. Mineral. 23, 381-421.

Christiansen, E.H., Burt, D.M., and Sheridan M.F., 1986, The geology of topaz rhyolites from the western United States: Geol. Soc. Am. Spec. Paper 205, 82 p.

Cocker, M.D., 1992. Geochemistry and economic potential of pegmatites in the Thomaston-Barnesville district, Georgia. Georgia Department of Natural Resources, Geologic Report 7, 81 pp.

Deer, W.A., Howie, R.A., Zussman, J., 1986. Disilicates and ring silicates, in Rock-forming minerals, 1A. London, Longman, 372-409.

De Vito, C., Pezzotta, F., Ferrini, V., Aurisicchio, C., 2006. Ti-Nb-Ta oxides in the Anjanabonoina pegmatite, central Madagascar: a record of magmatic and postmagmatic events. Can. Mineral. 44, 87-104.

Ercit, T.S. (1992): Oxide mineralogy of the Mattawa pegmatite district – extreme Ta fractionation for muscovite-class pegmatites. *Geol. Assoc. Can. – Mineral. Assoc. Can., Program Abstr.* 17, A32.

Ercit, T.S., Groat, L.A., Gault, R.A., 2003. Granitic pegmatites of the O'Grady batholith, N.W.T., Canada: a case study of the evolution of the elbaite subtype of rare-element granitic pegmatites. Can. Mineral. 41, 117-137.

Feiss, P.G., Maybin, A.H., III, Riggs, S.R., Grosz, A.E. 1991. Mineral resources of the Carolinas. *in* The Geology of the Carolinas (Horton, J.W., Jr. and Zullo, V.A., eds). The University of Tennessee Press.

Foord, E.E., Martin, R.F., 1979. Amazonite from the Pikes Peak batholith. Mineralogical Record, 10, 373-384.

Foord, E.E., Černý, P., Jackson, L.L., Sherman, D.M., Eby, R.K., 1995. Mineralogical and geochemical evolution of micas from miarolitic pegmatites of the anorogenic Pikes Peak batholith, Colorado. Mineral. Petrol. 55, 1-26.

Goldberg, S.A., Butler, J.R., Mies, J.W., 1986. Subdivision of the Blue Ridge thrust complex, western Carolina and adjacent Tennessee. Geol. Soc. Am. Abstracts with Programs, v. 18, p. 616-617.

Goldberg, S.A., Butler, J.R., Mies, J.W., Traupe, C.H., 1989. The southern Appalachian orogen in northwestern North Carolina and adjacent states. International Geological Congress Field Trip T365 Guidebook. American Geophysical Union, Washington, D.C. 55 p.

Goldberg, S.A., Butler, J.R., Traupe, C.H., Adams, M.G., 1992a. The Blue Ridge thrust complex northwest of the Grandfather Mountain window, North Carolina and Tennessee, *in* Dennison, J.M., and Stewart, K.G., eds, Geologic field guides to North Carolina and vicinity. Chapel Hill, North Carolina, Department of Geology, University of North Carolina at Chapel Hill, Geologic Guidebook No. 1, p. 213-233.

Goldberg, S.A., Trupe, C.H., Adams, M.G., 1992b. Pressure-temperature-time constraints for a segment of the Spruce Pine thrust sheet, North Carolina Blue Ridge. Geol. Soc. Am. Abstracts with Programs, v. 24, 17.

Goldberg, S.A., Dallmeyer, R.D., 1997. Chronology of Paleozoic metamorphism and deformation in the Blue Ridge thrust complex, North Carolina and Tennesssee. Am. J. Sci. 297, 488-526.

Hatcher, R. D. Jr., 1978. Tectonics of the western Piedmont and Blue Ridge: review and speculation: Am. J. Sci. 278, 276-304.

Hatcher, R. D. Jr., 1989. Tectonic synthesis of the U.S. Appalachians. *in* Hatcher, R.D., Jr., Thomas, W.A. and Viele, G.W., eds., The Geology of North America, The Appalachian-Ouachita Orogen in the United States, vol. F-2 p.511-535.

Hawthorne, F.C., Cooper, M.A., Simmons, W.B., Falster, A.U., Laurs, B.M., Armbruster, T., Rossman, G.R., Peretti, A., Günter, D., Grobéty, B. 2004. Pezzottaite, $Cs(Be_2Li)Al_2Si_6O_{18}$, A spectacular new beryl-group mineral from the Sakavalana pegmatite, Fianarantsoa province, Madagascar. vMineral. Rec. 35, 369-378.

Heier, K.S., 1962. Trace elements in feldspars- a review. Norsk Geol. Tidsskr. 42, 415-454.

Heinrich, E.W., 1950. Accessory sulfides in North Carolina pegmatites. Am. J. Sci. 248, 112-123.

Johnson, B.J., Miller, B.V., Stewart, K.G., 2001. The nature and timing of Acadian deformation in the Southern Appalachian Blue Ridge constrained by the Spruce Pine plutonic suite, western North Carolina. Geol. Soc. Am. Abstracts with Programs, v.33, no. 2, p 30.

Kish, S.A., 1989. Paleozoic thermal history of the Blue Ridge in southwestern North Carolina- constraints based upon mineral cooling ages and the ages of intrusive rocks. Geol. Soc. Am. Abstracts with Programs, v. 21, 45.

Larsen, R.B., 2002, The distribution of rare-earth elements in K-feldspar as an indicator of petrogenetic processes in granitic pegmatites: examples from two pegmatite fields in southern Norway. Can. Mineral. 40, 137-151.

Laurs, B.M, Dilles, J.H., Snee, L.W., 1996. Emerald mineralization and metasomatism of amphibolite, Khaltaro granitic pegmatite-hydrothermal vein system, Haramosh Mountains, Northern Pakistan. Can. Mineral. 34, 1253-1286.

Laurs B.M., Simmons W.B., Rossman G.R., Quinn E.P., McClure S.F., Peretti A., Armbruster T., Hawthorne, F.C., Falster, A.U., Günther D., Cooper, M.A. and Grobéty B. 2003 Pezzottaite from Ambatovita, Madagascar: a new gem mineral. Gems & Gemology, 39, 284-301.

Lesure, F.G., 1968. Mica deposits of the Blue Ridge in North Carolina. U.S. Geol. Surv. Prof. Pap. 577, 124 pp.

London, D., 1992. The application of experimental petrology to the genesis and crystallization of granitic pegmatites. Can. Mineral. 30, 499-540.

London, D., 2005. Granitic pegmatites : an assessment of current concepts and directions for the future. Lithos 80, 281-303.

London, D., 2008. *Pegmatites*. The Canadian Mineralogist Special Publication 10, Quebec, Canada, 347 pp.

Martin, R.F. 1989. Metasomatic "ground preparation" and

the origin of anorogenic granites. Symp. Precambrian Granitoids, Helsinki, Abstr., 87.

Martin, R.F., De Vito, C., 2005. The patterns of enrichment in felsic pegmatites ultimately depend on tectonic setting. Can. Mineral. 43, 2027-2048.

Mauthner, M.H.F., 1996. Mineralogy, geochemistry, and geochronology of the Little Nahanni Pegmatite Group, Logan Mountains, southwestern Northwest Territories. MSc. thesis, Univ. of British Columbia, Vancouver, 192 pp. (unpublished).

McSween, H.Y., Jr., Speer, J.A., Fullagar, P.D., 1991. Plutonic rocks, in Horton, J.W. and Zullo, V.A., eds., The geology of the Carolinas: Carolina Geological Society Fiftieth Anniversary Volume, 109-126.

Meintzer, R.E., 1987, The mineralogy and geochemistry of granitoid rocks and related pegmatites of the Yellow-knife pegmatite field, Northwest Territories: [Ph.D., Thesis], Manitoba, University of Manitoba, 708 p. (unpublished)

Miller, B.V., Fetter, A.H., Stewart, K.G., 2006. Plutonism in three orogenic pulses, Eastern Blue Ridge Province, southern Appalachians. Geol. Soc. Am. Bull. 118, 171-184.

Miller, C.F., Fullagar, P.D., Sando, T.W., Kish, S.A., Solomon, G.C., Russell, G.S., Wood Steltenpohl, L.F., 1997. Low-potassium, trondhjemitic to granodioritic plutonism in the eastern Blue Ridge, southwestern North Carolina-northeastern Georgia, in Sinha, A.K., Whalen, J.B., and Hogan, J.P., editors, The nature of magmatism in the Appalachian orogen: Geol. Soc. Am. Memoir 191, p. 235-254.

Miller, C.F., Hatcher, R.D., Jr., Harrison, T.M., Coath, C.D., Gorisch, E.B., 1998. Cryptic crustal events elucidated through zone imaging and ion microprobe studies of zircon, southern Appalachian Blue Ridge, North Carolina-Georgia: Geology, v. 26, p. 419-422.

Olson, J.C., 1944. Economic geology of the Spruce Pine district, North Carolina. North Carolina Department of Conservation And Development, Mineral Resources Division Bulletin 43, 67 p.

Pearce, J.A., Harris, N.B.W., Tindle, A.G., 1984. Trace element discrimination diagrams for the tectonic interpretation of granitic rocks. J. Petrol. 25, 956-993.

Pezzotta, F., 2001. Madagascar, a mineral and gemstone paradise. Extralapis English 1, 97 p.

Pezzotta, F., Diella, V., Guastoni, A. 2005. Scandium silicates from the Baveno and Cuasso al Monte NYF-granites, Southern Alps (Italy): Mineralogy and genetic inferences. Am. Mineral. 90, 1442-1452.

Rankin, D.W., 1975. The continental margin of eastern North America in the southern Appalachians: The opening and closing of the Proto-Atlantic Ocean: Am. J. Sci. 275-A, 298-336.

Rankin, D.W., Espenshade, G.H., Shaw, K.W., 1973. Stratigraphy and structure of the metamorphic belt in north-eastern North Carolina and southwestern Virginia: a study from the Blue Ridge across the Brevard fault zone to the Sauratown Mountains anticlinorium. Am. J. Sci.

273-A, 1-40.

Selway, J.B., Černý, P., Hawthorne, F.C., 1998. Feruvite from lepidolite pegmatites at Red Cross Lake, Manitoba. Can. Mineral. 36, 433-439.

Shearer, C.K., Papike, J.J., Laul, J.C., 1985. Chemistry of potassium feldspar from three zoned pegmatites, Black Hills, South Dakota: implications concerning pegmatite evolution. Geochim. Cosmochim. Acta 49, 663-673.

Shigley, J.E., Foord, E.E., 1984. Gem-quality red beryl from the Wah Wah Mountains, Utah. Gems Gemol. 20, 208-221.

Smeds, S.-A., 1994. Zoning and fractionation trends of a peraluminous NYF granitic pegmatite field at Falun, south-central Sweden. GFF 116, 175-184.

Stevenson, R.K., Martin, R.F., 1986. Implications of the presence of amazonite in the Broken Hill and Geco metamorphosed sulfide deposits. Can. Mineral. 24, 729-745.

Stewart, K.G., Adams, M.G., Trupe, C.H., 1997. Paleozoic structural evolution of the Blue Ridge thrust complex, western North Carolina. in Stewart, K.G., Adams, M.G. and Trupe, C.H., eds., Paleozoic structure, metamorphism, and tectonics of the Blue Ridge of western North Carolina. Carolina Geological Society Field Trip and Annual Meeting, p. 21-31.

Surour, A.A., Takla, M.A., Omar, S.A. 2002. EPR spectra and age determination of beryl from the Eastern Desert of Egypt. Annals Geol. Surv. Egypt. 55, 389-400.

Tappen, C.M., Smith, M.S., 2003. The Crabtree pegmatite, Spruce Pine District, North Carolina: mineralization and host rock relationships. Southeastern Geology, 41, 201-223.

Taylor, B.E., Foord, E.E., Friedrichsen, H., 1979. Stable isotope and fluid inclusion studies of gem-bearing granitic pegmatite-aplite dikes, San Diego County, California. Contrib. Mineral. Petrol., 68, 187-205.

Taylor, R.P., Fallick, A.E., Breaks, F.W., 1992. Volatile evolution in Archean rare-element granitic pegmatites: evidence from the hydrogen-isotopic composition of channel H_2O in beryl. Can. Mineral. 30, 877-893.

Taylor, S.R., Heier, K.S., Sverdrup, T.L., 1960. Trace element variation in three generations of feldspars from the Landsverk I pegmatite, Evje, southern Norway. Norsk Geol. Tidsskr. 40, 133-156.

Thomas, A.V., Spooner, E.T.C., 1988. Fluid inclusions in the system H_2O-CH_4-NaCl-CO_2 from metasomatic tourmaline within the border unit of the Tanco zoned granitic pegmatite, S.E. Manitoba. Geochim. Cosmochim. Acta 52, 1065-1075.

Tischendorf, G., Gottesmann, B., Förster, H-J., Trumbull, R.B., 1997. On Li-bearing micas: estimating Li from electron microprobe analyses and an improved diagram for graphical representation. Mineral. Mag. 61, 809-834.

Tomascak, P.B., 1991, Granites and rare-element pegmatites of the Aylmer Lake pegmatite field, Slave structural province, N.W.T.: Petrochemistry, mineralogy and

exploration quidelines: [M.S., Thesis], Manitoba, University of Manitoba, 215 p. (unpublished)

Trupe, C.H., Stewart, K.G., Adams, M.G., Waters, C.L., Miller, B.V., Hewitt, L.K., 2003. The Burnsville fault: evidence for the timing and kinematics of southern Appalachian Acadian dextral transform tectonics. Geol. Soc. Am. Bull. 115, 1365-1376.

Veal, W.B. 2004. Mineralogy of the Peraluminous Spruce Pine Plutonic Suite, Mitchell, Avery, and Yancey Counties, North Carolina. M.S.thesis, University of Georgia, Athens, 213 p.(unpublished).

Waters, C.L., Hewitt, L.K., Stewart, K.G., Miller, B.V., 2000. Technothermal evolution of the Ashe Metamorphic Suite south of the Grandfather Mountain window, NC: implications for Paleozoic orogenic events in the eastern Blue Ridge. Geol. Soc. Am. Abstracts with Programs, v.32, no. 2, p 81.

Wood, P. A., 1996. Petrogenesis of the Spruce Pine Pegmatites, North Carolina. MSc. thesis, Virginia Polytechnic Institute and State University, Blacksburg, 99 pp. (unpublished).

Zhu, Y.-F., Zeng, Y., Gu, L. 2006. Geochemistry of the rare metal-bearing pegmatite No. 3 vein and related granites in the Keketuohai region, Altay Mountains, northwest China. J. Asian Earth Sci. 27, 61-77.